The Astronomical Journal, 157:216 (32pp), 2019 June https://doi.org/10.3847/1538-3881/ab05dc

The Solar Neighborhood. XLV. The Stellar Multiplicity Rate of M Dwarfs Within 25 pc

Jennifer G. Winters[1,7], Todd J. Henry[2,7], Wei-Chun Jao[3,7], John P. Subasavage[4,7], Joseph P. Chatelain[5,7], Ken Slatten[2], Adric R. Riedel[6,7], Michele L. Silverstein[3,7], and Matthew J. Payne[1]
[1] Harvard-Smithsonian Center for Astrophysics, 60 Garden Street, Cambridge, MA 02138, USA; jennifer.winters@cfa.harvard.edu
[2] RECONS Institute, Chambersburg, PA 17201, USA
[3] Department of Physics and Astronomy, Georgia State University, Atlanta, GA 30302-4106, USA
[4] The Aerospace Corporation, 2310 E. El Segundo Boulevard, El Segundo, CA 90245, USA
[5] Las Cumbres Observatory, 6740 Cortona Drive, Suite 102, Goleta, CA 93117, USA
[6] Space Telescope Science Institute, Baltimore, MD 21218, USA
Received 2018 April 25; revised 2019 January 17; accepted 2019 January 18; published 2019 May 7

Abstract

We present results of the largest, most comprehensive study ever done of the stellar multiplicity of the most common stars in the Galaxy, the red dwarfs. We have conducted an all-sky volume-limited survey for stellar companions to 1120 M dwarf primaries known to lie within 25 pc of the Sun via trigonometric parallaxes. In addition to a comprehensive literature search, stars were explored in new surveys for companions at separations of 2″–300″. A reconnaissance of wide companions to separations of 300″ was done via blinking archival images. *I*-band images were used to search our sample for companions at separations of 2″–180″. Various astrometric and photometric methods were used to probe the inner 2″ to reveal close companions. We report the discovery of 20 new companions and identify 56 candidate multiple systems. We find a stellar multiplicity rate of 26.8 ± 1.4% and a stellar companion rate of 32.4 ± 1.4% for M dwarfs. There is a broad peak in the separation distribution of the companions at 4–20 au, with a weak trend of smaller projected linear separations for lower mass primaries. A hint that M-dwarf multiplicity may be a function of tangential velocity is found, with faster moving, presumably older, stars found to be multiple somewhat less often. We calculate that stellar companions make up at least 17% of mass attributed to M dwarfs in the solar neighborhood, with roughly 11% of M-dwarf mass hidden as unresolved companions. Finally, when considering all M-dwarf primaries and companions, we find that the mass distribution for M dwarfs increases to the end of the stellar main sequence.

Key words: binaries: general – solar neighborhood – stars: low-mass – stars: statistics

Supporting material: machine-readable tables

1. Introduction

Much like people, stars arrange themselves in various configurations—singles, doubles, multiples, clusters, and great aggregations known as galaxies. Each of these collections is different, depending on the proximity of the members and the shared history and composition of the stars involved. Stellar multiples and their properties (e.g., separations and mass ratios) provide fundamental clues about the nature of star formation, the distribution of baryonic mass in the Universe, and the evolution of stellar systems over time. How stars are parceled into singles, doubles, and higher order multiples also provides clues about the angular momentum distribution in stellar systems and can constrain whether planets may be found in these systems (Holman & Wiegert 1999; Raghavan et al. 2010; Wang et al. 2014; Winn & Fabrycky 2015; Kraus et al. 2016). Of all the populations in our Galaxy, the nearest stars provide the fundamental framework upon which stellar astrophysics is based because they contain the most easily studied representatives of their kinds. Because M dwarfs, often called "red dwarfs," dominate the nearby stellar population, accounting for roughly 75% of all stars (Henry et al. 2006), they are a critical sample to study in order to understand stellar multiplicity.

Companion searches have been done for M dwarfs during the past few decades, but until recently, most of the surveys have had inhomogeneous samples made up of on the order of 100 targets. Table 1 lists these previous efforts, with the survey presented in this work listed at the bottom for comparison. With samples of only a few hundred stars, our statistical understanding of the distribution of companions is quite weak, in particular when considering the many different types of M dwarfs, which span a factor of eight in mass (Benedict et al. 2016). In the largest survey of M dwarfs to date, Dhital et al. (2010) studied mid-K to mid-M dwarfs from the Sloan Digital Sky Survey that were not nearby and found primarily wide multiple systems, including white dwarf components in their analysis. In the next largest studies, only a fraction of the M dwarfs studied by Janson et al. (2012, 2014a) had trigonometric distances available, leading to a sample that was not volume-limited. Ward-Duong et al. (2015) had a volume-limited sample with trigonometric parallaxes from *Hipparcos* (Perryman et al. 1997, updated in van Leeuwen 2007), but the faintness limit of *Hipparcos* ($V \sim 12$) prevented the inclusion of later-M dwarf spectral types.[8]

Considering the significant percentage of all stars that M dwarfs comprise, a study with a large sample (i.e., more than 1000 systems) is vital in order to arrive at a conclusive understanding of red dwarf multiplicity, as well as to perform statistical analyses of the overall results, and on subsamples based on primary mass, metallicity, etc. For example, using a binomial distribution for error analysis, an expected

[7] Visiting Astronomer, Cerro Tololo Inter-American Observatory. CTIO is operated by AURA, Inc. under contract to the National Science Foundation.

[8] These final three studies were underway simultaneously with the study presented here.

Table 1
Previous M-dwarf Multiplicity Studies—Techniques

References	# of Stars	Technique	Search Region	MR[a]	Notes
Skrutskie et al. (1989)	55	Infrared Imaging	2″–14″	⋯	multiplicity not reported
Henry & McCarthy (1990)	27	Infrared Speckle	0.″2–5″	34 ± 9	
Henry (1991)	74	Infrared Speckle	0.″2–5″	20 ± 5	
Fischer & Marcy (1992)	28–62	Various	various	42 ± 9	varied sample
Simons et al. (1996)	63	Infrared Imaging	10″–240″	40	
Delfosse et al. (1999a)	127	Radial Velocities	<1.0″	⋯	multiplicity not reported
Law et al. (2006)	32	Lucky Imaging	0.″1–1.″5	7^{+7}_{-3}	M5–M8
Endl et al. (2006)	90	Radial Velocities	<1.″0	⋯	Jovian search
Law et al. (2008)	77	Lucky Imaging	0.″1–1.″5	$13.6^{+6.5}_{-4}$	late-type Ms
Bergfors et al. (2010)	124	Lucky Imaging	0.″2–5″	32 ± 6	young M0–M6
Dhital et al. (2010)	1342	Sloan Archive Search	7″–180″	⋯	wide binary search
Law et al. (2010)	36	Adaptive Optics	0.″1–1.″5	⋯	wide binary search
Dieterich et al. (2012)	126	*HST*-NICMOS	0.″2–7.″5	⋯	brown dwarf search
Janson et al. (2012)	701	Lucky Imaging	0.″08–6″	27 ± 3	young M0–M5
Janson et al. (2014a)	286	Lucky Imaging	0.″1–5″	21–27	>M5
Ward-Duong et al. (2015)	245	Infrared AO	10–10,000 au	23.5 ± 3.2	K7–M6
This survey	1120	Various	0″–300″	27.5 ± 1.4	all trig. distances

Note.
[a] Multiplicity Rate.

multiplicity rate (MR) of 30% on samples of 10, 100, and 1000 stars yields errors of 14.5%, 4.6%, and 1.4%, respectively, illustrating the importance of studying a large, well-defined sample of M dwarfs, preferably with at least 1000 stars.

Here we describe a volume-limited search for stellar companions to 1120 nearby M-dwarf primary stars. For these M-dwarf primaries[9] with trigonometric parallaxes placing them within 25 pc, an all-sky multiplicity search for stellar companions at separations of 2″–300″ was undertaken. A reconnaissance for companions with separations of 5″–300″ was done via the blinking of digitally scanned archival SuperCOSMOS *BRI* images, discussed in detail in Section 3.1. At separations of 2″–10″, the environs of these systems were probed for companions via *I*-band images obtained at telescopes located in both the northern and southern hemispheres, as outlined in Section 3.2. The Cerro Tololo Inter-American Observatory/Small and Moderate Aperture Research Telescope System (CTIO/SMARTS) 0.9 m and 1.0 m telescopes were used in the southern hemisphere, and the Lowell 42-inch and United States Naval Observatory (USNO) 40-inch telescopes were used in the northern hemisphere (see Section 3.2 for specifics on each telescope). In addition, indirect methods based on photometry were used to infer the presence of nearly equal-magnitude companions at separations smaller than ∼2″ (Section 3.3). Various subsets of the sample were searched for companions at subarcsecond separations using long-term astrometry at the CTIO/SMARTS 0.9 m (Section 3.3.3) and *Hipparcos* reduction flags (Section 3.3.4). Finally, an extensive literature search was conducted (Section 3.4). Because spectral type M is effectively the end of the stellar main sequence, the stellar companions revealed in this search are, by definition, M dwarfs as well. We do not include brown dwarf companions to M dwarfs in the statistical results for this study, although they are identified.

[9] We refer to any collection of stars and their companion brown dwarfs and/or exoplanets as a system, including single M dwarfs not currently known to have any companions.

In the interest of clarity, we first define a few terms. *Component* refers to any physical member of a multiple system. The *primary* is either a single star or the most massive (or brightest in *V*) component in the system, and *companion* is used throughout to refer to a physical member of a multiple system that is less massive (or fainter, again in *V*) than the primary star. Finally, we use the terms "red dwarf" and "M dwarf" interchangeably throughout.

2. Definition of the Sample

2.1. Astrometry

The RECONS 25 Parsec Database is a listing of all stars, brown dwarfs, and planets thought to be located within 25 pc, with distances determined only via accurate trigonometric parallaxes. Included in the database is a wealth of information on each system: coordinates, proper motions, the weighted mean of the parallaxes available for each system, *UBVRIJHK* photometry, spectral types in many cases, and alternate names. Additionally noted are the details of multiple systems: the number of components known to be members of the system, the separations and position angles for those components, the year and method of detection, and the delta-magnitude measurement and filter in which the relative photometry data were obtained. Its design has been a massive undertaking that has spanned at least eight years, with expectations of its release to the community in 2019.

The 1120 systems in the survey sample have published trigonometric parallaxes, π_{trig}, of at least 40 mas with errors of 10 mas or smaller that have been extracted from the RECONS 25 Parsec Database. As shown in Table 2, three primary sources of trigonometric parallax data for M dwarfs are currently available. The *General Catalogue of Trigonometric Stellar Parallaxes, Fourth Edition* (van Altena et al. 1995), often called the Yale Parallax Catalog (hereafter YPC), is a valuable compendium of ground-based parallaxes published prior to 1995 and includes just under half of the nearby M-dwarf parallaxes for our sample, primarily from parallax

Table 2
Parallax Sources for Multiplicity Search

Reference	# of Targets North of $\delta = 0$	# of Targets South of $\delta = 0$
YPC	389	125
HIP	83	146
RECONS—published	31	272
RECONS—unpublished	2	3
Literature (1995–2012)	51	18
TOTAL	556	564

programs at the Allegheny, Mt. Stromlo, McCormick, Sproul, US Naval, Van Vleck, Yale, and Yerkes Observatories. The *Hipparcos* mission (initial release by Perryman et al. (1997) and revised results used here by van Leeuwen (2007); hereafter HIP) updated 231 of those parallaxes, and contributed 229 new systems for bright ($V \lesssim 12.5$) nearby M dwarfs. Overall, 743 systems have parallaxes from the YPC and HIP catalogs.

The next largest collection of parallaxes measured for nearby M dwarfs is from the RECONS[10] team, contributing 308 red dwarf systems to the 25 pc census via new measurements (Costa et al. 2005, 2006; Jao et al. 2005, 2011, 2014, 2017; Henry et al. 2006, 2018; Subasavage et al. 2009; Riedel et al. 2010, 2011, 2014, 2018; von Braun et al. 2011; Mamajek et al. 2013; Dieterich et al. 2014; Bartlett et al. 2017; Winters et al. 2017), published in *The Solar Neighborhood* series of papers (hereafter TSN) in *The Astronomical Journal*.[11] Finally, other groups have contributed parallaxes for an additional 69 nearby M dwarfs. As shown in Table 2, RECONS' work in the southern hemisphere creates a balanced all-sky sample of M dwarfs with known distances for the first time, as the southern hemisphere has historically been under-sampled. An important aspect of the sample surveyed here is that because all 1120 systems have accurate parallaxes, biases inherent to photometrically-selected samples are ameliorated.

A combination of color and absolute magnitude limits was used to select a sample of bona fide M dwarfs. Stars within 25 pc were evaluated to define the meaning of "M dwarf" by plotting spectral types from Reid et al. (1995), Hawley et al. (1996), Gray et al. (2003), and RECONS (Riedel et al. 2014) versus $(V-K)$ and M_V. Because spectral types can be imprecise, there was overlap between the K and M types, so boundaries were chosen to split the types at carefully defined $(V-K)$ and M_V values. A similar method was followed for the M-L dwarf transition using results primarily from Dahn et al. (2002). These procedures resulted in ranges of $8.8 \leqslant M_V \leqslant 20.0$ and $3.7 \leqslant (V-K) \leqslant 9.5$ for stars we consider to be M dwarfs. For faint stars with no reliable V available, an initial constraint of $(I-K) \leqslant 4.5$ was used to create the sample until V could be measured. These observational parameters correspond to masses of $0.63 < M/M_\odot < 0.075$, based on the mass–luminosity relation (MLR) presented in Benedict et al. (2016). We note that no M dwarfs known to be companions to more massive stars are included in this sample. Systems that contained a white dwarf component were excluded from the sample, as the white dwarf was previously the brighter and more massive primary.

[10] REsearch Consortium On Nearby Stars, www.recons.org.
[11] A few unpublished measurements used in this study are scheduled for a forthcoming publication in this series.

Imposing these distance, absolute magnitude, and color criteria yields a sample of 1120 red dwarf primaries as of 2014 January 1, when the companion search sample list was frozen, with some new parallaxes measured by RECONS being added as they became available. The astrometry data for these 1120 systems are listed in Table 3. Included are the names of the M-dwarf primary, coordinates (J2000.0), proper motion magnitudes and position angles with references, the weighted means of the published trigonometric parallaxes and the errors, and the number of parallaxes included in the weighted mean and references. We note that for multiple systems, the proper motion of the primary component has been assumed to be the same for all members of the system. All proper motions are from SuperCOSMOS, except where noted. Proper motions with the reference "RECONS (in prep)" indicate SuperCOSMOS proper motions that will be published in the forthcoming RECONS 25 Parsec Database (W. C. Jao et al. 2019, in preparation), as these values have not been presented previously. In the cases of multiple systems for which parallax measurements exist for companions as well as for the primaries, these measurements have been combined in the weighted means. The five parallaxes noted as "in prep" will be presented in upcoming papers in the TSN series. Figure 1 shows the distribution on the sky of the entire sample investigated for multiplicity. Note the balance in the distribution of stars surveyed, with nearly equal numbers of M dwarfs in the northern and southern skies.

2.2. Sample Selection Biases

We describe here how the sample selection process could bias the result of our survey.

We note that our sample is volume-limited, not volume-complete. If we assume that the 188 M-dwarf systems in our sample that lie within 10 pc comprise a volume-complete sample and extrapolate to 25 pc assuming a uniform stellar density, we expect 2938 M-dwarf systems to lie within 25 pc.

We cross-matched our sample of M-dwarf primaries to the recently available parallaxes from the *Gaia* Data Release 2 (DR2; Gaia Collaboration et al. 2016, 2018) and found that 90% (1008 primaries) had *Gaia* parallaxes that placed them within 25 pc. Four percent fell outside of 25 pc with a *Gaia* DR2 parallax. The remaining 6% (69 primaries) were not found to have a *Gaia* DR2 parallax, but 47 (4%) are known to be in multiple systems with separations between the components on the order of or smaller than 1″. Nine of these 47 multiple systems are within the 10 pc horizon. A few of the remaining 22 that are not currently known to be multiple are definitively nearby, but have high proper motion (e.g., GJ 406) or are bright (e.g., GJ 411). We do not make any corrections to our sample based on this comparison because it is evident that a sample of stars surveyed for stellar multiplicity based on the *Gaia* DR2 would neglect binaries. We look forward, however, to the *Gaia* DR3, which will include valuable multiplicity information.

Figure 2 shows the distribution of the apparent I magnitudes of the red dwarfs surveyed, with a peak at $I = 8.5$–9.5. Because brighter objects are generally targeted for parallax measurements before fainter objects, for which measurements are more difficult, 85% of the sample is made up of bright stars ($I < 12.00$), introducing an implicit Malmquist bias. As unresolved multiple systems are usually overluminous, this survey's outcomes are biased toward a larger MR.

Table 3
Astrometry Data

Name	R.A. (hh:mm:ss)	Decl. (dd:mm:ss)	μ ($''$ yr^{-1})	P.A. (deg)	References	π (mas)	σ_π (mas)	# π	References
(1)	(2)	(3)	(4)	(5)	(6)	(7)	(8)	(9)	(10)
GJ 1001ABC	00 04 36.45	−40 44 02.7	1.636	159.7	71	77.90	2.04	2	15, 68
GJ 1	00 05 24.43	−37 21 26.7	6.106	112.5	28	230.32	0.90	2	68, 69
LHS 1019	00 06 19.19	−65 50 25.9	0.564	158.7	72	59.85	2.64	1	69
GJ 1002	00 06 43.19	−07 32 17.0	2.041	204.0	39	213.00	3.60	1	68
GJ 1003	00 07 26.71	+29 14 32.7	1.890	127.0	38	53.50	2.50	1	68
LHS 1022	00 07 59.11	+08 00 19.4	0.546	222.0	38	44.00	6.30	1	68
L 217−28	00 08 17.37	−57 05 52.9	0.370	264.0	40	75.17	2.11	1	73
HIP 687	00 08 27.29	+17 25 27.3	0.110	233.8	28	45.98	1.93	1	69
G 131−26AB	00 08 53.92	+20 50 25.4	0.251	194.4	53	54.13	1.35	1	53
GJ 7	00 09 04.34	−27 07 19.5	0.715	079.7	72	43.61	2.56	2	68, 69
LEHPM 1−255	00 09 45.06	−42 01 39.6	0.271	096.7	72	53.26	1.51	1	73

Note.
[a] The weighted mean parallax includes the parallax of both the primary and the secondary components.
References. (1) Andrei et al. (2011); (2) Anglada-Escudé et al. (2012); (3) Bartlett et al. (2017); (4) Benedict et al. (1999); (5) Benedict et al. (2000); (6) Benedict et al. (2001); (7) Benedict et al. (2002); (8) Biller & Close (2007); (9) Costa et al. (2005); (10) Costa et al. (2006); (11) Dahn et al. (2002); (12) Deacon & Hambly (2001); (13) Deacon et al. (2005b); (14) Deacon et al. (2005a); (15) Dieterich et al. (2014); (16) Dupuy & Liu (2012); (17) Fabricius & Makarov (2000); (18) Faherty et al. (2012); (19) Falin & Mignard (1999); (20) Gatewood et al. (1993); (21) Gatewood et al. (2003); (22) Gatewood (2008); (23) Gatewood & Coban (2009); (24) Henry et al. (1997); (25) Henry et al. (2006); (26) Henry et al. (2018); (27) Hershey & Taff (1998); (28) Høg et al. (2000); (29) Ianna et al. (1996); (30) Jao et al. (2005); (31) Jao et al. (2011); (32) Jao et al. (2017); (33) Khovritchev et al. (2013); (34) Lèpine & Shara (2005); (35) Lèpine et al. (2009); (36) Lurie et al. (2014); (37) Luyten (1979a); (38) Luyten (1979b); (39) Luyten (1980a); (40) Luyten (1980b); (41) Martin & Mignard (1998); (42) Martinache et al. (2007); (43) Martinache et al. (2009); (44) Monet et al. (2003); (45) Pokorny et al. (2004); (46) Pourbaix et al. (2003); (47) Pravdo et al. (2006); (48) Pravdo & Shaklan (2009); (49) RECONS (in prep); (50) Reid et al. (2003); (51) Riedel et al. (2010); (52) Riedel et al. (2011); (53) Riedel et al. (2014); (54) Riedel et al. (2018); (55) Schilbach et al. (2009); (56) Schmidt et al. (2007); (57) Shakht (1997); (58) Shkolnik et al. (2012); (59) Smart et al. (2007); (60) Smart et al. (2010); (61) Söderhjelm (1999); (62) Subasavage et al. (2005a); (63) Subasavage et al. (2005b); (64) Teegarden et al. (2003); (65) Teixeira et al. (2009); (66) Tinney et al. (1995); (67) Tinney (1996); (68) van Altena et al. (1995); (69) van Leeuwen (2007); (70) von Braun et al. (2011); (71) Weis (1999); (72) Winters et al. (2015); (73) Winters et al. (2017).

(This table is available in its entirety in machine-readable form.)

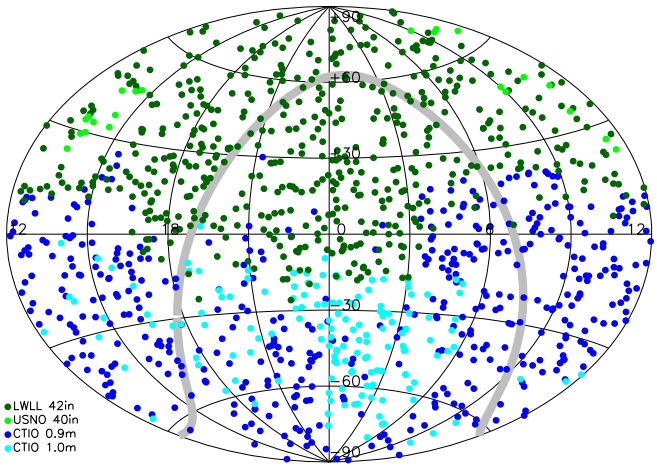

Figure 1. Distribution on the sky of all 1120 M-dwarf primaries examined for multiplicity. Different colors indicate the different telescopes that were used for the CCD imaging search: royal blue for the CTIO/SMARTS 0.9 m, dark green for the Lowell 42-inch, cyan for the CTIO/SMARTS 1.0 m, and bright green for the USNO 40-inch telescopes. The Galactic plane is outlined in gray. Illustrated is the uniformity of the sample in both hemispheres, due in large part to RECONS' parallax work in the southern hemisphere.

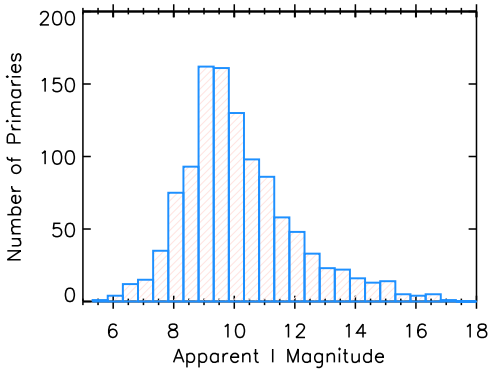

Figure 2. Distribution of *I*-band magnitudes of our sample of 1120 M dwarfs known to lie within 25 pc, illustrating that most (85%) of the target stars are brighter than $I = 12$.

We have also required the error on the published trigonometric parallax to be $\leqslant$10 mas in order to limit the sample to members that are reliably within 25 pc. Therefore it is possible that binaries were missed, as perturbations on the parallax due to an unseen companion can increase the parallax error. Forty-five M-dwarf systems with YPC or HIP parallaxes were eliminated from the sample due to their large parallax errors. We cross-checked these 45 targets against the *Gaia* DR2 with a search radius of 3′ to mitigate the positional offset of these typically high proper motion stars. Twenty-nine were returned with parallaxes by *Gaia*, 19 of which remained within our chosen 25 pc distance horizon. Four of these 19 had close companions detected by *Gaia*. If we assumed that the 16 non-detections were all multiple systems and all within 25 pc, the sample size would increase to 1155, and the MR would increase by 0.9%. We do not include any correction due to this bias. We note that the parallaxes measured as a result of RECONS' astrometry program, roughly one-third of the sample, would not factor into this negative bias, as all of these data were examined and stars with astrometric perturbations due to unseen companions flagged.

Additionally, there is mass missing within 25 pc in the form of M-dwarf primaries (Winters et al. 2015). However, because the MRs decrease as a function of primary mass (see Section 6.1.3 and Figure 19), the percentages of "missing" multiple systems in each mass bin are effectively equal. Based on the 10 pc sample, as above, we expect 969 M dwarfs more massive than 0.30 $M_{\odot}$ within 25 pc, but have 506 in our sample. The MR of 28.2% for the estimated 463 missing systems results in 131 (14%) missing multiples in this primary mass subset. We expect 1109 M dwarfs with primaries 0.15–0.30 $M_{\odot}$ within 25 pc, but have 402 in our sample. The MR of 21.4% for the estimated 707 missing systems results in 151 (14%) missing multiples in this primary mass subset. Finally, we expect 859 M dwarfs with primaries 0.075–0.15 $M_{\odot}$ within 25 pc, but have 212 in our sample. The MR of 16.0% for the estimated 647 missing systems results in 104 (12%) missing multiples in this primary mass subset. Therefore we do not include a correction for this bias.

2.3. Optical and Infrared Photometry

Existing *VRI* photometry for many of the M dwarfs in the sample was culled from the literature, much of which has been presented previously for the southern M dwarfs in Winters et al. (2011, 2015, 2017); however, a number of M dwarfs in the sample had no published reliable optical photometry available. As part of the effort to characterize the M dwarfs in the survey, new absolute photometry in the Johnson–Kron–Cousins $V_J R_{KC} I_{KC}$[12] filters was acquired for 81, 3, and 49 stars at the CTIO/SMARTS 0.9 m, CTIO/SMARTS 1.0 m, and Lowell 42-inch telescopes, respectively, and is presented here for the first time. Identical observational methods were used at all three sites. As in previous RECONS efforts, standard star fields from Graham (1982), Bessel (1990), and/or Landolt (1992, 2007, 2013) were observed multiple times each night to derive transformation equations and extinction curves. In order to match those used by Landolt, apertures 14″ in diameter were used to determine the stellar fluxes, except in cases where close contaminating sources needed to be deblended. In these cases, smaller apertures were used and aperture corrections were applied. Further details about the data reduction procedures, transformation equations, etc., can be found in Jao et al. (2005), Winters et al. (2011), and Winters et al. (2015).

In addition to the 0.9 m, 1.0 m, and 42-inch observations, three stars were observed at the USNO Flagstaff Station 40-inch telescope. Basic calibration frames, bias and sky flats in each filter are taken either every night (bias) or over multiple nights in a run (sky flats) and are applied to the raw science data. Standard star fields from Landolt (2009, 2013) were observed at multiple airmasses between ∼1.0 and ∼2.1 each per night to calculate extinction curves. All instrumental magnitudes, both for standards and science targets, are extracted by fitting spatially-dependent point-spread functions (PSFs) for each frame using Source Extractor (*SExtractor*; Bertin & Arnouts 1996) and *PSFEx* (Bertin 2011), with an aperture diameter of 14″. Extensive comparisons of this technique to basic aperture photometry have produced consistent results in uncrowded fields.

[12] These subscripts will be dropped henceforth. The central wavelengths for the V_J, R_{KC}, and I_{KC} filters at the 0.9 m are 5438 Å, 6425 Å, and 8075 Å, respectively; filters at other telescopes are similar.

Optical and infrared photometry for the 1448 components of the 1120 M-dwarf systems is presented in Table 4, where available. JHK_s magnitudes were extracted from 2MASS (Skrutskie et al. 2006) and confirmed by eye to correspond to the star in question during the blinking survey. Included are the names of the M dwarfs (Column 1), the number of known components in the systems (2), J2000.0 coordinates (3, 4), *VRI* magnitudes (5, 6, 7), the number of observations and/or references (8), the 2MASS JHK_s magnitudes (9, 10, 11), and the photometric distance estimate. Next are listed the ΔV magnitudes between stellar companions and primaries (12), the deblended V magnitudes V_{db} (13), and estimated masses for each component (14). Components of multiple systems are noted with a capital letter (A, B, C, D, E) after the name in the first column. If the names of the components are different, the letters identifying the primary and the secondary are placed within parentheses, e.g., LHS1104(A) and LHS1105(B). If the star is a companion in a multiple system, "0" is given in Column (2). "J" for joint photometry is listed with each blended magnitude. Brown dwarf companions are noted by a "BD" next to the "0" in Column 2, and often do not have complete photometry, if any.

For new photometry reported here, superscripts are added to the references indicating which telescope(s) was used to acquire the *VRI* photometry: "09" for the CTIO/SMARTS 0.9 m, "10" for the CTIO/SMARTS 1.0 m, "40" for the USNO 40-inch telescope, and "42" for the Lowell 42-inch telescope. If the ΔV is larger than 3, the magnitude of the primary is treated as unaffected by the companion(s). All masses are estimated from the absolute V magnitude, which has been calculated from the deblended V magnitude for each star in Column (13), the parallax in Table 3, and the empirical MLRs of Benedict et al. (2016). If any type of assumption or conversion was made regarding the ΔV (as discussed in Section 5.3.1), it is noted.

As outlined in Winters et al. (2011), photometric errors at the 0.9 m are typically 0.03 mag in V and 0.02 mag in R and I. To verify the Lowell 42-inch data,[13] Table 5 presents photometry for four stars observed at the Lowell 42-inch and at the CTIO/SMARTS 0.9 m telescopes, as well as six stars with *VRI* from the literature. Results from the 42-inch and 0.9 m telescopes match to 0.06 mag, except for the R magnitude of GJ 1167, which can be attributed to a possible flare event observed at the time of observation at the 42-inch telescope, as the V and I magnitudes are consistent. This object is, in fact, included in a flare star catalog of UV Cet-type variables (Gershberg et al. 1999). An additional six stars were observed by Weis,[14] and the photometry matches to within 0.08 mag for all six objects, and typically to 0.03 mag. Given our typical 1σ errors of at most 0.03 mag for *VRI*, we find that the Lowell 42-inch data have differences of 2σ or smaller in 28 of the 30 cases shown in Table 5.

3. The Searches and Detected Companions

Several searches were carried out on the 1120 nearby M dwarfs in an effort to make this the most comprehensive investigation of multiplicity ever undertaken for stars that dominate the solar neighborhood. Information about the

[13] No rigorous comparisons are yet possible for our sample of red dwarfs for the CTIO/SMARTS 1.0 m and USNO 40-inch telescopes because only three stars have been observed at each.

[14] All photometry from Weis has been converted to the Johnson–Kron–Cousins (JKC) system using the relation in Bessell & Weis (1987).

Table 4
Photometry Data

Name	# Obj	R.A.	Decl.	V_J	R_{KC}	I_{KC}	# nts/ref	J	H	K_s	π_{ccd}	σ_π	ΔV	V_{db}	Mass
		(dd:mm:ss)	(hh:mm:ss)	(mag)	(mag)	(mag)		(mag)	(mag)	(mag)	(pc)	(pc)	(mag)	(mag)	($M_\odot$)
(1)	(2)	(3)	(4)	(5)	(6)	(7)	(8)	(9)	(10)	(11)	(12)	(13)	(14)	(15)	(16)
GJ 1001B	0BD	00 04 34.87	−40 44 06.5	22.77J	19.04J	16.67J	/10[d]	13.11J	12.06J	11.40J	…	…	…	…	…
GJ 1001C	0BD	00 04 34.87	−40 44 06.5	…	…	…	…	…	…	…	…	…	…	…	…
GJ 1001A	3	00 04 36.45	−40 44 02.7	12.83	11.62	10.08	/40	8.60	8.04	7.74	12.5	1.9	…	12.83	0.234
GJ 1	1	00 05 24.43	−37 21 26.7	8.54	7.57	6.41	/4	5.33	4.83[a]	4.52	5.6	0.9	…	8.54	0.411
LHS 1019	1	00 06 19.19	−65 50 25.9	12.17	11.11	9.78	/21	8.48	7.84	7.63	16.6	2.6	…	12.17	0.335
GJ 1002	1	00 06 43.19	−07 32 17.0	13.84	12.21	10.21	/40	8.32	7.79	7.44	5.4	1.0	…	13.84	0.116
GJ 1003	1	00 07 26.71	+29 14 32.7	14.16	13.01	11.54	/37	10.22	9.74	9.46	36.0	7.0	…	14.16	0.203
LHS 1022	1	00 07 59.11	+08 00 19.4	13.09	12.02	10.65	/37	9.39	8.91	8.65	28.9	5.2	…	13.09	0.311
L 217-28	1	00 08 17.37	−57 05 52.9	12.13	11.00	9.57	/40	8.21	7.63	7.40	13.2	2.0	…	12.13	0.293
HIP 687	1	00 08 27.29	+17 25 27.3	10.80	9.88	8.93	/35	7.81	7.17	6.98	18.5	3.2	…	10.80	0.582

Notes. A "J" next to a photometry value indicates that the magnitude is blended due to one or more close companions. A square bracket next to the photometric distance estimate indicates that the joint photometry of the multiple system was used to calculate the distance estimate, which is thus likely underestimated. A "u" following the photometry reference indicates that we present an update to previously presented RECONS photometry.

[a] 2MASS magnitude error greater than 0.05 mag.
[b] An assumption was made regarding the Δmag.
[c] A conversion to ΔV was done from a reported magnitude difference in another filter.
[d] Photometry in SOAR filters and not converted to Johnson–Kron–Cousins system.
[e] Mass from Barbieri et al. (1996).
[f] Mass from Benedict et al. (2000).
[g] Mass from Benedict et al. (2016).
[h] Mass from Henry et al. (1999).
[i] Mass from Henry et al. (1999), Tamazian et al. (2006).
[j] Mass from Ségransan et al. (2000).
[k] Mass from Delfosse et al. (1999a).
[l] Mass from Díaz et al. (2007).
[m] Mass from Duquennoy & Mayor (1988).
[n] Mass from Herbig & Moorhead (1965).
[o] Photometry for "AC" instead of for the "B" component was mistakenly reported in Davison et al. (2015).

References. (1) This work; (2) Bartlett et al. (2017); (3) Benedict et al. (2016); (4) Bessel (1990); (5) Bessell (1991); (6) Costa et al. (2005); (7) Costa et al. (2006); (8) Dahn et al. (2002); (9) Davison et al. (2015); (10) Dieterich et al. (2014); (11) Harrington & Dahn (1980); (12) Harrington et al. (1993); (13) Henry et al. (2006); (14) Henry et al. (2018); (15) Høg et al. (2000); (16) Hosey et al. (2015); (17) Jao et al. (2005); (18) Jao et al. (2011); (19) Jao et al. (2017); (20) Koen et al. (2002); (21) Koen et al. (2010); (22) Lèpine et al. (2009); (23) Lurie et al. (2014); (24) Reid et al. (2002); (25) Riedel et al. (2010); (26) Riedel et al. (2011); (27) Riedel et al. (2014); (28) Riedel et al. (2018); (29) Weis (1984); (30) Weis (1986); (31) Weis (1987); (32) Weis (1988); (33) Weis (1991b); (34) Weis (1991a); (35) Weis (1993); (36) Weis (1994); (37) Weis (1996); (38) Weis (1999); (39) Winters et al. (2011); (40) Winters et al. (2015); (41) Winters et al. (2017).

(This table is available in its entirety in machine-readable form.)

Table 5
Overlapping Photometry Data

Name	$(V-K)$ (mag)	V_J (mag)	R_{KC} (mag)	I_{KC} (mag)	# obs	tel/ref
2MA J0738 +2400	4.86	12.98	11.81	10.35	1	42in
		12.98	11.83	10.35	2	0.9 m
G 43−2	4.76	13.23	12.08	10.67	1	42in
		13.24	12.07	10.66	2	0.9 m
2MA J1113 +1025	5.34	14.55	13.27	11.63	1	42in
		14.50	13.21	11.59	2	0.9 m
GJ 1167	5.59	14.16	12.67	11.10	1	42in
		14.20	12.82	11.11	1	0.9 m
LTT 17095A	4.22	11.12	10.12	9.00	1	42in
		11.11	10.11	8.94	⋯	1
GJ 15B	5.12	11.07	9.82	8.34	2	42in
		11.06	9.83	8.26	⋯	3
GJ 507AC	3.96	9.52	8.56	7.55	1	42in
		9.52	8.58	7.55	⋯	3
GJ 507B	4.64	12.15	11.06	9.66	1	42in
		12.12	11.03	9.65	⋯	3
GJ 617A	3.64	8.59	7.68	6.85	1	42in
		8.60	7.72	6.86	⋯	3
GJ 617B	4.67	10.74	9.67	8.29	1	42in
		10.71	9.63	8.25	⋯	2

References. (1) Weis (1993); (2) Weis (1994); (3) Weis (1996).

surveys is collected in Tables 6–12, including a statistical overview of the individual surveys in Table 6. Note that the number of detections includes confirmations of previously reported multiples in the literature. Specifics about the Blink Survey are listed in Table 7. Telescopes used for the CCD Imaging Survey in Table 8, while detection limit information for the CCD Imaging Survey is presented in Tables 9 and 10. Results for confirmed multiples are collected in Table 11, whereas candidate (as yet unconfirmed) companions are listed in Table 12.

We report the results of each search here; overall results are presented in Section 5.

3.1. Wide-field Blinking Survey: Companions at 5″–300″

Because most nearby stars have large proper motions, images of the stars taken at different epochs were blinked for common proper motion (CPM) companions with separations of 5″–300″. A wide companion would have a similar proper motion to its primary and would thus appear to move in the same direction at the same speed across the sky. Archival SuperCOMOS $B_J R_{59F} I_{IVN}$[15] photographic plate images $10' \times 10'$ in size were blinked using the Aladin interface of the Centre de Données astronomiques de Strasbourg (CDS) to detect companions at separations greater than ∼5″. These plates were taken from 1974 to 2002 and provide up to 28 years of temporal coverage, with typical epoch spreads of at least 10 years. Information for the images blinked is given in Table 7, taken from Morgan (1995), Subasavage (2007), and the UK Schmidt webpage.[16] Candidates were confirmed to be real by collecting *VRI* photometry and estimating photometric distances using the suite of relations in Henry et al. (2004); if the distances of the primary and candidate matched to within the errors on the distances, the candidate was deemed to be a physical companion. In addition to recovering 63 known CPM companions, one new CPM companion (2MA0936−2610C) was discovered during this blinking search, details of which are given in Section 4.1. No comprehensive search for companions at angular separations larger than 300″ was conducted.

[15] These subscripts will be dropped henceforth.
[16] http://www.roe.ac.uk/ifa/wfau/ukstu/telescope.html

Table 6
Companion Search Technique Statistics

Technique	Separation (″)	Searched (#)	Searched (%)	Detected (#)
Image Blinking	5–300	1110	99	64
CCD Imaging	2–10	1120	100	44
RECONS Perturbations	<2	324	29	39
HR Diagram Elevation	<2	1120	100	11
Distance Mismatches	<2	1112	99	37
Hipparcos Flags	<2	460	41	31
Literature/WDS Search	all	1120	100	290
Individual companions	TOTAL	1120	100	310

Table 7
Blink Survey Information

Filter	Epoch Span (yr)	Decl. Range (deg)	Mag. Limit (mag)	$\Delta\lambda$ (Å)
B_J (IIIaJ)	1974–1994	all-sky	∼20.5	3950–5400
R_{59F} (IIIaF)	1984–2001	all-sky	∼21.5	5900–6900
I_{IVN} (IVN)	1978–2002	all-sky	∼19.5	6700–9000
E_{POSS-I} (103aE)	1950–1957	$-20.5 < \delta < +05$	∼19.5	6200–6700
I_{KC}	2010–2014	all sky	∼17.5	7150–9000

Table 8
Telescopes Used for CCD Imaging Search and *VRI* Photometry

Telescope	FOV	Pixel Scale	# Nights	# Objects
Lowell 42in	22.′3 × 22.′3	0.″327 px^{-1}	21	508
USNO 40in	22.′9 × 22.′9	0.″670 px^{-1}	1	22
CTIO/ SMARTS 0.9 m	13.′6 × 13.′6	0.″401 px^{-1}	16	442
CTIO/ SMARTS 1.0 m	19.′6 × 19.′6	0.″289 px^{-1}	8	148

3.1.1. Blink Survey Detection Limits

The CPM search had two elements that needed to be evaluated in order to confidently identify objects moving with the primary star in question: companion brightness and the size of each system's proper motion.

A companion would have to be detectable on at least two of the three photographic plates in order to notice its proper motion, so any companion would need to be brighter than the magnitude limits given in Table 7 in at least two images. Because the search is for *stellar* companions, it is only necessary to be able to detect a companion as faint as the faintest star in the sample, effectively spectral type M9.5 V at 25 pc. The two faintest stars in the sample are DEN 0909 −0658, with $VRI = 21.55$, 19.46, and 17.18 and RG0050 −2722 with $VRI = 21.54$, 19.09, and 16.65. The *B* magnitudes

Table 9
Stars Used for Imaging Search Detection Limit Study

Name	I (mag)	FWHM (arcsec)	Tel	Note
GJ 285	8.24	0.8	0.9 m	
LP 848−50AB	12.47J	0.8	0.9 m	$\rho_{AB} < 2''$
SIP 1632−0631	15.56	0.8	0.9 m	
L 32−9A	8.04	1.0	0.9 m	$\rho_{AB} = 22''.40$
SCR 0754−3809	11.98	1.0	0.9 m	
BRI 1222−1221	15.59	1.0	0.9 m	
GJ 709	8.41	1.0	42in	
GJ 1231	12.08	1.0	42in	
Reference Star	16 (scaled)	1.0	42in	
GJ 2060AB	7.83J	1.5	0.9 m	$\rho_{AB} = 0''.485$
2MA 2053−0133	12.46	1.5	0.9 m	
Reference Star	16 (scaled)	1.5	0.9 m	
GJ 109	8.10	1.5	42in	
LHS 1378	12.09	1.5	42in	
2MA 0352+0210	16.12	1.5	42in	
Reference Star	8 (scaled)	1.8	0.9 m	
SCR 2307−8452	12.00	1.8	0.9 m	
Reference Star	16 (scaled)	1.8	0.9 m	
GJ 134	8.21	1.8	42in	
LHS 1375	12.01	1.8	42in	
SIP 0320−0446AB	16.37	1.8	42in	$\rho_{AB} < 0''.33$
GJ 720A	8.02	2.0	42in	$\rho_{AB} = 112''.10$
LHS 3005	11.99	2.0	42in	
2MA 1731+2721	15.50	2.0	42in	

Note. "J" on the I-band magnitudes of LP 848−50AB and GJ 2060AB indicates that the photometry includes light from the companion. The other subarcsecond binary, SIP 0320−0446AB, has a brown dwarf companion that does not contribute significant light to the photometry of its primary star.

Table 10
Imaging Search Detection Limit Summary

Seeing Conditions	Yes (#)	No (#)	Maybe (#)	Yes (#)	No (#)	Maybe (#)
		0.9 m			42in	
FWHM = 0.″8	64	8	3	…	…	…
I = 8 mag	36	7	2	…	…	…
I = 12 mag	23	1	1	…	…	…
I = 16 mag	5	…	…	…	…	…
FWHM = 1.″0	62	8	5	60	12	3
I = 8 mag	35	7	3	34	8	3
I = 12 mag	22	1	2	21	4	…
I = 16 mag	5	…	…	5	…	…
FWHM = 1.″5	58	12	5	55	12	8
I = 8 mag	33	9	3	33	6	6
I = 12 mag	20	3	2	17	6	2
I = 16 mag	5	…	…	5	…	…
FWHM = 1.″8	50	18	7	52	14	9
I = 8 mag	28	13	4	29	10	6
I = 12 mag	18	5	2	19	4	2
I = 16 mag	4	…	1	4	…	1
FWHM = 2.″0	…	…	…	46	17	12
I = 8 mag	…	…	…	24	12	9
I = 12 mag	…	…	…	18	5	2
I = 16 mag	…	…	…	4	…	1
TOTAL	234	46	20	213	55	32

for these stars are both fainter than the mag ∼20.5 limit of the B plate, and thus neither star was detected in the B image; however, their R and I magnitudes are both brighter than the limits of those plates and the stars were identified in both the R and I images. Ten other objects are too faint to be seen on the B plate, but as is the case with DEN0909−0658 and RG0050 −2722, all are bright enough for detection in the R and I images.

The epoch spread between the plates also needed to be large enough to detect the primary star moving in order to then notice a companion moving in tandem with it. As shown in the histogram of proper motions in Figure 3, most of the survey stars move faster than $0''.18$ yr^{-1}, the historical cutoff of Luyten's proper motion surveys. Hence, even a 10 yr baseline provides $1''.8$ of motion, our adopted minimum proper motion detection limit, easily discerned when blinking plates. However, 58 of the stars in the survey (∼5% of the sample) have $\mu < 0''.18$ yr^{-1}, with the slowest star having $\mu = 0''.03$ yr^{-1}; for this star, to detect a motion of $1''.8$, the epoch spread would need to be 60 yr. For 18 stars with decl. $-20 < \delta < +5°$, the older POSS-I plate (taken during 1950–1957) was used for the slow-moving primaries. This extended the epoch spread by 8–24 yr, enabling companions for these 18 stars to be detected, leaving 40 slow-moving stars to search.

The proper motions of 151 additional primaries were not initially able to be detected confidently because the epoch spread of the SuperCOSMOS plates was shorter than 5 yr. These 151 stars, in addition to the 40 stars with low μ mentioned above that were not able to be blinked using the POSS plates, were compared to our newly acquired I-band images taken during the CCD Imaging Survey, extending the epoch spread by almost 20 years in some cases. Wherever possible, the SuperCOSMOS I-band image was blinked with our CCD I-band image, but sometimes a larger epoch spread was possible with either the B- or R-band plate images. In these cases, the plate that provided the largest epoch spread was used. In order to upload these images to Aladin to blink with the archival SuperCOSMOS images, World Coordinate System (WCS) coordinates were added to the header of each image so that the two images could be aligned properly. This was done using *SExtractor* for the CTIO/SMARTS 0.9 m and the USNO 40-inch images and the tools at Astrometry.net for the Lowell 42-inch and the CTIO/SMARTS 1.0 m images.

After using the various techniques outlined above to extend the image epoch spreads, 1110 of 1120 stars were sucessfully searched in the Blink Survey for companions. In 10 cases, either the primary star's proper motion was still undetectable, the available CCD images were taken under poor sky conditions and many faint sources were not visible, or the frame rotations converged poorly. A primary result from this Blink Survey is that in the separation regime from $10''$ to $300''$, where the search is effectively complete, we find an MR of 4.7% (as discussed in Section 5.2). Thus, we estimate that only 0.5 CPM stellar companions ($10 * 4.7\%$) with separations $10''$–$300''$ were missed due to not searching 10 stars during the Blinking Survey.

Table 11
Multiplicity Information for Sample

Name	# Obj	Map	R.A. (hh:mm:ss)	Decl. (dd:mm:ss)	ρ ($''$)	θ (deg)	Year	Technique	References	Δmag (mag)	Filter	References
GJ 1001	0	BC	00 04 34.87	−40 44 06.5	0.087	048	2003	HSTACS	40	0.01	222	40
GJ 1001	3	A-BC	00 04 36.45	−40 44 02.7	18.2	259	2003	visdet	40	9.91	V_J	1
G 131−26	2	AB	00 08 53.92	+20 50 25.4	0.111	170	2001	AO det	13	0.46	H	13
GJ 11	2	AB	00 13 15.81	+69 19 37.2	0.859	089	2012	lkydet	62	0.69	i′	62
LTT 17095	2	AB	00 13 38.74	+80 39 56.8	12.78	126	2001	visdet	103	3.63	V_J	1
GJ 1005	2	AB	00 15 28.06	−16 08 01.8	0.329	234	2002	HSTNIC	30	2.42	V_J	9
2MA 0015−1636	2	AB	00 15 58.07	−16 36 57.8	0.105	090	2011	AO det	18	0.06	H	18
L 290−72	2	AB	00 16 01.99	−48 15 39.3	<1	⋯	2007	SB1	117	⋯	⋯	...
GJ 1006	2	AB	00 16 14.62	+19 51 37.6	25.09	059	1999	visdet	103	0.94	V_J	111
GJ 15	2	AB	00 18 22.88	+44 01 22.7	35.15	064	1999	visdet	103	2.97	V_J	1

Note. The codes for the techniques and instruments used to detect and resolve systems are: AO det—adaptive optics; astdet —detection via astrometric perturbation, companion often not detected directly; astorb—orbit from astrometric measurements; HSTACS—*Hubble Space Telescope's* Advanced Camera for Surveys; HSTFGS —*Hubble Space Telescope's* Fine Guidance Sensors; HSTNIC—*Hubble Space Telescope's* Near Infrared Camera and Multi-Object Spectrometer; HSTWPC—*Hubble Space Telescope's* Wide Field Planetary Camera 2; lkydet—detection via lucky imaging; lkyorb—orbit from lucky imaging measurements; radorb—orbit from radial velocity measurements; radvel— detection via radial velocity, but no SB type indicated; SB (1, 2, 3)—spectroscopic multiple, either single-lined, double-lined, or triple-lined; spkdet—detection via speckle interferometry; spkorb—orbit from speckle interferometry measurements; visdet —detection via visual astrometry; visorb—orbit from visual astrometry measurements.

References. (1) This work; (2) Allen & Reid (2008); (3) Al-Shukri et al. (1996); (4) Balega et al. (2007); (5) Balega et al. (2013); (6) Bartlett et al. (2017); (7) Benedict et al. (2000); (8) Benedict et al. (2001); (9) Benedict et al. (2016); (10) Bergfors et al. (2010); (11) Bessel (1990); (12) Bessell (1991); (13) Beuzit et al. (2004); (14) Biller et al. (2006); (15) Blake et al. (2008); (16) Bonfils et al. (2013); (17) Bonnefoy et al. (2009); (18) Bowler et al. (2015); (19) Burningham et al. (2009); (20) Chanamé & Gould (2004); (21) Cortes-Contreras et al. (2014); (22) Cvetković et al. (2015); (23) Daemgen et al. (2007); (24) Dahn et al. (1988); (25) Davison et al. (2014); (26) Dawson & De Robertis (2005); (27) Delfosse et al. (1999a); (28) Delfosse et al. (1999b); (29) Díaz et al. (2007); (30) Dieterich et al. (2012); (31) Docobo et al. (2006); (32) Doyle & Butler (1990); (33) Duquennoy & Mayor (1988); (34) Femenía et al. (2011); (35) Forveille et al. (2005); (36) Freed et al. (2003); (37) Fu et al. (1997); (38) Gizis (1998); (39) Gizis et al. (2002); (40) Golimowski et al. (2004); (41) Harlow (1996); (42) Harrington et al. (1985); (43) Hartkopf et al. (2012); (44) Heintz (1985); (45) Heintz (1987); (46) Heintz (1990); (47) Heintz (1991); (48) Heintz (1992); (49) Heintz (1993); (50) Heintz (1994); (51) Henry et al. (1999); (52) Henry et al. (2006); (53) Henry et al. (2018); (54) Herbig & Moorhead (1965); (55) Horch et al. (2010); (56) Horch et al. (2011a); (57) Horch et al. (2012); (58) Horch et al. (2015a); (59) Ireland et al. (2008); (60) Janson et al. (2012); (61) Janson et al. (2014a); (62) Janson et al. (2014b); (63) Jao et al. (2003); (64) Jao et al. (2009); (65) Jao et al. (2011); (66) Jenkins et al. (2009); (67) Jódar et al. (2013); (68) Köhler et al. (2012); (69) Kürster et al. (2009); (70) Lampens et al. (2007); (71) Law et al. (2006); (72) Law et al. (2008); (73) Leinert et al. (1994); (74) Lèpine et al. (2009); (75) Lindegren et al. (1997); (76) Luyten (1979a); (77) Malo et al. (2014); (78) Martín et al. (2000); (79) Martinache et al. (2007); (80) Martinache et al. (2009); (81) Mason et al. (2009); (82) Mason et al. (2018); (83) McAlister et al. (1987); (84) Montagnier et al. (2006); (85) Nidever et al. (2002); (86) Pravdo et al. (2004); (87) Pravdo et al. (2006); (88) Reid et al. (2001); (89) Reid et al. (2002); (90) Reiners & Basri (2010); (91) Reiners et al. (2012); (92) Riddle et al. (1971); (93) Riedel et al. (2010); (94) Riedel et al. (2014);(95) Riedel et al. (2018); (96) Salim & Gould (2003); (97) Schneider et al. (2011); (98) Scholz (2010); (99) Ségransan et al. (2000); (100) Shkolnik et al. (2010); (101) Shkolnik et al. (2012); (102) Siegler et al. (2005); (103) Skrutskie et al. (2006); (104) Tokovinin & Lépine (2012); (105) van Biesbroeck (1974); (106) van Dessel & Sinachopoulos (1993); (107) Wahhaj et al. (2011); (108) Ward-Duong et al. (2015); (109) Weis (1991b); (110) Weis (1993); (111) Weis (1996); (112) Winters et al. (2011); (113) Winters et al. (2017); (114) Winters et al. (2018); (115) Woitas et al. (2003); (116) Worley & Mason (1998); (117) Zechmeister et al. (2009).

(This table is available in its entirety in machine-readable form.)

3.2. CCD Imaging Survey: Companions at 2″–10″

To search for companions with separations 2″–10″, astrometry data were obtained at four different telescopes: in the northern hemisphere, the Hall 42-inch telescope at Lowell Observatory and the USNO 40-inch telescope, both in Flagstaff, AZ, and in the southern hemisphere, the CTIO/SMARTS 0.9 m and 1.0 m telescopes, both at Cerro Tololo Inter-American Observatory in Chile. Each M-dwarf primary was observed in the I_{KC} filter with integrations of 3, 30, and 300 seconds in order to reveal stellar companions at separations 2″–10″. This observational strategy was adopted to reveal any close equal-magnitude companions with the short 3 s exposures, while the long 300 s exposures would reveal faint companions with masses at the end of the main sequence. The 30 s exposures were taken to bridge the intermediate phase space. Calibration frames taken at the beginning of each night were used for typical bias subtraction and dome flat-fielding using standard IRAF procedures.

Technical details for the cameras and specifics about the observational setups and numbers of nights and stars observed at each telescope are given in Table 8. The telescopes used for the imaging campaign all have primary mirrors roughly 1 m in size and have CCD cameras that provide similar pixel scales. Data from all telescopes were acquired without binning pixels. The histogram in Figure 4 illustrates the seeing measured for the best images of each star surveyed at the four different telescopes. Seeing conditions better than 2″ were attained for all but one star, GJ 507, with some stars being observed multiple times. While the 0.9 m telescope has a slightly larger pixel scale than the 1.0 m and the 42-inch telescopes, as shown in Figure 4, the seeing was typically better at that site, allowing for better resolution. Only 22 primaries (fewer than 2% of the survey) were observed at the USNO 40-inch telescope, so we do not consider the coarser pixel scale to have significantly affected the survey. Overall, the data from the four telescopes used were of similar quality and the results could be combined without modification.

A few additional details of the observations are worthy of note:

1. A total of 442 stars were observed at the CTIO/SMARTS 0.9 m telescope, where consistently good seeing, telescope operation, and weather conditions make

Table 12
Suspected Multiple Systems

Name	# Stars	R.A. (hh:mm:ss)	Decl. (dd:mm:ss)	Flag	Reference
GJ 1006A	3?	00 16 14.62	+19 51 37.6	dist	1
HIP 6365	2?	01 21 45.39	−46 42 51.8	X	3
LHS 1288	2?	01 42 55.78	−42 12 12.5	X	3
GJ 91	2?	02 13 53.62	−32 02 28.5	X	3
G 143.3	2?	03 31 47.14	+14 19 17.9	X	3
BD-21 1074A	4?	05 06 49.47	−21 35 03.8	dist	1
GJ 192	2?	05 12 42.22	+19 39 56.5	X	3
GJ 207.1	2?	05 33 44.81	+01 56 43.4	possSB	4
SCR 0631-8811	2?	06 31 31.04	−88 11 36.6	elev	1
LP 381-4	2?	06 36 18.25	−40 00 23.8	G	3
SCR 0702-6102	2?	07 02 50.36	−61 02 47.7	elev,pb?	1,1
LP 423-31	2?	07 52 23.93	+16 12 15.0	elev	1
SCR 0757-7114	2?	07 57 32.55	−71 14 53.8	dist	1
GJ 1105	2?	07 58 12.70	+41 18 13.4	X	3
LHS 2029	2?	08 37 07.97	+15 07 45.6	X	3
LHS 259	2?	09 00 52.08	+48 25 24.7	elev	1
GJ 341	2?	09 21 37.61	−60 16 55.1	possSB	4
GJ 367	2?	09 44 29.83	−45 46 35.6	X	3
GJ 369	2?	09 51 09.63	−12 19 47.6	X	3
GJ 373	2?	09 56 08.68	+62 47 18.5	possSB	4
GJ 377	2?	10 01 10.74	−30 23 24.5	dist	1
GJ 1136A	3?	10 41 51.83	−36 38 00.1	X,possSB	3,4
GJ 402	2?	10 50 52.02	+06 48 29.4	X	3
LHS 2520	2?	12 10 05.59	−15 04 16.9	dist	1
GJ 465	2?	12 24 52.49	−18 14 32.3	pb?	2
DEN 1250-2121	2?	12 50 52.65	−21 21 13.6	elev	1
GJ 507.1	2?	13 19 40.13	+33 20 47.7	X	3
GJ 540	2?	14 08 12.97	+80 35 50.1	X	3
2MA 1507-2000	2?	15 07 27.81	−20 00 43.3	dist,elev	1
G 202-16	2?	15 49 36.28	+51 02 57.3	G	3
LHS 3129A	3?	15 53 06.35	+34 45 13.9	dist	1
GJ 620	2?	16 23 07.64	−24 42 35.2	G	3
GJ 1203	2?	16 32 45.20	+12 36 45.9	X	3
LP 69-457	2?	16 40 20.65	+67 36 04.9	elev	1
LTT 14949	2?	16 40 48.90	+36 18 59.9	X	3
HIP 83405	2?	17 02 49.58	−06 04 06.5	X	3
LP 44-162	2?	17 57 15.40	+70 42 01.4	elev	1
LP 334-11	2?	18 09 40.72	+31 52 12.8	X	3
SCR 1826-6542	2?	18 26 46.83	−65 42 39.9	elev	1
LP 44-334	2?	18 40 02.40	+72 40 54.1	elev	1
GJ 723	2?	18 40 17.83	−10 27 55.3	X	3
HIP 92451	2?	18 50 26.67	−62 03 03.8	possSB	4
LHS 3445A	3?	19 14 39.15	+19 19 03.7	dist	1
GJ 756	2?	19 21 51.42	+28 39 58.2	X	3
LP 870-65	2?	20 04 30.79	−23 42 02.4	dist	1
GJ 1250	2?	20 08 17.90	+33 18 12.9	dist	1
LEHPM 2-783	2?	20 19 49.82	−58 16 43.0	elev	1
GJ 791	2?	20 27 41.65	−27 44 51.9	X	3
LHS 3564	2?	20 34 43.03	+03 20 51.1	X	3
GJ 811.1	2?	20 56 46.59	−10 26 54.8	X	3
L 117-123	2?	21 20 09.80	−67 39 05.6	X	3
HIP 106803	2?	21 37 55.69	−63 42 43.0	X	3
LHS 3748	2?	22 03 27.13	−50 38 38.4	X	3
G 214-14	2?	22 11 16.96	+41 00 54.9	X	3
GJ 899	2?	23 34 03.33	+00 10 45.9	X	3
GJ 912	2?	23 55 39.77	−06 08 33.2	X	3

Note. Flag description: "dist" means that the *ccddist* is at least $\sqrt{2}$ times closer than the *trigdist* due to the object's overluminosity; "elev" means that the object is elevated above the main sequence in the HR diagram in Figure 10 due to overluminosity; "possSB" means that the object has been noted as a possible spectroscopic binary by Reiners et al. (2012); "pb?" indicates that a possible perturbation was noted. The the single letters are *Hipparcos* reduction flags as follows: *G* is an acceleration solution where a component might be causing a variation in the proper motion; *V* is for variability-induced movers, where one component in an unresolved binary could be causing the photocenter of the system to be perturbed; *X* is for a stochastic solution, where no reliable astrometric parameters could be determined, and which may indicate an astrometric binary.

References. (1) This work; (2) Heintz (1986); (3) Lindegren et al. (1997); (4) Reiners et al. (2012).

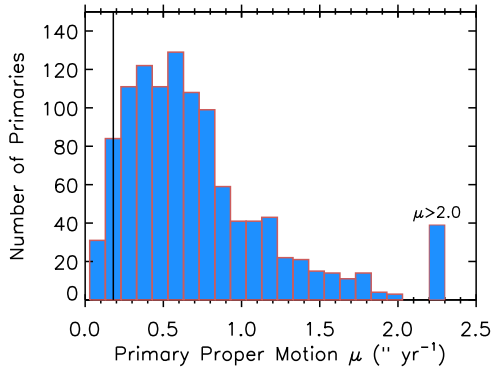

Figure 3. Histogram of the proper motion of the primary (or single) component in each system, with the vertical line indicating $\mu = 0\farcs18$ yr^{-1}, the canonical lower proper motion limit of Luyten's surveys. The majority (95%) have proper motions, μ, larger than $0\farcs18$ yr^{-1}.

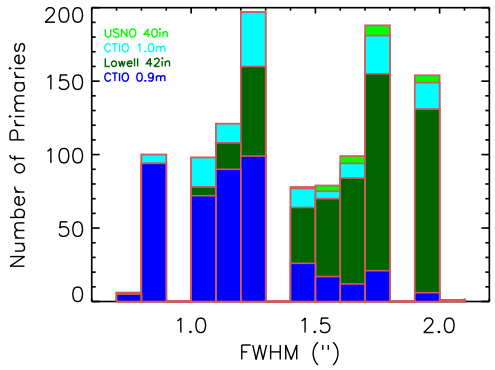

Figure 4. Seeing FWHM measured for target star frames used in the *I*-band CCD imaging search. The four different telescopes used are represented as royal blue for the CTIO/SMARTS 0.9 m, dark green for the Lowell 42-inch, cyan for the CTIO/SMARTS 1.0 m, and bright green for the USNO 40-inch telescopes. Note the generally superior seeing conditions for targets observed at the 0.9 m.

observations at this site superior to those at the other telescopes used, as illustrated in Figure 4.

2. While being re-aluminized in 2012 December, the primary mirror at the Lowell 42-inch telescope was dropped and damaged. The mask that was installed over the damaged mirror as a temporary fix resulted in a PSF flare before a better mask was installed that slightly improved the PSF. Of the 508 stars observed for astrometry at Lowell, 457 were observed before the mishap and 51 after.
3. *I*-band images at both the Lowell 42-inch and CTIO/SMARTS 1.0 m telescopes suffer from fringing, the major cause of which is night sky emission from atmospheric OH molecules. This effect sometimes occurs with back-illuminated CCDs at optical wavelengths longer than roughly 700 nm where the light is reflected several times between the internal front and back surfaces of the CCD, creating constructive and destructive interference patterns, or fringing (Howell 2000, 2012). In order to remove these fringes, *I*-band frames from multiple nights with a minimum of saturated stars in the frame were selected, boxcar smoothed, and then average-combined into a fringe map. This fringe map was then subtracted from all *I*-band images using a modified IDL code originally crafted by Snodgrass & Carry (2013).

Four new companions were discovered during this portion of the survey. Details on these new companions are given in Section 4.1. In each case, archival SuperCOSMOS plates were blinked to eliminate the possibility that new companions were background objects. We detected 32 companions with separations 2″–10″, as well as 12 companions with $\rho < 2''$, including the four noted above.

3.2.1. CCD Imaging Survey Detection Limits

The M_I range of the M-dwarf sequence is roughly 8 magnitudes ($M_I = 6.95$–14.80 mag, specifically, for our sample). Therefore an analysis of the detection limits of the CCD imaging campaign was done for objects with a range of *I* magnitudes at $\rho = 1''$–$5''$ and at Δmags = 0–8 in one-magnitude increments for different seeing conditions at the two main telescopes where the bulk (85%) of the stars were imaged: the CTIO/SMARTS 0.9 m and the Lowell 42-inch telescopes. While the companion search in the CCD frames extended to 10″, sources were detected even more easily at separations 5″–10″ than at 5″, so it was not deemed necessary to perform the analysis for the larger separations.

Because the apparent *I*-band magnitudes for the stars in the sample range from 5.32 to 17.18 (as shown in Figure 2), objects with *I*-band magnitudes of approximately 8, 12, and 16 were selected for investigation. Only 88 primaries (7.8% of the sample) have $I < 8$, so it was not felt necessary to create a separate set of simulations for these brighter stars. The stars used for the detection limit analysis are listed in Table 9 with their *I* magnitudes, the FWHM at which they were observed and at which telescope, and any relevant notes.

Each of the selected test stars was analyzed in seeing conditions of $1\farcs0$, $1\farcs5$, and $1\farcs8$, but because the seeing at CTIO is typically better than that at Anderson Mesa, we were able to push to $0\farcs8$ for the 0.9 m, and had to extend to $2\farcs0$ for the Lowell 42-inch telescope. These test stars were verified to have no known *detectable* companions within the 1″–5″ separations explored in this part of the project. We note that one of the targets examined for the best resolution test, LP 848−50AB, has an astrometric perturbation due to an unseen companion at an unknown separation, but that in data with a FWHM of $0\farcs8$, the two objects were still not resolved. As the detection limit determination probes separations 1″–5″, using this star does not affect the detection limit analysis. The other binaries used all had either larger or smaller separations than the 1″–5″ regions explored, effectively making them point sources.

The IDL SHIFT task was used to shift and add the science star as a proxy for an embedded companion, scaled by a factor of 2.512 for each magnitude difference. In cases where the science star was saturated in the frame, a reference star was selected from the shorter exposure taken in similar seeing in which the science star was not saturated. Its relative magnitude difference was calculated so that it could be scaled to the desired brightness in the longer exposure, and then it was embedded for the analysis. In all cases, the background sky counts were subtracted before any scaling was done.

Stars with $I = 8$ were searched for companion sources in IRAF via radial and contour plots using the 3 s exposure to probe $\Delta I = 0$, 1, 2, and 3, the 30 s exposure for $\Delta I = 4$ and 5, and the 300 s exposure for $\Delta I = 6$, 7, and 8. Similarly, twelfth-magnitude stars were probed at $\Delta I = 0$, 1, 2, and 3 using the 30 s exposure and at $\Delta I = 4$ with the 300 s frame. Finally, the 300 s exposure was used to explore the regions around the

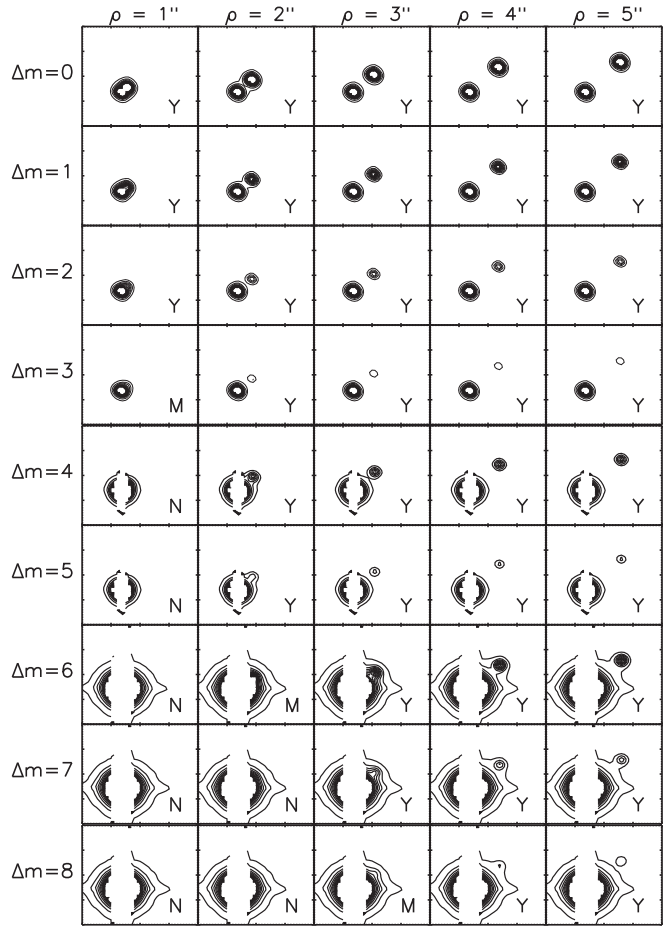

Figure 5. Detection limits for the CTIO/SMARTS 0.9 m: Contour plots for L 32-9A, with $I = 8.04$ in $1\farcs0$ seeing conditions for an embedded companion at $\rho = 1''$–$5''$ with Δmags = 0–8. The Y, N, and M labels indicate *yes*, *no*, or *maybe* for whether or not the embedded companion is detectable. The 3 s exposure was used for Δmags = 0–3, the 30 s exposure was used for Δmags = 4–5, and the 300 s exposure was used for Δmags = 6–8. Thirty-five simulated companions were detected, seven were undetectable, and three were possibly detected.

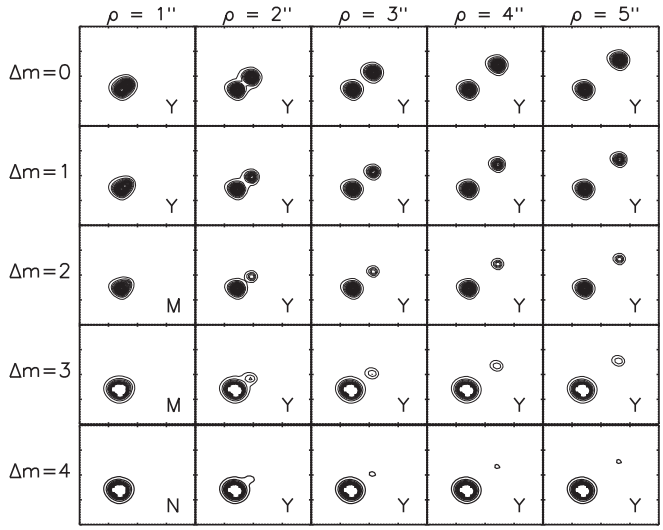

Figure 6. Detection limits for the CTIO/SMARTS 0.9 m: Contour plots for SCR 0754−3809, with $I = 11.98$ mag at $1\farcs0$ seeing conditions for an embedded companion at $\rho = 1''$–$5''$ with Δmags = 0–4. The Y, N, and M labels indicate *yes*, *no*, or *maybe* for whether or not the embedded companion is detectable. The 30 s exposure was used for Δmags = 0, 1, 2, and the 300 s exposure was used for Δmags = 3, 4. Twenty-two simulated companions were detected, one was undetectable, and two were possibly detected.

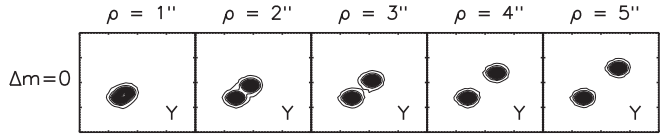

Figure 7. Detection limits for the CTIO/SMARTS 0.9 m: Contour plots for BRI 1222−1221, with $I = 15.59$ mag at $1\farcs0$ seeing conditions for an embedded companion at $\rho = 1''$–$5''$ with Δmags = 0. The Y, N, and M labels indicate *yes*, *no*, or *maybe* for whether or not the embedded companion is detectable. The 300 s exposure was used. All 5 simulated companions were detected.

sixteenth-magnitude objects for evidence of a stellar companion at $\Delta I = 0$.

In total, 600 contour plots were made using IDL and inspected by eye. A subset of 75 example plots for stars with $I = 8.04$, 11.98, and 15.59 observed in seeing conditions of $1\farcs0$ at the 0.9 m are shown in Figures 5–7. The "Y," "N," and "M" labels in each plot indicate *yes*, *no*, or *maybe* for whether or not the injected synthetic companion was detectable by eye at the separation, magnitude, and seeing conditions explored. As can be seen, the target star with $I = 8.04$ is highly saturated in the frames used for ΔI greater than 4. Overall, the companion can be detected in 62 of the 75 simulations, not detected in eight cases, and possibly detected in five more cases. The conditions in which the companion remains undetected in some cases are at small ρ and at $\Delta I > 4$, typically around bright stars. Note that these images do not stand alone—contour plots for target stars are also compared to plots for other stars in the frames, allowing an additional check to determine whether the star in question is multiple.

The full range of ΔI for the M-dwarf sequence is roughly eight magnitudes, so $\Delta I > 8$ represents detections of early-L dwarf and brown dwarf companions. There were no companions detected with $\Delta I > 8$ around the brighter stars in the simulations, indicating that this survey was *not* sensitive to these types of faint companions at separations $1''$–$5''$ around the brightest M dwarfs in the sample, although they would be detected around many of the fainter stars (none were found).

Table 10 presents a summary of the results of the detections of the embedded companions. Overall, the simulated companions were detected 75% of the time for all brightness ratios on both telescopes, were not detected 17% of the time, and were possibly detected in 9% of the simulations. For the simulations of bright stars with $I = 8$, 70% of the embedded companions were detected. For stars with $I = 12$, companions were detected in 79% of the time, and for the faint stars with $I = 16$, companions were detected in 93% of the cases tested. At $\rho = 1''$, the embedded companions were detected in 28% of cases, not detected in 52% of cases, and possibly detected in 20% of cases. Thus, we do not claim high sensitivity at separations this small. In total, for $\rho \geqslant 2''$, we successfully detected the simulated companions 86% of the time, did not detect them 8% of the time, and possibly detected them 6% of the time.

We note that this study was not sensitive to companions with large Δmags at separations $\sim 1''$–$2''$ from their primaries. While the long-exposure *I*-band images obtained during the direct imaging campaign would likely reveal fainter companions at $\rho \sim 2''$–$5''$, the saturation of some of the observed brighter stars creates a CCD bleed along columns in the direction in which

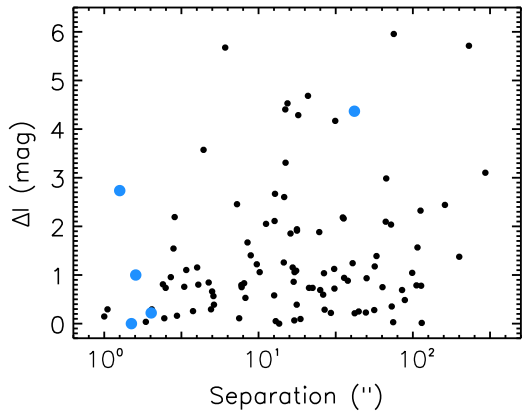

Figure 8. Log-linear plot of ΔI vs. angular separation to illustrate the observational limits of our Blinking and CCD Imaging Surveys. Solid black points indicate known companions that were confirmed, while the new companions discovered during our searches are shown as larger blue points.

the CCDs read out. Faint companions located within $\sim$1″–2″ of their primaries, but at a position angle near 0° or 180° would be overwhelmed by the CCD bleed of the saturated star and not be detected. We do not include any correction due to this bias, as it mostly applies to companions at separations <2″ from their primaries, below our stated detection limit sensitivity.

3.2.2. Detection Limits Summary

Figure 8 illustrates detected companions in the Blinking and CCD Imaging Surveys, providing a comparison for the detection limits derived here. We note that the largest ΔI detected was roughly 6.0 mag (GJ 752B), while the largest angular separation detected was 295″ (GJ 49B).

Figure 9 indicates the coverage curves for our two main surveys as a function of projected linear separation. Using the angular separation limits of each survey (2″–10″ for the imaging survey and 5″–300″ for the blinking survey) and the trigonometric distances of each object to determine the upper and lower projected linear separation limit for each M-dwarf primary in our sample, we show that either the imaging or blinking survey would have detected stellar companions at projected distances of 50–1000 au for 100% of our sample.

3.3. Searches at Separations ⩽2″

In addition to the blinking and CCD imaging searches, investigations for companions at separations smaller than 2″ were possible using a variety of techniques, as detailed below in Sections 3.3.1–3.3.4. The availability of accurate parallaxes for all stars and of *VRIJHK* photometry for most stars made possible the identification of overluminous red dwarfs that could be harboring unresolved stellar companions. Various subsets of the sample were also probed using long-term astrometric data for stars observed during RECONS' astrometry program, as well as via data reduction flags indicating astrometric signatures of unseen companions for stars observed by *Hipparcos*.

3.3.1. Overluminosity via Photometry: Elevation above the Main Sequence

Accurate parallaxes and *V* and *K* magnitudes for stars in the sample allow the plotting of the observational HR diagram

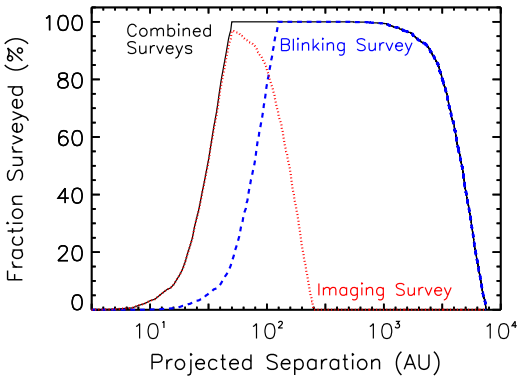

Figure 9. Fraction of our sample surveyed as a function of log-projected linear separation. The curve for the imaging campaign is shown as a red dotted line, while the blinking campaign coverage is shown as a blue dashed line. The solid black line indicates the combined coverage of the two campaigns. We show that our surveys are complete for stellar companions at projected linear separations of roughly 50–1000 au, 75% complete at separations 40–3000 au, and 50% complete at separations 30–4000 au.

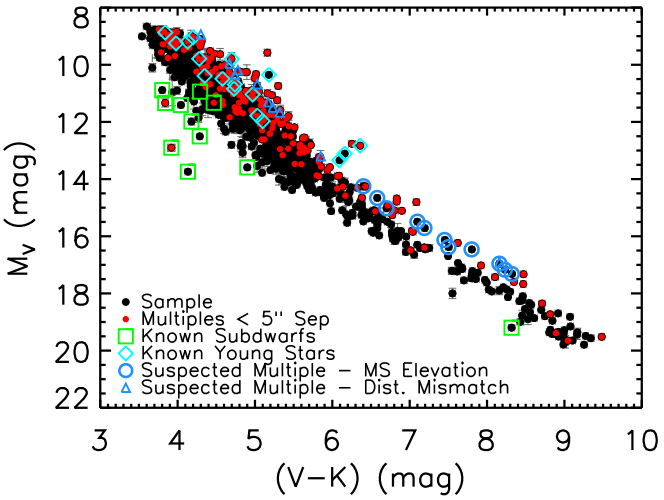

Figure 10. Observational HR diagram for 1120 M dwarf primaries, with M_V plotted vs. $(V-K)$ color. All primaries are plotted as black points. Overplotted are known close multiples with separations smaller than 5″ having blended photometry (red points), known subdwarfs (open green squares), and known young objects (open cyan diamonds). Error bars are shown in gray and are smaller than the points in most cases. The large *K* magnitude errors for four objects (GJ 408, GJ 508.2, LHS 3472, and LP 876-26AB) have been omitted for clarity. As expected, known multiples with merged photometry are often elevated above the middle of the distribution. The 11 stars suspected to be new unresolved multiples due to their elevated positions relative to the main sequence are indicated with open blue circles. The 10 stars suspected to be new unresolved multiples due to their distance mismatches from Figure 11 are indicated with open blue triangles. Note that the candidate multiples detected by main-sequence elevation are mostly mid- to late-type M dwarfs, while the suspected multiples identified by the distance mismatch technique are primarily early-type M dwarfs.

shown in Figure 10, where M_V and the $(V-K)$ color are used as proxies for luminosity and temperature, respectively. Unresolved companions that contribute significant flux to the photometry cause targets to be overluminous, placing them above the main sequence. Known multiples with separations <5″[17] are evident as points clearly elevated above the

[17] This 5″ separation appears to be the boundary where photometry for multiple systems from the literature—specifically from Bessell and Weis—becomes blended. For photometry available from the SAAO group (e.g., Kilkenny, Koen), the separation is $\sim$10″ because they use large apertures when calculating photometric values.

Table 13
Young Members

Name	# Objects	R.A. (hh:mm:ss)	Decl. (dd:mm:ss)	μ ($''$ yr^{-1})	P.A. (deg)	References	$v_{\rm tan}$ (km s^{-1})	Youth Indicator	Moving Group	References
LTT 10301AB	2	00 50 33.23	+24 49 00.9	0.203	101.9	5	11	ol	Argus	3
G 80-21	1	03 47 23.35	−01 58 19.8	0.323	147.8	5	25	Li	AB Dor	3
2MA 0414−0906	1	04 14 17.29	−09 06 54.3	0.168	325.2	4	19	Li	none	3
LP 776−25	1	04 52 24.42	−16 49 22.2	0.243	150.7	2	18	ol	AB Dor	3
GJ 2036AB	2	04 53 31.20	−55 51 37.3	0.149	060.6	5	8	BF	AB Dor	3
LP 717−36AB	2	05 25 41.67	−09 09 12.6	0.197	164.7	6	19	ol	AB Dor	3
AP COL	1	06 04 52.16	−34 33 36.0	0.330	003.6	6	13	Li	Argus	3
CD-35 2722AB	2	06 09 19.22	−35 49 31.1	0.057	186.4	4	6	BF	AB Dor	3
GJ 2060ABC	3	07 28 51.37	−30 14 49.2	0.212	207.9	5	15	BF	AB Dor	3
G 161-71	1	09 44 54.19	−12 20 54.4	0.321	277.1	1	21	ol	Argus	1
GJ 382	1	10 12 17.67	−03 44 44.4	0.314	219.0	5	12	ol	AB Dor	3
TWA 22AB	2	10 17 26.91	−53 54 26.5	0.149	264.4	6	12	Li	Beta Pic	3
GJ 393	1	10 28 55.56	+00 50 27.6	0.950	219.3	5	32	ol	AB Dor	3
GJ 490ABCD	4	12 57 40.26	+35 13 30.3	0.307	240.9	5	29	BF	Tuc-Hor	3
GJ 856AB	2	22 23 29.08	+32 27 33.1	0.329	129.1	5	24	Li	AB Dor	3
GJ 871.1AB	2	22 44 57.96	−33 15 01.7	0.230	123.1	5	25	(Li)	Beta Pic	3
HIP 114066	1	23 06 04.83	+63 55 33.9	0.185	108.5	5	21	Li	AB Dor	3

Note. The youth indicators are as follows: BF —a bona fide and well-known member of a moving group; Li—the presence of lithium; ol—over-luminous.
References. (1) Bartlett et al. (2017); (2) Høg et al. (2000); (3) Riedel et al. (2017); (4) Shkolnik et al. (2012); (5) van Leeuwen (2007); (6) Winters et al. (2015).

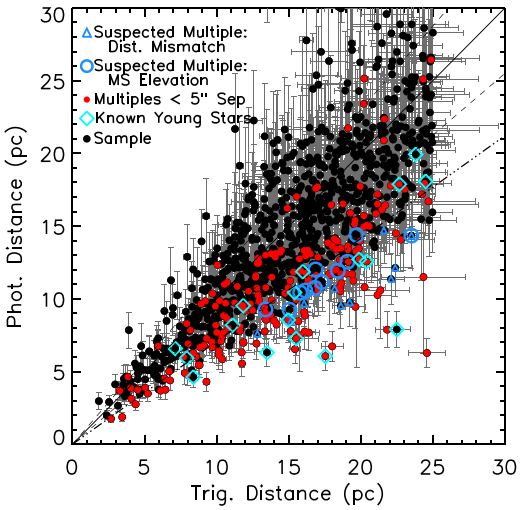

Figure 11. Comparison of distance estimates from *VRIJHK* photometry vs. distances using $\pi_{\rm trig}$ for 1091 of the M-dwarf primaries in the sample. The 29 stars with photometric distances >30 pc are not included in this plot. Errors on the distances are noted in gray. The diagonal solid line represents 1:1 agreement in distances, while the dashed lines indicate the 15% uncertainties associated with the CCD distance estimates from Henry et al. (2004). The dash–dotted line traces the location where the trigonometric distance exceeds the photometric estimate by a factor of $\sqrt{2}$, corresponding to an equal-luminosity/mass pair of stars. Known unresolved multiples with blended photometry are indicated with red points. The 11 candidate unresolved multiples from the HR diagram in Figure 10 are enclosed with open blue circles. The 10 new candidates that may be unresolved multiples from this plot are enclosed with open blue triangles.

presumed single stars on the main sequence, and merge with a few young objects. Subdwarfs are located below and to the left of the singles, as they are old, metal-poor, and underluminous at a given color. Eleven candidate multiples lying among the sequence of known multiples have been identified by eye via this HR diagram. These candidates are listed in Table 12 and are marked in Figures 10 and 11. Note that these candidates are primarily mid- to late-M dwarfs. Known young stars and subdwarfs were identified during the literature search and are listed in Tables 13 and 14, along with their identifying characteristics. More details on these young and old systems are given in Sections 3.4.2 and 3.4.3.

3.3.2. Overluminosity via Photometry: Trigonometric and CCD Distance Mismatches

Because both *VRI* and 2MASS *JHK* photometry are now available for nearly the entire sample, photometric distances based on CCD photometry (*ccddist*) were estimated and compared to the accurate trigonometric distances (*trigdist*) available from the parallaxes. Although similar in spirit to the HR diagram test discussed above that uses *V* and *K* photometry, all of the *VRIJHK* photometry is used for each star to estimate the *ccddist* via the technique described in Henry et al. (2004), thereby leveraging additional information. As shown in Figure 11, suspected multiples that would otherwise have been missed due to the inner separation limit ($2''$) of our main imaging survey can be identified due to mismatches in the two distances. For example, an unresolved equal-magnitude binary would have an estimated *ccddist* closer by a factor of $\sqrt{2}$ compared to its measured *trigdist*. Unresolved multiples with more than two components, e.g., a triple system, could be even more overluminous, as could young, multiple systems. By contrast, cool subdwarfs are underluminous, and therefore their photometric distances are overestimated.

With this method, 50 candidate multiples were revealed with *ccddists* that were $\sqrt{2}$ or more times closer than their *trigdists*. Of these, 40 were already known to have at least one close companion (36 stars) or to be young (four stars), verifying the technique. The remaining 10 are new candidates and are listed in Table 12.

3.3.3. RECONS Perturbations

A total of 324 red dwarfs in the sample have parallax measurements by RECONS, with the astrometric coverage spanning 2–16 yr. This number is slightly higher than the 308

Table 14
Subdwarf Members

Name	# Objects	R.A. (hh:mm:ss)	Decl. (dd:mm:ss)	μ ($''$ yr^{-1})	P.A. (deg)	References	v_{tan} (km s^{-1})	Spectral Type	References
LHS 1490	1	03 02 06.36	−39 50 51.9	0.859	221.3	8	58	M5.0 VI	4
GJ 1062	1	03 38 15.70	−11 29 13.5	3.033	152.0	7	230	M2.5 VI	3
LHS 189AB	2	04 25 38.35	−06 52 37.0	1.204	145.7	2	105	M3.0 VIJ	4
LHS 272	1	09 43 46.16	−17 47 06.2	1.439	279.2	5	92	M3.0 VI	3
GJ 455AB	2	12 02 18.08	+28 35 14.2	0.791	268.0	7	74	M3.5 VIJ	3
LHS 2852	1	14 02 46.67	−24 31 49.7	0.506	315.6	8	41	M2.0 VI	3
LHS 375	1	14 31 38.25	−25 25 32.9	1.386	269.0	7	158	M4.0 VI	3
SSSPM J1444−2019	1	14 44 20.33	−20 19 25.5	3.507	236.0	6	270	M9.0 VI:	6
GJ 2116	1	15 43 18.33	−20 15 32.9	1.173	195.3	8	119	M2.0 VI	1
LHS 3409	1	18 45 52.24	+52 27 40.7	0.843	298.0	7	81	M4.5 VI	3
LHS 64AB	2	21 07 55.39	+59 43 19.4	2.098	209.0	7	238	M1.5 VIJ	3

References. (1) Bidelman (1985); (2) Costa et al. (2006); (3) Gizis (1997); (4) Jao et al. (2008); (5) Jao et al. (2011); (6) Schilbach et al. (2009); (7) van Altena et al. (1995); (8) Winters et al. (2015).

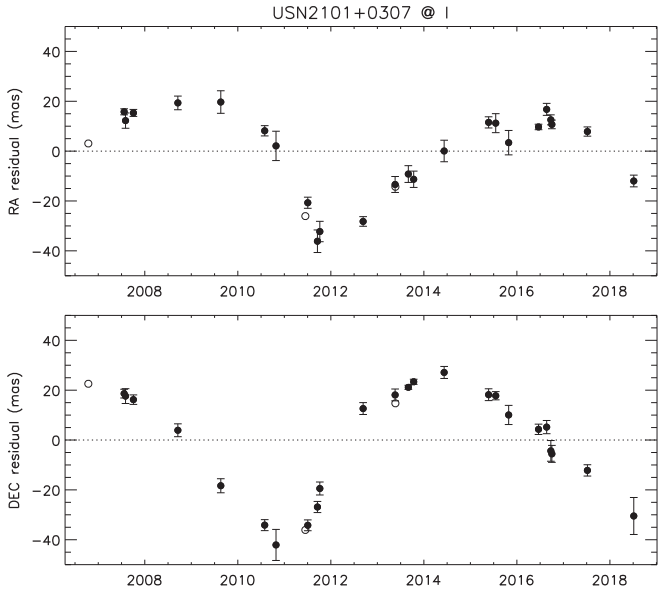

Figure 12. Nightly mean astrometric residual plots in R.A. and decl. for USN2101+0307. The astrometric signature of the system's proper motion and parallax has been removed, leaving clear indication that an unseen companion is perturbing the position of the primary star.

parallaxes listed in Table 2 due to updated and more accurate RECONS parallax measurements that improved upon YPC parallaxes with high errors. The presence of a companion with a mass and/or luminosity different from the primary causes a perturbation in the photocenter of the system that is evident in the astrometric residuals after solving for the proper motion and parallax. This is the case for 39 of the observed systems, which, although sometimes still unseen, are listed as confirmed companions in Table 11, where references are given. Because 13 of these 39 stars with perturbations were detected during the course of this project, we note them as new discoveries, although they were first reported in other papers (e.g., Bartlett et al. 2017; Jao et al. 2017; Winters et al. 2017; Henry et al. 2018; Riedel et al. 2018). A new companion to USN2101 +0307 was reported in Jao et al. (2017). We present here the nightly mean astrometric residual plots in R.A. and decl. for this star (shown in Figure 12), which exhibits a perturbation due to its unseen companion. This system is discussed in more detail in Section 4.1.

This is the only technique used in this companion search that may have revealed brown dwarf companions. None of the companions have been resolved, so it remains uncertain whether the companion is a red or brown dwarf. As we noted in Winters et al. (2017), the magnitude of the perturbation in the photocenter of the system, α, follows the relation $\alpha = (B - \beta)a$, where B is the fractional mass $M_B/(M_A + M_B)$, β is the relative flux expressed as $(1 + 10^{0.4\Delta m})^{-1}$, and a is the semimajor axis of the relative orbit of the two components (van de Kamp 1975). The degeneracy between the mass ratio/flux difference and the scaling of the photocentric and relative orbits results in an uncertainty in the nature of the companion. We are able to assume that the companion is a red dwarf if the system is overluminous, which is the case for eight of these systems. Therefore we conservatively assume that all the companions are red dwarfs. These particular systems are high-priority targets for high-resolution speckle observations through our large program on the Gemini telescopes that is currently in progress, with a goal of resolving and characterizing the companions.

3.3.4. Hipparcos *Reduction Flags*

All 460 stars in the sample with *Hipparcos* parallaxes were searched for entries in the Double and Multiple Systems Annex (DMSA; Lindegren et al. 1997) of the original *Hipparcos* Catalog to reveal any evidence of a companion. Of these 460 stars, 229 have a parallax measured only by *Hipparcos*, while 231 also have a parallax measurement from another source. Various flags exist in the DMSA that confirm or infer the presence of a companion: C—component solutions where both components are resolved and have individual parallaxes; G—acceleration solutions, i.e., due to variable proper motions, which could be caused by an unseen companion; O—orbits from astrometric binaries; V—variability-induced movers (VIMs), where the variability of an unresolved companion causes the photocenter of the system to move or be perturbed; X—stochastic solutions, for which no astrometric parameters could be determined and which may indicate that the star is actually a short-period astrometric binary.

Most of the AFGK systems observed by *Hipparcos* that have flags in the DMSA have been further examined or reanalyzed by Pourbaix et al. (2003, 2004), Platais et al. (2003), Jancart et al. (2005), Frankowski et al. (2007), and Horch et al. (2002, 2011a, 2011b, 2015b, 2017); however, only few of the M-dwarf systems have been investigated to date. Stars with C and O flags were often previously known to be binary, are considered to be confirmed multiples, and are included in Table 11. We found that G, V, or X flags existed for 31 systems in the survey—these suspected multiples are listed in Table 12.

3.4. Literature Search

Finally, a literature search was carried out by reviewing all 1120 primaries in *SIMBAD* and using the available bibliography tool to search for papers reporting additional companions. While *SIMBAD* is sometimes incomplete, most publications reporting companions are included. Papers that were scrutinized in detail include those reporting high-resolution spectroscopic studies (typically radial velocity planet searches or rotational velocity results that might report spectroscopic binaries), parallax papers that might report perturbations, high-resolution imaging results, speckle interferometry papers, and other companion search papers. A long list of references for multiple systems found via the literature search is included in Table 11.

In addition, the Washington Double Star Catalog (WDS), maintained by Brian Mason,[18] was used extensively to find publications with information on multiple systems. Regarding the WDS, we note that (1) not all reported companions are true physical members of the system with which they are listed, and (2) only resolved companions (i.e., no spectroscopic or astrometric binaries) are included in the catalog. Thus, care had to be taken when determining the true number of companions in a system. Information pertaining to a star in the WDS was usually only accessed after it was already known that the system was multiple and how many components were present in the system, so this was not really troublesome. However, the WDS sometimes had references to multiplicity publications that *SIMBAD* had not listed. Thus, the WDS proved valuable in identifying references and the separations, magnitude differences, and other information included in Table 11.

Finally, all of the multiple systems were cross-checked against the *Gaia* DR2 through the Aladin interface. Thirty-two known multiple systems had positional data, but no parallax, while 14 known systems were not found. Of the 575 stellar components presented in this sample, 133 were not found to have separate data points. The majority of these companions are located at subarcsecond angular separations from their primaries, with a rare few having separations $1''$–$3''$. An additional 15 companions had unique coordinates, but no individual parallax or proper motion. We anticipate that future *Gaia* data releases will provide some of the currently missing information for these low-mass multiple systems.

Information for all multiple systems (including brown dwarf components) is presented in Table 11, with *n-1* lines for each system, where *n* is the total number of components in the system. For example, a quadruple system will have three lines of information that describe the system. The name is followed by the number of components in the system and the configuration map of the components detailed in that line of the table. If the line of data pertains to higher order systems containing component configurations for subsystems (e.g., "BC" of a triple system), the number of components noted will be "0," as the full membership of the system will already have been noted in the line of data containing the "A" component. These data are followed by epoch J2000.0 coordinates, the angular separation (ρ) in arcseconds, the position angle (θ) in degrees measured east of north, the year of the measurement, the code for the technique used to identify the component, and the reference. We assign a separation of $<1''$ for all astrometric and spectroscopic binaries (unless more information is available) and/or to indicate that a companion has been detected, but not yet resolved. We note that where orbit determinations from the literature are reported, the semimajor axis, *a*, is listed instead of ρ. If *a* was not reported in the reference given, it was calculated from the period and the estimated masses of the components in question via Kepler's third law.

The final three columns give a magnitude difference (Δmag) between the components indicated by the configuration map, the filter used to measure this Δmag, and the reference for this measurement. Photometry from photographic plates is denoted by "V*." In many cases, there are multiple separation and Δmag measurements available in the literature from different groups using different techniques. An exhaustive list of these results is beyond the scope of this work; instead, a single recent result for each system is listed. In a few cases, the position angles and/or Δmag measurements are not available. We discuss how these systems are treated in Section 5.3.1.

3.4.1. Suspected Companions

Forty-nine singles suspected to be doubles were revealed during this survey, three of which (GJ 912, GJ 1250, and SCR 1826−6542) have so far been confirmed with continuing follow-up observations. An additional five doubles are suspected to be triples, yielding a current total of 54 suspected additional companions (only one companion per system in all cases) listed in Table 12, but *not* included in Table 11.[19] Systems in Table 12 are listed with the suspected number of components followed by a question mark to indicate the system's suspect status, followed by J2000.0 coordinates, a flag code for the reason a system is included as having a candidate companion, and the reference. Notes to the table give detailed descriptions of the flags. Of the 56 suspected companions, 31 are from the *Hipparcos* DMSA, in which they are assigned G, V, or X flags. A number of primaries that were suspected to be multiple due to either an underestimated *ccddist* or an elevated position on the HR diagram were found through the literature search to have already been resolved by others and have been incorporated into Table 11 and included in the analysis as confirmed companions. There remain 21 systems in Table 12 with *ccddist* values that do not match their trigonometric parallax distances and/or that are noticeably elevated above the main sequence that have not yet been confirmed. A few more systems had other combinations of indicators that they were multiple, e.g., an object with a

[18] The primary copy is kept at USNO and a back-up copy is housed at Georgia State University.

[19] For consistency, companions to GJ 912, GJ 1250, and SCR 1826−6542are included in Table 12 and in the "Suspects" portion of the histogram in Figure 16.

perturbation might also have a distance mismatch. Six stars were reported as suspected binaries in the literature. GJ 207.1, GJ 341, GJ 373, GJ 1136A, and HIP 92451 were noted by Reiners et al. (2012) as possible spectroscopic binaries, and GJ 465 was identified by Heintz (1986) as a possible astrometric binary. These are listed in Table 12. We reiterate that none of these *suspected* companions have been included in any of the analyses of the previous section or that follow; only *confirmed* companions have been used.

3.4.2. Young Stellar Objects

Within the solar neighborhood are young moving groups that have contributed members to the multiplicity sample. Within the studied collection are 16 confirmed young M dwarfs, 9 of which are known to be multiple, yielding an MR of 56 ± 19%. We note that this result is not statistically robust due to the small number of objects with which it was calculated. Presented in Table 13 are these known nearby young red dwarfs, with their astrometric data duplicated from Table 3. In addition, the tangential velocity $v_{\rm tan}$ is listed, along with the youth indicators, the moving group with which they are associated, and the reference. The youth indicators are as follows: BF—a bona fide and well-known member of a moving group; Li—the presence of lithium; ol—over-luminous. Any member of a multiple system where one component exhibits any of these indicators is also assumed to be young, as in the case of GJ 871.1AB. We note that we do not exclude any of the identified young M-dwarf members from our sample. This would arbitrarily bias our sample, as a comprehensive search for these objects in the current sample has not been conducted.

3.4.3. Old, Cool Subdwarfs

There are a small number of old halo members, also known as cool subdwarfs, that happen to be passing through the solar neighborhood. The objects have been identified either spectroscopically or stand out on a reduced proper motion diagram. Out of the 11 confirmed subdwarf members with trigonometric parallaxes found within 25 pc, only 3 are multiple systems, resulting in an MR of 27 ± 16%. This is very similar to that of the M-dwarf population as a whole (26.8 ± 1.4%; see Section 5.2) and in agreement with a larger sample of 62 K and M subdwarfs has been studied by Jao et al. (2009), who found a rate of of 26 ± 6%. As with the young stars, with such a small number of objects, this result is not statistically robust. The known subdwarfs in our sample are identified in Table 14. In addition to the astrometric data for each system that have been duplicated from Table 3, the calculated tangential velocities $v_{\rm tan}$ and spectral types from the literature are listed. We note that we do not exclude any of the identified M-type subdwarfs from our study. This would arbitrarily bias our sample, as a comprehensive search for these objects in the current sample has not been conducted.

3.4.4. Substellar Companions

Because this study focuses on the *stellar* companions of M dwarfs, it was important to determine which companions were stellar and which were *substellar*. Dieterich et al. (2014) found that the boundary between stars and brown dwarfs is near the L2.0V spectral type; efforts are underway to determine to what mass this spectral type corresponds. As mentioned in Section 2, $M_V = 20.0$ and $(V - K) = 9.5$ were used as cutoffs for the faintest and reddest (and correspondingly least massive) M dwarfs. Analysis of the main sequence in the HR diagram created from the RECONS list of stars and brown dwarfs within 25 pc indicates that $M_V = 21.5$ and $(V - K) = 10.3$ correspond to spectral type L2.0V, and therefore the end of the stellar main sequence. Thus, for this large statistical study, we consider objects fainter or redder than these limits to be substellar brown dwarfs.

Via the literature search, 18 brown dwarf companions to 15 M-dwarf primaries were identified. These are noted in Table 4 with a "BD" for the component in the object column (Column 2). Although no comprehensive searches have been done for brown dwarfs as companions to the 1120 M dwarfs targeted here (including ours), we note that as currently known, the rate of M-dwarf primaries with known brown dwarf companions is 1.3 ± 0.3%. This is a factor of 21 lower than the stellar MR, considering the stellar and brown dwarf companions detected to date. While more brown dwarf companions will undoubtedly be found in the future, it seems that they are genuinely much rarer than stellar companions. We note that astrometric detection via a perturbation is the only technique used in this survey that was sensitive to brown dwarf companions, and only a few stars (GJ 1215 and SCR 1845−6357) have so far been found to be orbited by brown dwarfs via perturbations in data from our astrometric survey at the CTIO/SMARTS 0.9 m.

We do not include any brown dwarf companions in the analysis that follows, nor are planetary companions addressed in this work.

4. Notes on Individual Systems

4.1. New Companions

Several new companions were discovered during the surveys, or were confirmed after being noticed during the long-term astrometry program at the CTIO/SMARTS 0.9 m. They are listed in order of R.A.. In each case, archival SuperCOSMOS plates were blinked to eliminate the possibility that new companions were background objects.

1. *GJ 84.1C (0205−2804).* was found during the imaging survey separated by 1.″5 from GJ 84.1B at a position angle of 299° and with a $\Delta I = 0.23$ mag, making the system a triple. The SuperCOSMOS *B* and *R* plates, taken 1977 September and 1994 November, respectively, provide a Δt of 17.2 years. Blinking these two plates using the CDS Aladin interface showed that the B component, with a proper motion of 0.″549 yr^{-1}, moved 9.″4. Projecting the star's position forward 17 years to the date of the observation (2011 October) indicates that there was no background star at the position of the B component at that time. Astrometry from the *Gaia* DR2 confirms our discovery, with reported parallaxes of 38.29 ± 0.03, 38.51 ± 0.08, and 38.15 ± 0.10 mas for the now three components. We therefore consider this star a new member of the system.
2. *2MA 0936−2610C (0936−2610).* During the blinking survey, we detected a new companion to this previously known double star at $\rho = 41.''8$, $\theta = 315°$, making this a triple system. The ΔV between the AB pair and the C component is 6.9 mag. There is no *Gaia* DR2 parallax available for the AB pair yet, but the trigonometric distance of 18.50 ± 0.05 pc for the C component (54.04 ± 0.12 mas; Gaia Collaboration et al. 2018) is in

agreement with the ground-based parallax of 53.75 ± 1.42 mas (18.6 pc; Riedel et al. 2018) of the AB pair. We therefore consider this star a new member of the system.

3. *UPM 1710−5300B (1710−5300).* was found during the imaging survey as a companion separated by 1.″2 from its primary at a position angle of 339°, with $\Delta I = 1.2$ mag. The archival *B* and *R* plates, taken 1977 July and 1993 April, respectively, provide a Δt of 15.8 years. Blinking these two plates showed that the primary component, with a proper motion of 0.″207 yr^{-1}, moved 4.″1. Projecting the star's position forward 20 years to the date of the observation (2013 April) indicates that there was no background star of similar brightness at the position of the primary component at that time. Astrometry from the *Gaia* DR2 confirms our discovery, with reported parallaxes of 45.54 ± 0.12 and 45.05 ± 0.15 mas for the two components. We consider this star a new binary system.
4. *LHS 5348 (1927−2811).* This binary system discovery was previously reported in Winters et al. (2017) along with its parallax measurement; however, we include it here with updated multiplicity information, as it was discovered during the multiplicity survey. It is separated by 0.″89 from its primary at a position angle of 283°, with $\Delta I = 2.3$ mag. The archival *B* and *I* plates, taken 1976 September and 1996 July, respectively, provide a Δt of 19.8 years. Blinking these two plates showed that the primary component, with a proper motion of 0.″509 yr^{-1}, moved 10″. Projecting the star's position forward 17 years to the date of the observation (2013 May) indicates that there was no background star of similar brightness at the position of the primary component at that time. While there are two data points in the *Gaia* DR2 at the positions of the two components, only one reports a parallax in agreement with the distance of the system. The other has no associated parallax measurement. We nevertheless consider this a new binary system and anticipate that future *Gaia* data releases will confirm our discovery.
5. *2MA 1951−3510B (1951−3510).* was found during the imaging survey as a companion separated by 1.″9 from its primary at a position angle of 131°, with $\Delta I = 0.3$ mag. The *B* and *R* plates, taken 1976 July and 1990 September, respectively, provide a Δt of 14.1 years. Blinking these two plates showed that the primary component, with a proper motion of 0.″373 yr^{-1}, moved 5.″3. Projecting the star's position forward 23 years to the date of the observation (2013 May) indicates that there was no background star of similar brightness at the position of the primary component at that time. Astrometry from the *Gaia* DR2 confirms our discovery, with reported parallaxes of 88.20 ± 0.08 and 88.27 ± 0.09 mas for the two components (Gaia Collaboration et al. 2018). We consider this a new binary system.
6. *USN 2101+0307 (2101+0307).* This object shows a clear astrometric perturbation, which was not reported in Jao et al. (2017), although it was noted as a binary. As shown in Figure 12, the orbit has not yet wrapped, with more than 10 years of data available for this system. The photometric distance estimate of 13.9 ± 2.2 pc disagrees marginally with the trigonometric distance of 17.7 ± 0.6 pc. This indicates that the system is slightly overluminous, which indicates that the companion contributes some light to the system and is therefore likely a star and not a brown dwarf. The companion is not resolved in the *Gaia* DR2.

4.2. Interesting Systems

There are some systems that require more detail than that given in Table 11, typically those that constitute more than two components or that are particularly interesting. These are listed here with the first four digits of R.A. and decl. in sexagesimal hours and degrees, respectively. Note that below, we adopt the moniker GJ to identify all Gl, GL, and GJ stars, also known as "Gliese" stars.

GJ 2005ABC (0024−2708). This system is a triple, not a quadruple. Upon further analysis of the *HST-FGS* data, the D component reported in Henry et al. (1999) is a false detection and is not real.

GJ 1046AB (0219−3646). The SB companion is a probable brown dwarf with 168.848 -day period (Kürster et al. 2008); also described by Zechmeister et al. (2009). Bonfils et al. (2013) also note that the companion is a brown dwarf or substellar in nature.

GJ 109 (0244+2531). This object is tagged as a VIM (variability-induced mover) in the *Hipparcos* catalog, which could imply duplicity. However, Pourbaix et al. (2003) have shown this to be an incorrect tag in their reanalysis and recalculation of the $(V-I)$ colors. This object is not included as a candidate multiple.

GJ 165AB (0413+5031). Allen et al. (2007) refer to Gl 165B (which we here call GJ 165B) as an L4 dwarf; however, this is likely a typo for GD 165B, which is reported as a bona fide brown dwarf companion to a white dwarf in Kirkpatrick & McCarthy (1994) and McLean et al. (2003). The coordinates of GD 165B are $\alpha = 14{:}24{:}39.09$, $\delta = +09{:}17{:}10.4$, so it is not the same object as GJ 165B. Kirkpatrick & McCarthy (1994) discuss both Gl 65B and GD 165B. GJ 165AB seems to be a possible equal-magnitude binary (Heintz 1992), while McAlister et al. (1987) provide separation information from speckle observations. These data are noted in Table 11.

LTT 11399 (0419+3629). Both Worley (1961) and Worley (1962) report that this is a binary with a separation of 6.″4 at 226°. Balega et al. (2007) observed this star using speckle interferometry but were unable to resolve it. It is also marked as having a stochastic solution in Lindegren et al. (1997). Closer inspection and backtracking of its proper motion indicate that the alleged component is a background star. We consider this to be a single star and do not list it in Table 12.

GJ 273 (Luyten's Star) (0727+0513). This star was reported in Ward-Duong et al. (2015) as having a close companion; however, based on previous observations of this object with myriad methods (IR speckle (Leinert et al. 1997), long-term astrometric monitoring (15.2 yr Gatewood 2008), high-resolution spectroscopy (Nidever et al. 2002; Bonfils et al. 2013), etc.), we conclude that the reported companion is likely an unassociated background object. We treat this object as single.

GJ 289 (0748+2022). Marcy & Benitz (1989) note that Gl 289 (GJ 289) is an SB2, but this is likely a typo for GJ 829, which is noted in Marcy et al. (1987) as being a probable SB2. We did not see reports of GJ 289 being an SB2 noted anywhere else in the literature. We treat GJ 289 as a single object.

GJ 1103 (0751−0000). Reiners et al. (2012) cite Delfosse et al. (1998) for GJ 1103(A) being an SB. However, Delfosse et al. (1998) note only that they exclude GJ 1103 from their sample due to it being a binary. They do not claim that it is an SB. In the LHS Catalog (Luyten 1979a), where it is listed as LHS 1951, it is advertised to have a companion LHS 1952 with a separation of 3″ at $\theta = 78°$, with component magnitudes of $m_R = 13.0$ and 15.5, and $m_{pg} = 15.0$ and 17.5. We searched for the companion by examining both RECONS astrometry frames, in which the seeing was sometimes 1.″2 or better; and via the blinking campaign. No companion was found. We conclude that GJ 1103 is single.

GJ 450 (1151+3516). This object was reported as a low-probability binary candidate with a low-velocity amplitude by Young et al. (1987), who measured five epochs of precise radial velocities. However, more recent high-resolution observations with ELODIE and SOPHIE over a range of resolutions ($R = 40{,}000$–$75{,}000$) make no mention of this object being multiple (Houdebine 2010), nor was a companion detected with lucky imaging (Jódar et al. 2013) or with infrared adaptive optics observations (Ward-Duong et al. 2015). We therefore consider this object to be single.

GJ 452 (1153−0722). Gould & Chanamé (2004) report a likely white dwarf companion at $\rho = 9″$ and $\theta = 110°$ that was detected in 1960 by Luyten (1980a). However, blinking SuperCOSMOS plate images (epochs 1984–1997) with the 300-second integration taken at the CTIO/SMARTS 0.9 m reveals no co-moving companion. Backtracking the proper motion of the star to epoch 1960 places a background star at the appropriate separation and position angle of the reported companion. We thus consider this object to be single.

GJ 1155AB (1216+0258). This object was previously thought to have a white dwarf companion, but Gianninas et al. (2011) report that the white dwarf is actually a misclassified M dwarf. A survey of SDSS objects by Kleinman et al. (2004) did not spectroscopically confirm the companion as a white dwarf. We therefore consider the companion to be an M dwarf.

GJ 465 (1224−1814). Heintz (1986) notes this object may yet be a long-term binary. We note this system as a candidate multiple in Table 12.

GJ 471 (1231+0848). Poveda et al. (1994) report that this object is a CPM companion to the binary GJ 469AB with a separation of 2490″. While the weighted mean trigonometric distances from van Altena et al. (1995) and van Leeuwen (2007) agree within the error bars (73.13 ± 1.28 mas for GJ 471 versus 74.77 ± 3.39 mas for GJ 469AB), their proper motions are significantly different: 822 mas yr^{-1} at $\theta = 231°$ for GJ 471 versus 685 mas yr^{-1} at $\theta = 248°$ for GJ 469AB. Thus, we consider GJ 471 a single star.

GJ 477AB (1235−4556). This object is flagged in the *Hipparcos* DMSA (Lindegren et al. 1997) as having a stochastic solution, indicating that it is a probable short-period astrometric binary. Zechmeister et al. (2009) note it as an SB1 using VLT+UVES, with the companion being low-mass or a brown dwarf. We treat the companion as a stellar component.

GJ 1167 (1309+2859). Jahreiß et al. (2008) note a B component with $\mu = 0.″292$ yr^{-1}, $\theta = 234.°9$, but then note that the two stars are not physically associated, as the photometric distance for B is 190 pc while the trigonometric distance for A is 12 pc. We calculate the *ccddist* for A to be 14.2 pc. Janson et al. (2012) note that A is single in their survey. We conclude that GJ 1167"B" is not a CPM companion to GJ 1167A and that GJ 1167 is a single system.

GJ 541.2AB (1417+4526). This system had too small a proper motion (47 mas yr^{-1} at a position angle of 109.8°; van Leeuwen 2007) to confirm its secondary component with a separation of 55.″2 at a position angle of 204°. Our image, taken in 2013, provided 18 years of coverage when blinked with the 1995 SuperCOSMOS plate, but resulted in the system moving less than an arcsecond during our blinking survey. However, the *Gaia* DR2 catalog confirms this system as a binary, reporting parallaxes and proper motions for both components that agree both with each other and the HIP parallax of 52.60 ± 1.25 mas: $\pi_A = 51.43 \pm 0.03$ mas and $\mu_A = 47.3$ mas yr^{-1}, $\theta_A = 113°$; $\pi_B = 51.74 \pm 0.16$ mas and $\mu_B = 47.8$ mas yr^{-1}, $\theta_B = 113°$. We therefore treat this system as binary.

GJ 680 (1735−4840). A companion at $\rho = 3.″94$, $\theta = 323.°7$ with $\Delta H = 1.93$ mag was reported in Ward-Duong et al. (2015). However, while performing PSF photometry in the crowded field in order to deblend the magnitudes of the primary and secondary, we noted that the alleged secondary had not moved with the primary between epochs of photometry taken 18 months apart. With a proper motion of 462 mas yr^{-1}, the two stars would have moved a pixel and a half. This was the case with the primary, but not the alleged secondary. Therefore, we deem the companion a background star and not physically associated.

GJ 687 (1736+6820). Montet et al. (2014) cite Jenkins et al. (2009) for the M3.5 companion that they note in their Table 2, but the spectral type of the *primary* is M3.5. Jenkins et al. (2009) do not note any additional information about a companion.

We find that the WDS lists GJ 687 as the B component to the F5 star HD 160861. The parallax for the F5 star is 11.20 mas (89 pc; van Leeuwen 2007), which places this object at a much larger distance than the M dwarf, which has $\pi = 220.47$ mas (4.5 pc; van Altena et al. 1995; van Leeuwen 2007). It appears that the "A" component, the F5 star (at $\alpha = 17{:}36{:}42$, $\delta = +68{:}22{:}59$, compared to $\alpha = 17{:}36{:}25.9$, $\delta = +68{:}20{:}20$ for GJ 687) is an SB, for which the measurement by McAlister et al. (1987) pertains. Tokovinin (1992) notes GJ 687 as both an astrometric and speckle binary in the table in that paper named "Long-period spectroscopic binaries." This, too, is likely for the F dwarf, however. The companion is deemed to be optical, and we consider GJ 687 to be single.

LTT 15769 (1945+3223). This system is listed as double in the *Hipparcos* DMSA (Lindegren et al. 1997) with $\rho = 12.″76$, $\theta = 339°$ with a quality code of "D," indicating an uncertain solution. Blinking the SuperCOSMOS *R* plate image with an *I*-band image taken with the Lowell 42-inch image results in an epoch difference of 19 years and reveals the motion of the primary, but not that of the bright "secondary" with a ΔH_p of 2.3 mag. We thus refute this low-probability companion and deem the system "single."

GJ 793 (2030+6527). Weis (1991b) lists this object in the "Rejected Pairs" table (Table 5) and note that the alleged companion is not listed in either the Luyten or Giclas catalogs. The SuperCOSMOS photographic plates had an epoch spread of only one year, so we used the 300 s image taken during our imaging campaign at the Lowell 42-inch telescope to blink with the SuperCOSMOS *I*-band archival image. This resulted

in a $\delta t = 20$ yr. No CPM companion was detected. We confirm that this object is single.

GJ 873 (2246+4420). This object was reported by van de Kamp & Worth (1972) to be an astrometric binary, but this detection was later found to be due to systemmatic errors in the micrometric separation measurements (Heintz 1976).

Young et al. (1987) initially report this object as a high-probability SB1, but then note in the appendix to that paper that the detection is tentative due to the low-velocity amplitude of the signal.

Hełminiak et al. (2009) also investigate this system, citing a "B" component that they infer is a real binary with spectral type G, but not associated with the "A" component, our M dwarf. We confirm by blinking that the two are not physically bound because the G-dwarf binary has a very different proper motion ($\alpha_\mu = 8.6$ mas, $\delta_\mu = -2.0$ mas) from that of the M-dwarf component ($\alpha_\mu = -705$ mas, $\delta_\mu = -461$ mas), and thus the two systems do not move together. In addition, the V magnitudes for the two "components" are not physically possible if they are located at similar distances: the M dwarf has $V = 10.22$, while the G dwarf has $V = 10.66$.

Tanner et al. (2010) report two unconfirmed companions found via AO, but the two candidates are too faint to have 2MASS magnitudes available.

Finally, Docobo et al. (2010) observed this object using speckle interferometry on a 6 m telescope and did not resolve a companion. They were able to resolve companions down to angular separations of 22 mas, corresponding to 0.11 au at the object's distance of 5 pc.

We consider this object to be a single star.

5. Overall Results

We first report the multiplicity and companion rates for the 1120 M dwarfs surveyed before any corrections are applied. The MR is the percentage of all systems that are multiple, regardless of whether the system is double, triple, or higher order. For example, discovering that a member of a binary system has an additional close companion makes the system a triple, but would not affect the MR. The *companion rate* (CR) is the average number of companions per primary in the sample, so higher order multiples *do* affect this rate, as they add a companion to the statistics. The equations describing these percentages are given below, where N_S is the number of singles, N_D is the number of doubles, N_T is the number of triples, N_{Qd} is the number of quadruples, and N_{Qn} is the number of quintuples, the highest order multiples so far known among M-dwarf primaries within 25 pc. The denominator in both cases is 1120.

$$\mathrm{MR} = 100 * \frac{N_D + N_T + N_{Qd} + N_{Qn}}{N_S + N_D + N_T + N_{Qd} + N_{Qn}} \quad (1)$$

$$\mathrm{CR} = 100 * \frac{N_D + 2N_T + 3N_{Qd} + 4N_{Qn}}{N_S + N_D + N_T + N_{Qd} + N_{Qn}}. \quad (2)$$

We analyze all companions in relation to the primary of the system, even if they are members of sub-binaries or -triples.

5.1. Uncorrected Multiplicity and Companion Rates for Confirmed Companions

Among the 1120 M dwarfs searched, there are 265 multiple systems with 310 new and confirmed *stellar* companions to their primaries, resulting in an initial uncorrected MR of MR = 23.7 ± 1.3% and an uncorrected stellar companion rate of CR = 27.7 ± 1.3%. The ratios of singles:doubles:triples: higher order systems is 856:223:37:3, corresponding to 76:20:3:0.3%. For comparison, Raghavan et al. (2010) found 56:33:8:3% for singles:doubles:triples:higher order systems for companions (including brown dwarfs) in a sample of 454 solar-type stars. If we include the known brown dwarf companions to M dwarfs, the ratios change only slightly, to 844:230:41:2:2, corresponding to 75:21:4:0.3%.

5.2. Adjustment to the Multiplicity and Companion Rates at Small Separations

Because this survey was not uniformly sensitive to systems with companions at $\rho < 2''$, a correction should be made in order to determine a final MR. The sample of M dwarfs within 10 pc appears to be at least 90% complete based on decades of RECONS work. Thus, this volume-limited 10 pc sample provides a reasonably complete set of stars that can provide insight into the stellar CR at small separations. If effectively all of the primaries have been targeted by some type of high-resolution technique, an adjustment based on the stellar MR of those objects for the closest companions can be determined and applied to the sample of 1120 M dwarfs in the full survey outlined here. We note that $2''$ separations correspond to 20 au at 10 pc, but to 50 au at 25 pc. Thus, we perform the correction based on a 50 au separation.

A literature search for spectroscopic and high-resolution imaging studies targeting M dwarfs within 10 pc was performed to determine the companion population at small separations. These two techniques cover most of the separation phase space for stellar companions at separations $\rho < 50$ au. It was found that all but two systems either already had a close companion at $\rho < 50$ au, or had been observed with high-resolution techniques, e.g., spectroscopy, *HST* imaging, speckle interferometry, lucky imaging, or long-term astrometry. Because 186 of the 188 M dwarfs within 10 pc have been searched, we infer that we can use the 10 pc sample to correct for unresolved companions with $\rho < 50$ au at distances 10–25 pc.

Figure 13 presents a graph of the running stellar multiplicity at different angular and projected linear separations as a function of distance for the sample of M dwarfs found within 25 pc. For the 13 M dwarfs with only substellar companions, the system was considered single for the purpose of the stellar multiplicity calculation, while the two systems that had both an M dwarf and a substellar companion were considered multiple. For higher order multiple systems with more than one companion, the smallest separation between the primary and a companion was chosen to mitigate the likely incompleteness at small ρ in the top panel. All stellar companions at all separations are included in the bottom panel.

The striking feature of Figure 13 (top) is that most stellar companions to red dwarfs are found at angular separations smaller than $2''$ (50 au). Thus, it is not surprising that the two main campaigns for detecting companions undertaken here yielded few new objects, yet those searches needed to be done systematically. It is evident that the two sets of companions at separations greater than $2''$ are effectively constant from 10 to 25 pc, indicating that there are not significant numbers of overlooked companions at large separations from their primaries. The MRs for companions with angular separations

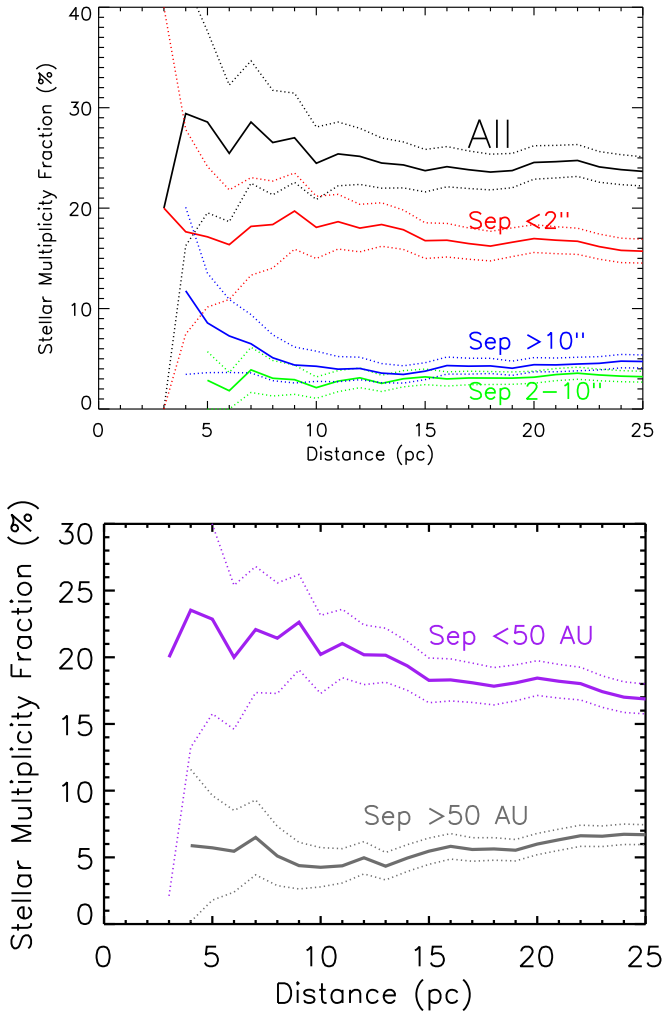

Figure 13. Cumulative multiplicity rate at different angular (top) and projected linear (bottom) separations for the 265 multiples among 1120 M-dwarf systems, binned by 1 pc and subdivided into separations of $\rho < 2''$, $2'' < \rho < 10''$, and $\rho > 10''$ (top) and separations of $\rho < 50$ au and $\rho > 50$ au (bottom). The two rates for companions with separations greater than $2''$ remain fairly constant from 10 to 25 pc, while the rate for separations smaller than $2''$ decreases slightly from ∼10 to 25 pc, and particularly from 13 to 25 pc, indicating that a correction is warranted. The bottom panel shows the translation of angular into projected linear separations, which emphasizes the decreasing trend at $\rho < 50$ au. Neither suspected nor substellar companions are included in these graphs. The dotted lines indicate the binomial errors on each line. The large scatter and errors on the curves at distances less than 10 pc are due to small samples of stars.

$2''$–$10''$ and $>10''$ are 3.2% and 4.7%, respectively, indicating that only 7.9 ± 0.8% of the nearest M dwarfs have companions beyond $2''$. In contrast, the curve for companions with separations smaller than $2''$ decreases from 10 to 25 pc, implying that more close companions remain to be found from 10 to 25 pc. Many of these are presumably the candidates discussed in Section 3.4.1 and listed in Table 12.

The bottom panel illustrates the cumulative MR subdivided into projected linear separations smaller than and greater than 50 au. Neither curve is flat. A decreasing trend is evident in the curve showing separations <50 au, illustrating that multiple systems are missing at those separations. An increasing trend in the >50 au curve hints that multiple systems are missing at large separations as well; however, this corresponds to one missing companion, which is within the errors of our correction (as described below), so we do not apply a correction for this.

By comparing the MR for $\rho < 50$ au at 10 pc ($38/188 = 20.2 \pm 2.9\%$) to the rate at 10–25 pc ($153/932 = 16.4 \pm 1.2\%$), we find a correction of an additional 3.8 ± 0.6% multiple systems that can be appropriately applied to stars from 10 to 25 pc. This corresponds to 35 multiple systems among the 932 stars in this shell, bringing the total number of M-dwarf multiples within 25 pc to 265 + 35 = 300 for 1120 primaries. Thus, the corrected MR for the entire sample is 26.8 ± 1.4%, indicating that roughly three-quarters of M dwarfs are single, compared to only half of solar-type stars.

We use the same method to calculate the correction to the CR and find a CR of 23.9 ± 3.1% at 10 pc and a correction of 5.7 ± 0.8%. The correction corresponds to 53 missing companions to the 932 primaries at 10–25 pc. This brings the total number of companions to 310 + 53 = 363 for 1120 primaries and results in a corrected CR of 32.4 ± 1.4%.

Thus, M dwarfs have an MR of 20.2 ± 1.2% and a CR of 23.9 ± 1.4% at separations smaller than 50 au.

We note that we have identified 56 candidate multiple systems, 51 of which are currently believed to be single; the other 5 are already known to have a companion at a large angular separation. An additional 4 of these 51 candidates are located within 10 pc. All 4 have been observed with both high-resolution spectroscopy and imaging, with no companions detected. If any are found to have a companion, the correction will change, but that appears unlikely to happen.

5.3. Masses for Red Dwarfs in the Sample

In order to perform any quantitative analysis of the multiplicity results related to stellar mass, a conversion from M_V to mass using an MLR was necessary for each primary and stellar companion in the sample. For single M dwarfs or wide binaries with separate V photometry, this is straightforward. For multiples with separations smaller than roughly $4''$, system photometry was deblended at V using PSF fits. For multiples too close for PSF photometry, estimates of the Δmags were made based on the information available in the literature.

5.3.1. Deblending Photometry

For systems with companions at separations too small (typically $1''$–$4''$) to perform effective aperture correction photometry, PSF photometry was performed on frames acquired in Arizona and Chile during the imaging program in order to measure ΔV for each system. First, the contribution from the sky background was calculated from a "blank" part of the image. The region around the close pair being analyzed was then cropped to contain only the relevant pair, and the background subtracted. A Moffat curve was fit to the PSF of the primary, the flux determined from the fit, and then the primary was subtracted from the image, with care taken to minimize the residual counts from the primary. Gaussian and Lorentzian curves were also tested, but it was found that Moffat curves provided the best fits to PSFs from all of the 1meter-class telescopes used in this program. A Moffat curve was then fit to the secondary component's PSF and the flux calculated from the fit. The ratio of the fluxes (fr) of the primary and secondary yielded the ΔV ($\Delta V = -2.5\log(fr)$), which when combined with the composite V photometry, provided the

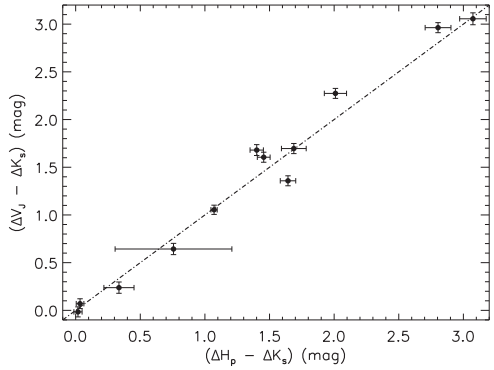

Figure 14. Magnitude differences as a function of color for 12 common proper motion pairs with HIP parallaxes and individual V_J, H_p, and K_s for each component. The dot–dashed line indicates a one-to-one relation. Illustrated is the good agreement between the ΔH_p and ΔV_J for each pair.

individual V magnitudes ($V_B = V_{AB} + 2.5\log(1 + 10^{0.4\Delta V})$; $V_A = V_B - \Delta V$) needed to estimate masses for each component in a multiple system.

For triples where all three components were closer than 4″, the pair with the widest separation was deblended first using the appropriate ΔV to calculate the deblended V magnitude for the single and the resulting pair. Then the ΔV relevant to the remaining pair was used to calculate individual V magnitudes for the components of the closest pair.

For the 96 close multiples with Δmags reported in the literature that were not in the V band, the relations reported in Riedel et al. (2014) were used to convert ΔR_{KC}, ΔI_{KC}, $\Delta i'$, or 2MASS ΔJ, ΔH, ΔK filters to ΔV_J. Magnitude differences in the *Hipparcos* H_p filter were considered to be equivalent to magnitude differences in V_J, as were any visual Δmags reported in the literature, e.g., those from any binary papers before ∼1995 that used photographic plates. For results using the Differential Speckle Survey Instrument (DSSI; Horch et al. 2009) reported in Horch et al. (2011a, 2012, 2015a), Δ562 was adopted to be ΔV and Δ692 was adopted to be ΔR. Horch et al. (2009) state that the 562 and 692 nm DSSI filters' central wavelengths are close to those of the V and R of the Johnson *UBVRI* system. For observations from the RIT-Yale Tip-tilt Speckle Imager (RYTSI; Meyer et al. 2006) reported in Horch et al. (2010, 2012), Δ550 measurements were adopted as ΔV, Δ698 were adopted as ΔR, and Δ754 nm measurements were adopted as ΔI. The Δ814 measurements reported in Reid et al. (2001) were assumed to be ΔI. For *HST* NICMOS data, the mean of the Δmags in the *F*207*M* and *F*222*M* filters were considered equivalent to ΔK_s. We note that we consider the Δmags in these specific filters to be equivalent, not the individual component magnitudes themselves. As an example, we show in Figure 14 the good agreement between the ΔH_p and ΔV_J magnitudes.

We note that for pairs with ΔV values higher than 3.0, the mass of the primary was calculated using the observed V magnitude as if it were single, as a companion with that ΔV contributes negligible flux (∼6% or less) to the system. Although the ΔVs are often not well defined at differences this large, the ΔV was simply added to the V magnitude of the primary and the mass estimated for the companion using that V.

The 43 pairs with unknown magnitude differences between the components (i.e., typically those with separations <1″) required estimates of the Δmag. For double-lined spectroscopic binaries (SB2s), the secondary component would need to contribute enough light to be able to see its spectral lines, making the system overluminous and underestimating the photometric distance. Therefore, if the *trigdist* was more than 1.4 times more distant than the *ccddist*, we adopted a Δmag = 0.5; if the trigonometric distance *trigdist* was 1.3–1.4 times more distant than the photometric distance *ccddist*, we adopted a Δmag = 1.0. Single-lined spectroscopic binaries (SB1s) and unresolved astrometric detections were treated identically. If the *trigdist* was larger than 1.3 times the *ccddist*, we adopted a Δmag = 2.0, inferring that light from the secondary component contributed to the photometry of the system; and if the *trigdist* was <1.3 times the *ccddist*, we adopted a Δmag = 3.0, as the companion did not appear to contribute light to the system. These estimates were all done for the filter in which the observations were done or reported; for example, an object being observed in the I band that was noted to have an astrometric perturbation was assigned a $\Delta I = 3$, which was then converted to ΔV, as long as its two distances agreed.

The ΔV and deblended V magnitudes for the individual components of multiple systems are given in Table 4, with a note if any of the aforementioned assumptions or conversions were made. This is the case for slightly fewer than half (138) of the pairs. We note that while some of the current ΔV estimates are imperfect, the only way to aquire masses of these systems' components is to measure their orbits, which was not a goal of this project.

5.3.2. Estimating Masses

A robust MLR for red dwarfs has recently been provided by Benedict et al. (2016), using extensive sets of *HST-FGS* and radial velocity data. We use their results on 47 stars with masses 0.07–0.62 $M_\odot$ (average errors of 0.005 $M_\odot$) to estimate masses for the red dwarfs in the survey outlined here. Using their mass–M_V relation, which has a scatter of 0.017 $M_\odot$, the massive end of the M dwarf spectral sequence for which we have adopted $M_V = 8.8$ corresponds to 0.63 $M_\odot$. The least massive M dwarf with $M_V = 20.0$ results in a mass of 0.075 $M_\odot$, consistent with the lowest mass M dwarf in Benedict et al. (2016), GJ 1245C with mass = 0.076 ± 0.001 $M_\odot$.

For the 24 systems with orbits presented in the literature that reported masses for individual components, these were used "as is," as long as the masses were true masses and not minimum masses, i.e., $M \sin^3 i$. In the nine cases where $M \sin^3 i$ was reported, we used the composite V-band photometry for the system, in combination with the mass ratio ($M_2 \sin^3 i / M_1 \sin^3 i$), to estimate the ΔV between the components. While the inclination of the system is not known, it is not needed, as the mass ratio remains the same regardless of inclination. However, the relation between the magnitude difference and mass ratio of the components is not linear (e.g., see Benedict et al. 2016) and will change with primary mass. We first assumed an initial ΔV to deblend the photometry of the components. We then used the parallax to calculate the absolute V-band photometry of each component. Finally, we used the MLR to estimate individual masses from the deblended photometry of the components and calculated the mass ratio. We iterated these steps, revising the ΔV, until the estimated mass ratio matched that reported in the literature

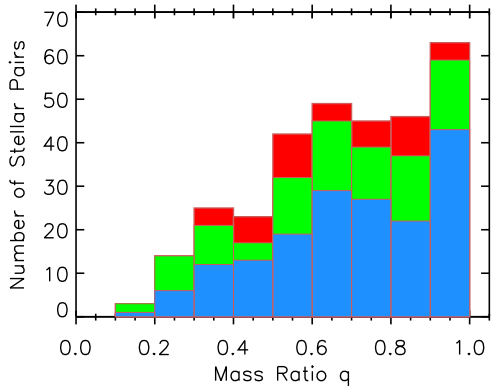

Figure 15. Histogram of the distribution of the mass ratios (M_2/M_1, M_3/M_1, etc.) of the 310 stellar pairs in the sample. In blue are plotted pairs for which no conversion or assumption to ΔV was made, green indicates a conversion to ΔV from another filter, and red indicates that an assumption was made regarding the Δmag. The distribution is likely incomplete at mass ratios lower than 0.5 and uniform from 0.5 to equal-mass ratios of 1.0, as the red shaded portions of the histogram will likely shift leftward in the future once more accurate mass measurements are available. We note that no corrections due to "missing" multiple systems have been incorporated into this distribution, nor are brown dwarf companions included.

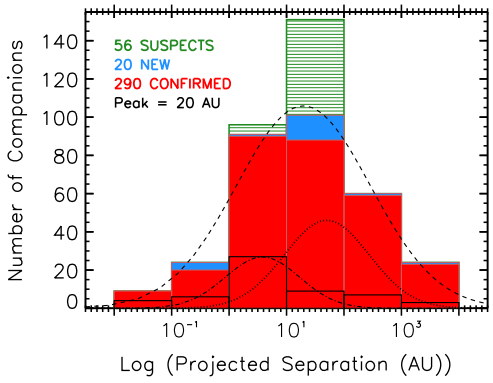

Figure 16. Histogram of the distribution of the projected separations of all stellar companions from their red dwarf primaries, in log form. The 290 confirmed (in red), 20 new (in blue), and 56 suspected companions (in green) are indicated. The dashed curve is a Gaussian that has been fit to the distribution of confirmed and new (but not suspected) companions and has a peak at 20 au, with $\sigma_{\log a} = 1.16$. The dot–dashed line is a fit to the 56 M-dwarf pairs within 10 pc, denoted by the black outline, indicating a peak at 4 au. For comparison, the dotted line indicates the fit for solar-type stars from Raghavan et al. (2010), which peaks at 51 au or $\log P = 5.03$, with $\sigma_{\log P} = 2.28$ yr.

for the system. The resulting ΔV estimates and masses are listed in Table 4.

Twenty-nine of the objects in our survey had masses presented in Benedict et al. (2016) that were used to define the MLR. This provides an opportunity to assess the accuracy of the mass estimates assigned here. We find a mean absolute deviation between the measured masses and our estimates of 10.5%, differences that can be attributed to cosmic scatter, as discussed in Benedict et al. (2016). Mass estimates for all components are listed in Table 4.

5.3.3. Mass Ratios

With mass estimates for all the stars in multiple systems in hand, we can evaluate the mass ratios of all companions relative to their primaries. Figure 15 shows the distribution of the mass ratios ($q = M_{\rm comp}/M_{\rm pri}$) for the 310 pairs in the sample. All companions were analyzed in relation to the primary of the system. There are 225 binaries, as well as 37 triples that result in 74 pairs of objects, one quadruple system yielding 3 pairs, and the two quintuple systems yielding 8 pairs. In the instances where Δmags reported in the literature for hierarchical systems was other than with respect to the "A" component, these data were calculated by first deblending the pair in question, calculating individual magnitudes, estimating individual masses, and then calculating the mass ratios in relation to the primary.

As shown in Figure 15, most of the pairs in the sample have mass ratios higher than 0.5 with a distribution that may very well be flat from $q = 0.5$–1.0. Once accurate mass determinations are available for the pairs represented in red in the histogram (primarily spectroscopic and astrometric binaries), the distribution may shift leftward somewhat, as we have assumed a conservative ΔV of 3 mag for some of these targets. For $q < 0.5$, there are a few incompleteness effects. First, we have excluded from the analysis the 18 known brown dwarf companions, which affect mass ratio evaluations more for M dwarfs than for any other type of star. Second, we show in Section 2.2 that primaries with masses 0.075–0.30 $M_\odot$ likely have companions that have eluded detection. These missing companions might fill in various parts of the distribution, but only for $q > 0.25$ (0.075 $M_\odot$/0.30 $M_\odot$), where 0.25 is the lowest q value possible in that mass regime when considering only *stellar* companions.

In order to assess whether the trend from $q = 0.5$–1.0 is real or due to a bias in the way the ΔV values were calculated (as described above), the histogram has been color-coded in order to identify any trends: blue represents pairs with Δmag in V (172 pairs), green represents pairs for which a conversion from a Δmag other than ΔV was made (96 pairs), and red represents pairs for which an assumption had to be made about the Δmag between the two components, e.g., unresolved spectroscopic and astrometric binaries (43 pairs). We do not see any strong systematic trend that correlates with the assumptions or conversions that were used for the mass estimates.

5.4. The Separation Distribution for the Nearby M Dwarfs

Figure 16 illustrates the projected separations of the 290 confirmed, 20 new, and 56 suspected stellar companions from their primaries. A Gaussian curve has been fit to the distribution of confirmed and new (but not suspected) companions as a function of log-separation, providing a reasonable fit to the distribution as known in the current data set. Exoploration of fitting a skewed Gaussian curve to the data resulted in a skew value very close to zero, with a peak at 20 au. Therefore, we justify our use of a normal Gaussian curve in this analysis. In an even larger sample that has been completely searched for companions at small separations, a different distribution may prove to be more appropriate.

The peak in the separation distribution of our sample falls at 20 au, with a broad spread. This distribution peaks at larger projected separations than the one presented in Janson et al. (2014a) for mid-type M dwarfs (6 au, their Figure 3). However, their search was for companions at angular separations 0.″08–6″ from their primaries at inferred distances within 52 pc (corresponding to 4–312 au), whereas our study searched for companions at angular separations out to 300″, corresponding to separations as large as 7500 au at the survey horizon of 25 pc. In addition, their results are based on a sample

containing 91 pairs in 85 multiples (from 79 binaries and six triples), compared to our 310 pairs in 265 multiples. Similarly, the distribution peak that we find is also at much larger separations than the 5.3 au peak reported for stars $0.1 \lesssim M/M_{\odot} \lesssim 0.5$ by Duchêne & Kraus (2013), i.e., M dwarfs. However, we recognize that our search is not complete at small separations and that the upper limits we have assumed for the separations of systems without measurements are likely overestimates. Therefore, we show the distribution of the 56-M dwarf pairs within 10 pc outlined in black. The dot–dashed line indicates a peak at 4 au for the 10 pc subsample, which is very close to the peaks reported above in Janson et al. (2014a) and Duchêne & Kraus (2013). Comparing our sample to solar-type stars, the peak for M dwarfs at 20 au (dashed line) is roughly one-half the distance for the peak at 51 au for the 259 companions found to 454 stars (dotted line) by Raghavan et al. (2010). In summary, stellar companions to M dwarfs are most often found at separations 4–20 au, i.e., similar to those of the gas giant planets in our solar system, and at least half the distance of stellar companions to more massive, solar-type stars.

The distribution shown in Figure 16 represents the projected separations observed, but two possible shifts in the distribution for these confirmed companions should be noted. Incorporating the correction of a factor of 1.26 from Fischer & Marcy (1992) for those systems for which no orbital information is known (all but 33 of the systems presented here) would shift the distribution to larger separations. In the opposite sense, we adopted projected separations of 1″ for unresolved systems, which is the case for 33 of the confirmed and new companions, plus all of the 56 suspected systems; these generally should be considered upper limits. Consequently, the distribution shown in Figure 16 will shift leftward to smaller separations once all known close companions have orbital semimajor axes determined.

6. Discussion

6.1. Understanding how Primary Mass Determines Companion Types, Separations, and the MR

Exploring how the multiplicity of M-dwarf systems depends on various characteristics provides hints about star formation processes. Because the target sample includes more than 1000 stars and more than 300 pairs, we can evaluate trends in multiplicity as functions of mass and separation.

6.1.1. Mass Ratio as a Function of Primary Mass

Figure 17 shows the mass ratios of all 310 pairs in the sample as a function of primary mass. We note that the distribution is fairly uniform, with no preference for equal-mass systems. There appear to be a dearth of equal-mass companions to the more massive M dwarfs (masses 0.52–0.62 $M_{\odot}$). The apparent trend of mass ratios converging to unity with the decrease in primary mass is expected because we have set a hard limit on companion masses by only including stellar companions, and there is a decreasing amount of mass phase space available as the primary's mass approaches this stellar boundary.

As noted in Section 3.4.4, brown dwarf companions have been excluded from the analysis. The percentage of M dwarfs with known brown dwarf companions is 1.3%, a fraction too low to fill in the open region on the graph where low-mass primaries have no secondaries at high mass ratios. We note that this rate is consistent with the number of solar-type stars with brown dwarf companions in the sample studied by Raghavan et al. (2010): $7/454 = 1.5 \pm 0.6\%$. Furthermore, as shown by Dieterich et al. 2012, there are not many brown dwarfs found around small stars.

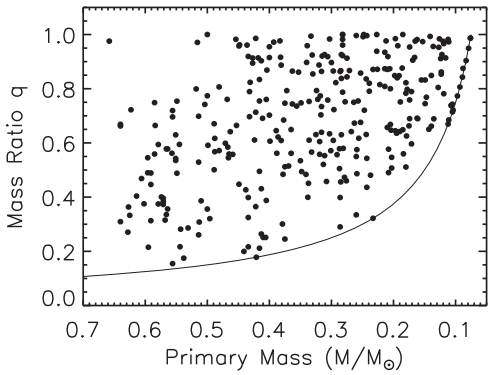

Figure 17. Mass ratios of 310 pairs as a function of primary mass. A trend of mass ratios increasing to unity for low-mass primaries is noted. The solid line indicates the mass ratio boundary relative to the lowest mass star considered here for this survey, with $M = 0.075\ M_{\odot}$.

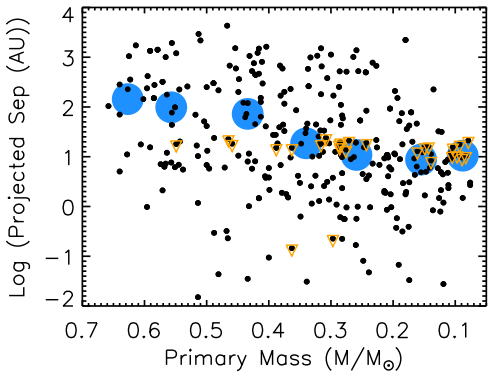

Figure 18. Log of the projected separation in au as a function of primary mass for the 310 stellar pairs. The more massive M-dwarf primaries seem to lack companions at very close separations. A weak trend of decreasing projected separation with primary mass is seen, as emphasized by the large blue points indicating the log of the median projected linear separation, with the median primary mass binned by 0.10 $M_{\odot}$. Pairs with estimated upper limits on their separations have been indicated with inverted orange triangles.

6.1.2. Separation as a Function of Primary Mass

Next, we examine the explicit dependence of separation on primary mass, as shown in Figure 18. Of note is the trend of decreasing projected separation with primary mass. In orange are highlighted the pairs with upper estimates on their separations. Because these pairs are generally spectroscopic and astrometric binaries, they typically have far smaller angular separations than the assumed 1″. Specifically, the astrometric pairs in the sample with measured orbits have separations 0.″0184–0.″239, while the spectroscopic binaries in the sample with measured orbits have separations 0.″001–0.″346. Thus, they will likely move to smaller separations once higher resolution observations are obtained and/or their orbits are measured.

The overall trends of Figures 17 and 18 illustrate that lower mass M dwarfs tend to have stellar companions at higher mass ratios and smaller separations than more massive M dwarfs.

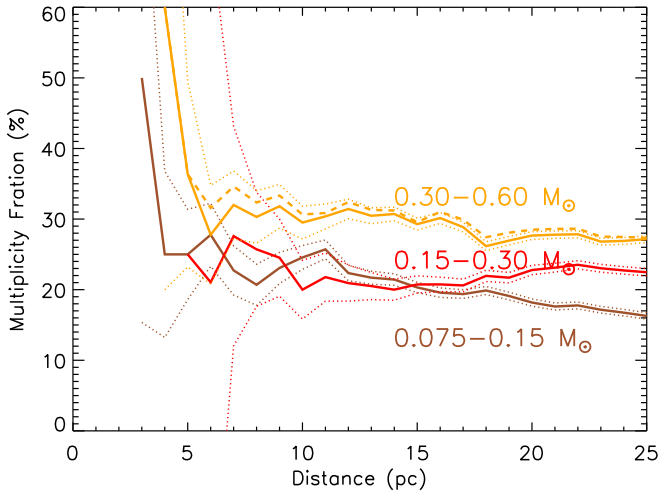

Figure 19. Cumulative stellar multiplicity rate by primary mass. Shown are the running multiplicity rates of the three mass subsets binned by one parsec, with the masses of the primaries calculated from deblended photometry: primary masses 0.30–0.60 $M_{\odot}$ (orange line), with an uncorrected multiplicity rate at 25 pc of 28.2 ± 2.1%; primary masses 0.15–0.30 $M_{\odot}$ (red line) with an uncorrected multiplicity rate at 25 pc of 21.4 ± 2.0%; and primary masses 0.075–0.15 $M_{\odot}$ (brown line), with an uncorrected multiplicity rate at 25 pc of 16.0 ± 2.5%. The dashed orange line indicates the addition of the 28 systems that have a primary mass higher than 0.60 $M_{\odot}$. The dotted lines on each curve indicate the Poisson errors. The large scatter and errors on the curves at distances smaller than 10 pc are due to small number statistics. Neither suspected nor substellar companions are included. The highest mass bin has a higher multiplicity rate than the two lower mass bins. It appears likely that multiple systems are missing from the lowest mass bin at distances 18 to 25 pc, as the curve decreases at those distances.

6.1.3. The Multiplicity Rate as a Function of Primary Mass

It is known that the MR decreases with the mass of the primary star for spectral types O through G (Duchêne & Kraus 2013), and one of the primary goals of our survey is to determine if that trend continues as a function of primary mass through the M dwarfs.

Figure 19 illustrates the MR dependence for three mass regimes subdivided into mass bins that span factors of two—0.30–0.60 $M_{\odot}$, 0.15–0.30 $M_{\odot}$, and 0.075–0.15 $M_{\odot}$—as a function of distance for the target stars. No corrections have been applied for undetected companions in any of the three subsamples. The dashed orange line shows the contribution of the 28 systems that have a primary mass higher than 0.60 $M_{\odot}$, of which 10 are multiple. It is evident that the highest mass bin of stars has the largest MR at 15 pc (31.1 ± 3.4%), roughly 10% greater than for lower masses (19.4 ± 2.8% and 19.8 ± 3.6% for the mid- and low-mass bins, respectively) at the same distance horizon. These values are consistent with Figure 3 in Janson et al. (2012) and Figure 7 in Janson et al. (2014a), although their sample only extends to spectral type M6, so they do not address our lowest mass bin. It also appears that there are slight dropoffs in detected multiples for the highest and lowest mass bins from 15 to 25 pc, whereas the MR for the medium-mass bin remains fairly flat. The dropoff for the highest mass stars is only 2%, a shift that we deem insignificant. However, the dropoff for the lowest mass stars is 4% from 15 to 25 pc and in fact is 9% from 11 to 25 pc. This is likely because the lowest mass primaries are the most difficult to study, so some companions have yet to be detected. Nonetheless, the overall situation is clear: high-mass M dwarfs have more stellar companions than low-mass M dwarfs.

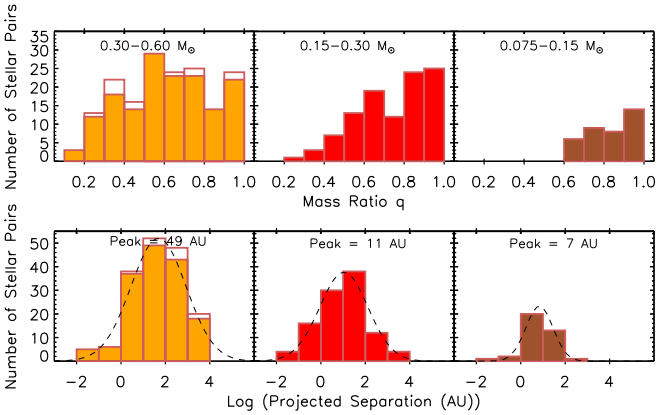

Figure 20. Mass ratios and log-separation distributions for subsamples of M dwarfs as a function of primary masses. Mass ratios for primaries with masses 0.30–0.60 $M_{\odot}$ (in orange, top left) with the 10 multiple systems with primaries more massive than 0.60 $M_{\odot}$ shown unfilled; for primaries with masses 0.15–0.30 $M_{\odot}$ (in red, top middle); and mass ratios for primaries with masses 0.075–0.15 $M_{\odot}$ (in brown, top right). The mass ratio ranges shrink as a function of decreasing primary mass in part due to the imposed lower stellar companion mass limit of 0.075 $M_{\odot}$, although some effect due to gravitational binding energy is likely. Distribution of the projected separations for companions to stars with 0.30–0.60 $M_{\odot}$ (bottom left), with the 10 multiple systems with primaries more massive than 0.60 $M_{\odot}$ shown unfilled; for companions to stars with 0.15–0.30 $M_{\odot}$ (bottom middle); for companions to stars with 0.075–0.15 $M_{\odot}$ (bottom right). The axis scales are the same for both trio of plots to highlight the differences between each mass subsample. The peaks of the projected separation distributions shift to smaller separations with decreasing primary mass subset.

With our large sample, it is also possible to evaluate the mass ratio and separation distributions by mass subset. Figure 20 presents the mass ratios (top row of three plots) and the log of the projected separations in au (bottom row of three plots, discussed below) of the 310 stellar components by mass subset.

It is evident that the number of multiples in each subset decreases with decreasing primary mass, as shown more explicitly in Figure 19. Of note is the wide range in the mass ratios for the most massive primaries, indicating that such stars tend to form with companions filling nearly the entire suite of possible masses. There is also a general shift to higher mass ratios with decreasing primary masses. This trend is somewhat expected because we have set a hard limit on companion masses by only including stellar companions, and there is a decreasing amount of mass phase space available as the primary's mass approaches this stellar/substellar boundary; as noted in Section 3.4.4, brown dwarf companions have been excluded from the analysis. Thus, it appears that lower mass red dwarfs may only form and/or gravitationally retain companions when they are of comparable mass and at small separations. We conclude that M dwarfs have nearly every type of lower mass companion star.

We next evaluate how the mass of the primary drives the separations at which companions are found. The bottom three panels of Figure 20 show the log-projected separation distributions for the three mass subsets. Again, the axis scales are the same between plots, and no substellar or suspected companions are included in these histograms. As in the top row of plots, the number of multiples decreases as a function of primary mass. It is evident that the distribution peaks move to smaller separations as a function of decreasing primary mass, following the trend from solar-type stars to M dwarfs as a whole. Comparison of our distribution peak for the mid-mass subsample, which corresponds most closely to the mid-M

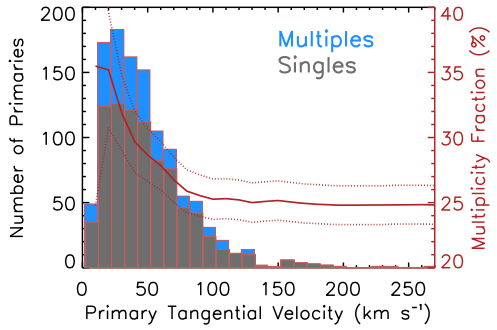

Figure 21. Histogram of primary tangential velocity. The tangential velocity of the primary (or single) component in each system is plotted in gray, with the primaries of confirmed multiple systems indicated in blue. Overplotted in red is the curve of the running multiplicity rate as a function of $v_{\rm tan}$, indicating that slower moving objects tend to have companions slightly more often. Poisson errors on the multiplicity fraction are indicated by dotted lines.

sample surveyed in Janson et al. (2014a), shows a peak within the range of the projected separations (11 au) of the peak reported from their survey (3–10 au).

6.2. Understanding how Tangential Velocity Influences the Multiplicity Rate and Companion Separations

Because it is known that the tangential velocity, $v_{\rm tan}$, of a star generally increases with age due to gravitational kicks from objects in the Milky Way (usually from giant molecular clouds), cool subdwarfs will generally have higher velocities (e.g., $v_{\rm tan} > 200\,{\rm km\,s^{-1}}$; Jao et al. 2017) than young stars (estimated to be $v_{\rm tan} < 35\,{\rm km\,s^{-1}}$).[20] Thus, we investigate M dwarf multiplicity as a function of $v_{\rm tan}$, which we use as a proxy for age. Figure 21 shows the $v_{\rm tan}$ distribution of the observed sample, using the $v_{\rm tan}$ of the primary component, where singles are shown in gray and multiples in blue. There are noticeably more multiple systems with $v_{\rm tan} < 50\,{\rm km\,s^{-1}}$ than at higher $v_{\rm tan}$. The overplotted red curve gives the running MR as a function of $v_{\rm tan}$, showing a general decrease in multiplicity with increasing $v_{\rm tan}$. The apparent drop in the MR at $v_{\rm tan} \approx 15\,{\rm km\,s^{-1}}$ is due to the incompleteness of the sample at low proper motions and corresponding $v_{\rm tan}$ values and is not a real trend. This implies that as small stars age and experience kicks in their travels through the Galaxy, they lose companions. Alternatively, these older stars may have experienced different multiplicity formation rates at the outset, either because of different (presumably lower) metallicities or different star formation environments.

Figure 22 further illustrates how multiplicity changes with $v_{\rm tan}$, showing the log of the projected separation as a function of $v_{\rm tan}$. The blue open circles represent the log of the median projected separation in $25\,{\rm km\,s^{-1}}$ bins, illustrating a weak trend of increasing projected separation with increasing $v_{\rm tan}$. The pairs for which the separations are upper limits are more numerous at the slower end of the plot, indicating that the median $v_{\rm tan}$ may decrease even further there when true separations are available for those close pairs. Thus, the overall trends are that faster moving stars have fewer companions, and

[20] This is a 1σ deviation from the tangential velocity of the oldest nearby young moving group AB Doradus. We consider this a reasonable maximum $v_{\rm tan}$ rate for young stars after comparing the total space motions of the ten nearby young moving groups listed in Table 1 of Mamajek (2016) with ages $\lesssim$150 Myr. The mean for all 10 (including AB Doradus) is $25\,{\rm km\,s^{-1}}$.

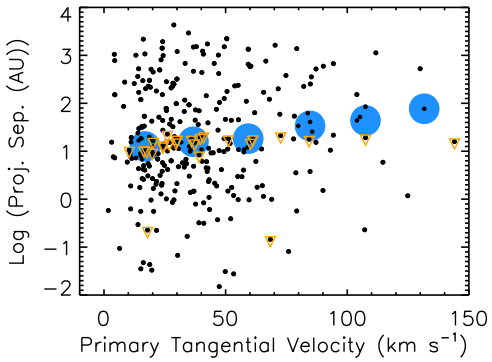

Figure 22. Log of the projected separation in au as a function of tangential velocity for the 310 stellar pairs. Not shown is the one subdwarf binary with $v_{\rm tan} > 150\,{\rm km\,s^{-1}}$. A weak trend of increasing projected separation with increasing tangential velocity is seen. This is emphasized by the large blue points indicating the log of the median projected linear separation as a function of the median tangential velocity in bins of $25\,{\rm km\,s^{-1}}$. Pairs with estimated upper limits on their separations have been indicated with inverted orange triangles.

that the separations of multiples with higher velocities tend to be larger than their slower moving counterparts.

6.3. The Luminosity and Mass Distributions

Shown in Figure 23 are luminosity distributions for our sample in M_V, calculated both before (top) and after (bottom) deblending "joint" photometry with contributions from close companions. Primaries are indicated in red, while companions are shown in blue. The vertical lines at $M_V = 9.25$, 11.80, and 13.86 correspond to masses of 0.60, 0.30, and 0.15 $M_\odot$ and indicate the factors of two in mass used to further divide the 25 pc sample for the analysis presented in 6.1. It is evident that a substantial number of companions were hiding in the blended photometry of the M-dwarf primaries.

Figure 24 illustrates the mass distribution for the 1214 M dwarfs with individual photometry with masses calculated from blended photometry (top) and the distribution for all 1432 M dwarf components (primaries plus all secondaries) found within 25 pc in the survey after deblending photometry (bottom). Both histograms show a gentle but steady rise to the end of the stellar main sequence, which we have defined to be 0.075 $M_\odot$. This trend is emphasized by the additions of the companions in each histogram, as they are all lower masses than their primaries by definition. Given that there are missing M-dwarf systems within 25 pc that are preferentially of low mass, the mass distribution will ultimately be even steeper than shown.

6.3.1. Mass Contributions from Primaries and Hidden Companions

We now consider the contributions to the Galactic mass budget by M dwarfs. Without any prior knowledge of unresolved companions, a naive estimate of the mass of the 1214 M dwarfs in the sample with indivdually measured photometry, from which masses are estimated, yields 381 $M_\odot$. This includes the 1120 M dwarf primaries plus their 94 well-separated secondaries.

However, of the 265 primaries in the sample of multiples, 210 have 257 companions located at angular separations smaller than 2″ from either their primaries or their widely separated secondaries, resulting in "joint," or blended, V magnitudes. After deblending, we find that the 1120 primaries

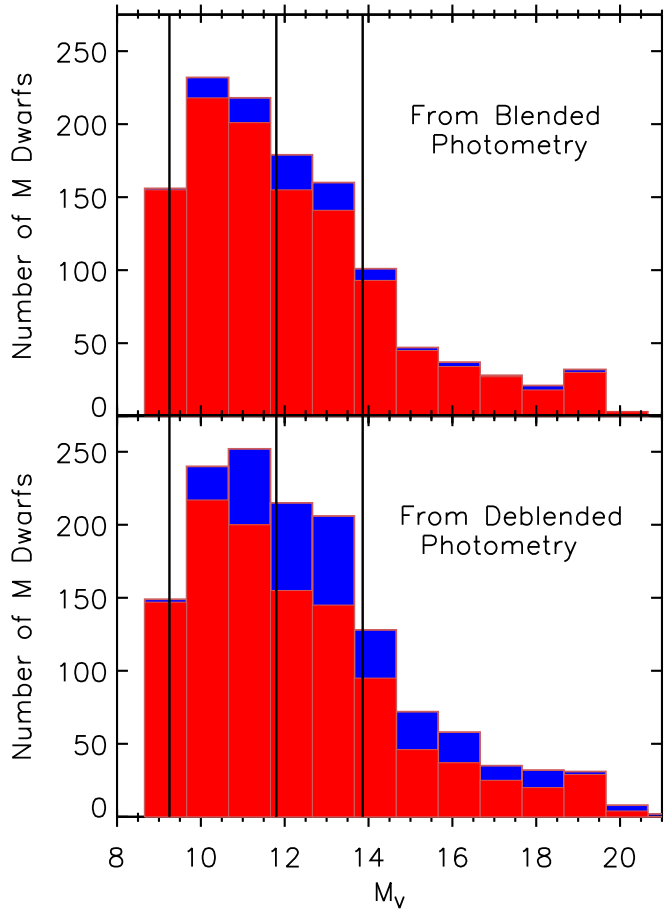

Figure 23. Luminosity distributions. (Top) The luminosity distribution for the 1214 M dwarfs in the sample with individual photometry. M_V has been calculated from the blended photometry. (Bottom) The luminosity distribution for all 1432 M dwarf primaries and secondaries in the sample with M_V calculated from deblended photometry. Primaries are plotted in red, and companions in blue. The vertical lines denote the subdivisions by factors of two in mass explored throughout the study. The contributions from the companions in the deblended luminosity distribution are greater than in the blended luminosity distribution.

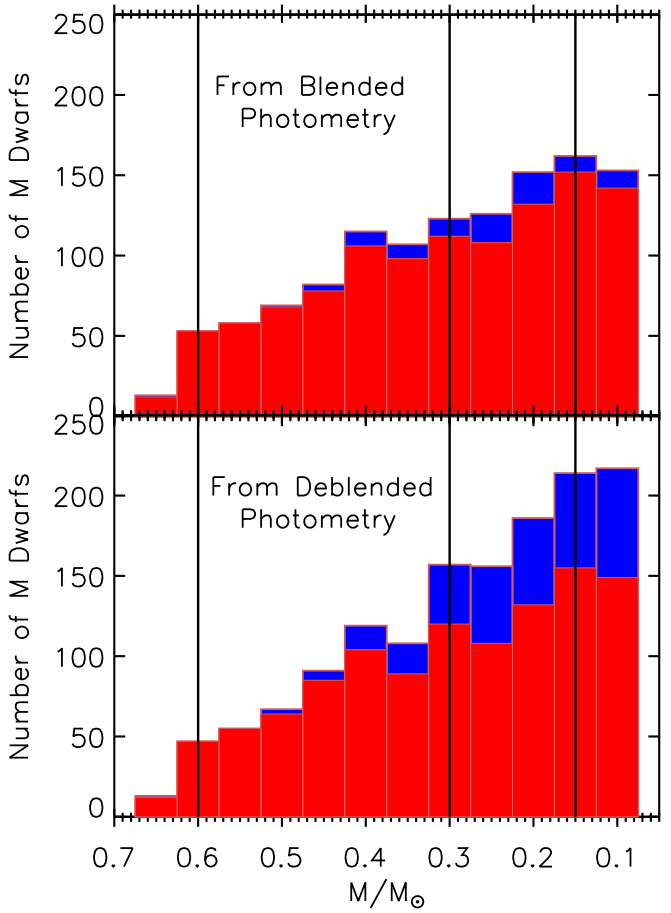

Figure 24. Mass distributions. (Top) The mass distribution for the 1214 M dwarfs in the sample with masses estimated from blended photometry. (Bottom) The mass distribution for all 1432 M dwarfs in the sample with masses estimated from deblended photometry. Primaries are plotted in red; stellar companions in blue. The vertical lines denote the subdivisions by factors of two in mass explored throughout the study. There is a noticeable difference in the shapes of the distributions, as the contributions from the low-mass companions contribute to the rise of the mass distribution to the end of the main sequence.

contribute 336 $M_\odot$. The deblended companions have added 45 $M_\odot$ to the total M-dwarf mass, indicating that 11% was hidden as unresolved stars. We find that at least 17% (66 $M_\odot$/402 $M_\odot$) of M-dwarf mass is found in companions, with unresolved companions contributing at least 68% (45 $M_\odot$/66 $M_\odot$) of the companion mass and donating 11% (45 $M_\odot$/402 $M_\odot$) to the total mass budget of M dwarfs. We emphasize that these values are all lower limits, as this collection of M dwarfs has not been thoroughly canvassed for companions at separations smaller than 2″, where most M-dwarf companions are found.

6.4. Comparisons to Previous Work on Other Stellar Populations

We now put the results from this survey in perspective by making comparisons to results from other M-dwarf multiplicity surveys, as well as to surveys of more massive stars. We then discuss how unresolved companions affect the red dwarf luminosity and mass distributions. Finally, directions for future work will be outlined.

6.4.1. Comparison to Other M-dwarf Surveys

As noted in Section 1, previous surveys have been done to determine M-dwarf multiplicity, but most have studied samples on the order of a hundred stars. Some of the surveys (Skrutskie et al. 1989; Delfosse et al. 1999a) did not report an MR in their results, so they will not be addressed. Others explored the regions around M dwarfs in search of different types of objects (brown dwarfs in the case of Dieterich et al. 2012 and Jovian mass planets in the case of Endl et al. 2006) or at different separation regimes (Dhital et al. 2010 and Law et al. 2010 explored only the wide binary rate) and are thus not relevant to the present comparison. For example, searches for substellar objects can provide lower limits for the types of companions found around M dwarfs, but stellar companions are not always reported. Law et al. (2006, 2008) probed different sample sizes of late-type M dwarfs using lucky imaging and report MRs that are different from each other by a factor of two, but still within their large errors. We note that the uncorrected MR calculated here for the lowest mass bin of M dwarfs—16.0 ± 2.5%—agrees with that reported in Law et al. (2008): $13.6^{+6.5}_{-4}$%.

A number of the other samples studied for M-dwarf multiplicity determination were volume-limited. Henry & McCarthy (1990) searched the 5 pc sample of M dwarfs, while Henry (1991) and Simons et al. (1996) extended the volume searched to 8 pc. Fischer & Marcy (1992) searched a varied sample of M dwarfs within 20 pc. The samples of Bergfors et al. (2010), Janson et al. (2012), and Janson et al. (2014a) were all within 52 pc, but most distances were photometric parallaxes.

We find that our MR result agrees with most of the more recent surveys. Bergfors et al. (2010), Janson et al. (2012), and Janson et al. (2014a) report MRs of 32%, 27%, and 21%–27%, respectively. Our results also agree with the earlier studies of Henry & McCarthy (1990) and Henry (1991) (34% and 20%) within the errors, but are smaller than the studies of Fischer & Marcy (1992) and Simons et al. (1996) (42% and 40%). It is likely that some of the earlier studies simply did not have enough targets from which to calculate accurate results with low statistical errors.

The only other sizeable survey that was volume-limited and had trigonometric parallaxes available was that of Ward-Duong et al. (2015); however, their sample included late K dwarfs and did not include any late-M dwarfs. We find a slightly larger MR than the $23.5 \pm 3.2\%$ of Ward-Duong et al. (2015), although results agree within the errors. Examination of the sample studied here reveals an additional 308 M dwarfs with parallaxes from sources other than van Leeuwen (2007) that place them within 15 pc, 247 of which are within the color-limits of their sample ($3.65 < (V-K) \lesssim 6.8$).[21]

Because all of the targets in our multiplicity sample have accurate trigonometric parallaxes, the study presented here has a number of advantages over studies conducted by others. All of the targets considered were reliably known to be within 25 pc. Because we measured *VRI* photometry for almost all targets lacking it, we were able to use a homogeneous set of data on the same photometric system, combined with the existing parallaxes, to calculate M_V and thus, estimate masses. Most other surveys were forced to use less accurate types of distances to draw conclusions from their data. We were also able to calculate projected separations that were more accurate than those of others, as our sample has trigonometric distances. Finally, our survey was comprehensive in two search regimes, while it was also able to infer the presence of candidate companions using other methods.

6.4.2. Comparison to More Massive Stars

Listed in Table 15 are the multiplicity statistics for stars of other main-sequence spectral types, along with the percentages of all stars by that spectral type. While brown dwarfs are not main-sequence objects, they have been included for comparison. The percentage of stars that they comprise has been purposely left blank, as they are not stars, and in fact, the size of the brown dwarf population is not well constrained.

While the MR decreases as a function of primary mass, it is evident that the number of stars increases with decreasing mass. Massive stars of types OBA are the rarest, accounting for fewer than 1% of all stars (Binney & Merrifield 1998), while solar-type FGK stars make up ~21% of all stars (Binney & Merrifield 1998). The M dwarfs make up 75% of all stars; thus, their multiplicity statistics have the largest impact. The K dwarf MR is the most uncertain, with no comprehensive multiplicity search having yet been done for that spectral type, although efforts to remedy this are currently underway by members of the RECONS group. The thorough study presented here provides an anchor for the statistics at the low end of the stellar main sequence, enabling a complete picture of stellar multiplicity.

Figure 25 indicates the MRs for dwarf stars, with values taken from the literature for the more massive main-sequence stars. The clear decrease in multiplicity with decreasing primary mass is evident.

From this comprehensive picture of stellar multiplicity, we can determine the MR of all star systems. Consider one million stars. Table 16 duplicates the percentages of stars for each main-sequence spectral type and the MR for each of those spectral types from Table 15. In addition, however, is listed the number of stars per one million that each spectral type would contribute and how many of those would be multiple. The extra three percent of stars not shown in the second column are made up of giants, supergiants, and white dwarfs

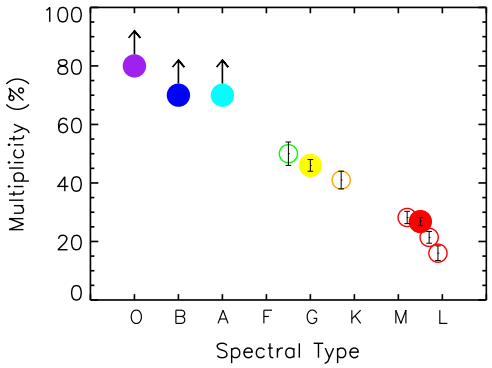

Figure 25. Multiplicity rate as a function of spectral type. Shown is the MR for dwarf stars, with the rates for M dwarfs presented here in red. Open red points are the uncorrected MRs for the three mass bins explored throughout this paper, while the solid point is the total corrected MR for all M dwarfs. Values for stars more massive than M dwarfs are taken from the literature, as listed in Table 15. The open green and orange points are the blue and red subsamples from Raghavan et al. (2010), while the solid yellow point is the average reported in that paper. The arrows indicate the MRs that are likely lower limits. We do not include the L dwarfs here. Clearly, the MR is a function of decreasing mass.

Table 15
Multiplicity of Main-sequence Stars

Spectral Type	% of Stars	References	Mult. Rate	Comp Rate	References
O	<0.1	2	>80	130	5, 3
B	0.1	2	>70	100	6, 3
A	0.6	2	>70	100	6, 3
F	3.3	2	50 ± 4	75	6
G	7.8	2	46 ± 2	75	6
K	10.2	2	41 ± 3	56	6
M	75.0	4	26.8 ± 1.4	32.4 ± 1.4	1
L, T	⋯		22	22	3

Note. The columns indicate the spectral type of object, the percentage of stars that each spectral type comprises, along with the reference. Next, the multiplicity rate, the companion rate, and the reference are listed.
References. (1) This work; (2) Binney & Merrifield (1998); (3) Duchêne & Kraus (2013); (4) Henry et al. (2006); (5) Mason et al. (2009); (6) Raghavan et al. (2010).

[21] This red limit has been estimated from the color–color diagram in Figure 1 in their paper, as it is not specified.

Table 16
Multiplicity Example

Spectral Type	% of Stars	# of Stars	Mult. Rate	# Mult.
O	0.003	30	80	24
B	0.1	1,000	70	700
A	0.6	6,000	70	4,200
F	3.3	33,000	50	16,500
G	7.8	78,000	46	35,880
K	10.2	102,000	41	41,820
M	75.0	750,000	26.8	201,000
	97.0	970,030	31	300,124

(Binney & Merrifield 1998). Based on the numbers presented, we can conclude that the MR of all main-sequence star systems is $31 \pm 0.05\%$, and that therefore most stellar systems are single.

7. Conclusions

7.1. Summary of Results

1. We report 20 new and 56 suspected companions to M dwarfs within 25 pc.
2. We find a corrected MR of $26.8 \pm 1.4\%$ and a corrected CR of $32.4 \pm 1.4\%$ for M dwarfs.
3. We find that M dwarfs have MRs and CRs of $20.2 \pm 1.2\%$ and $23.9 \pm 1.4\%$ at projected linear separations <50 au.
4. We find the uncorrected MR of the three mass subsets (0.30–0.60 $M/M_{\odot}$, 0.15–0.30 $M/M_{\odot}$, and 0.075–0.15 $M/M_{\odot}$) to be $28.2 \pm 2.1\%$, $21.4 \pm 2.0\%$, and $16.0 \pm 2.5\%$.
5. We find a uniformity in the mass ratio distribution, with no apparent preference in companion mass for the nearby M dwarfs.
6. The distribution of the projected separations of the companions peaks at 4–20 au for M dwarfs, i.e., the scale of the gas giants in our solar system.
7. A weak trend of decreasing projected separation with primary mass was found.
8. A possible relation between multiplicity and tangential velocity was found, indicating that older, faster moving M dwarfs tend to have fewer companions at smaller separations as a population than their younger counterparts.
9. We find that at least 17% of M dwarf mass is contained in companions, with 11% of the total mass budget made up of "hidden" stellar companions.
10. Finally, we demonstrate that the mass distribution of our volume-limited sample rises to the end of the stellar main sequence.

7.2. What Is Yet to Come

While the multiplicity survey presented here was comprehensive for stellar companions to M dwarfs with separations 2″–300″, much work remains to be done. Currently underway are Robo-AO, high-resolution speckle imaging, and radial velocity studies to probe within 2″ of these nearby M dwarfs in order to complete our understanding of M-dwarf multiplicity at all separation regimes. The results from these ongoing surveys will provide the separation and delta-magnitude measurements needed for a more thorough understanding of the characteristics of these multiple systems, e.g., the mass ratio and separation distributions. In addition, the radial velocities being measured provide the third velocity component needed to calculate precise *UVW* space motions. These space motions will allow further exploration of the possible trend of stellar multiplicity with tangential velocity.

Gaia will have five years or more of exquisite astrometric measurements that will enable the detection of binaries. Any astrometric binary orbits should provide inclinations, and thus the dynamical masses of each component when combined with ground-based spectroscopic orbits. In addition, *Gaia* should reveal many of the very low-mass stars that have escaped detection to date, providing a more complete picture of the nearby M-dwarf population that we will study in the future.

We thank the anonymous referee for a rigorous review that greatly improved the manuscript. J.G.W. is especially grateful to Jonathan Irwin, Willie Torres, and Eric Mamajek for illuminating and clarifying discussions and suggestions, and to Douglas Gies, Harold McAlister, Russel White, Sebastién Lépine, and David Charbonneau for constructive comments. We thank Brian Mason for access to the Washington Double Star Catalog, a copy of which is housed at Georgia State University. J.G.W. extends a heartfelt thanks to David Fanning for the availability of his IDL Coyote Graphics System.

We thank the members of the SMARTS Consortium, who have enabled the operations of the small telescopes at CTIO since 2003, as well as observers and observer support at CTIO, specifically Arturo Gomez, Mauricio Rojas, Hernan Tirado, Joselino Vasquez, Alberto Miranda, and Edgardo Cosgrove. We are indebted to the support staff and astronomers at Lowell Observatory for their assistance, particularly Len Bright, Larry Wasserman, Brian Skiff, and Ted Dunham.

Data products from the Two Micron All Sky Survey, which is a joint project of the University of Massachusetts and the Infrared Processing and Analysis Center/California Institute of Technology, funded by the National Aeronautics and Space Administration (NASA) and the NSF have been used extensively, as have the SIMBAD database and the Aladin and Vizier interfaces, operated at CDS, Strasbourg, France. This work has made ample use of the Smithsonian Astrophysical Observatory/NASA Astrophysics Data System. This work has made use of data from the European Space Agency (ESA) mission *Gaia* (https://www.cosmos.esa.int/gaia), processed by the *Gaia* Data Processing and Analysis Consortium (DPAC, https://www.cosmos.esa.int/web/gaia/dpac/consortium). Funding for the DPAC has been provided by national institutions, in particular the institutions participating in the *Gaia* Multilateral Agreement.

This work was made possible by National Science Foundation (NSF) grants 09-08402, 0507711, 1109445, and 141206, Sigma Xi Grants-In-Aid-of-Research, the generous budget allotment of Georgia State University that made possible access to the SMARTS telescopes at CTIO and Lowell, and the Georgia State University Dissertation grant. J.G.W. was supported by a grant from the John Templeton Foundation for a portion of the time that it took to finalize these results. The opinions expressed here are those of the authors and do not necessarily reflect the views of the John Templeton Foundation.

Software: IRAF (Tody 1986, 1993), SExtractor (Bertin & Arnouts 1996), PSFEx (Bertin 2011).

ORCID iDs

Jennifer G. Winters https://orcid.org/0000-0001-6031-9513
Wei-Chun Jao https://orcid.org/0000-0003-0193-2187
John P. Subasavage https://orcid.org/0000-0001-5912-6191
Adric R. Riedel https://orcid.org/0000-0003-1645-8596
Michele L. Silverstein https://orcid.org/0000-0003-2565-7909
Matthew J. Payne https://orcid.org/0000-0001-5133-6303

References

Allen, P. R., Koerner, D. W., McElwain, M. W., Cruz, K. L., & Reid, I. N. 2007, AJ, 133, 971
Allen, P. R., & Reid, I. N. 2008, AJ, 135, 2024
Al-Shukri, A. M., McAlister, H. A., Hartkopf, W. I., Hutter, D. J., & Franz, O. G. 1996, AJ, 111, 393
Andrei, A. H., Smart, R. L., Penna, J. L., et al. 2011, AJ, 141, 54
Anglada-Escudé, G., Boss, A. P., Weinberger, A. J., et al. 2012, ApJ, 746, 37
Balega, I. I., Balega, Y. Y., Gasanova, L. T., et al. 2013, AstBu, 68, 53
Balega, I. I., Balega, Y. Y., Maksimov, A. F., et al. 2007, AstBu, 62, 339
Barbieri, C., De Marchi, G., Nota, A., et al. 1996, A&A, 315, 418
Bartlett, J. L., Lurie, J. C., Riedel, A., et al. 2017, AJ, 154, 151
Benedict, G. F., McArthur, B. E., Franz, O. G., Wasserman, L. H., & Henry, T. J. 2000, AJ, 120, 1106
Benedict, G. F., McArthur, B., Chappell, D. W., et al. 1999, AJ, 118, 1086
Benedict, G. F., McArthur, B. E., Franz, O. G., et al. 2001, AJ, 121, 1607
Benedict, G. F., McArthur, B. E., Forveille, T., et al. 2002, ApJL, 581, L115
Benedict, G. F., Henry, T. J., Franz, O. G., et al. 2016, AJ, 152, 141
Bergfors, C., Brandner, W., Janson, M., et al. 2010, A&A, 520, A54
Bertin, E. 2011, in ASP Conf. Ser. 442, Astronomical Data Analysis Software and Systems XX, ed. I. N. Evans et al. (San Francisco, CA: ASP), 435
Bertin, E., & Arnouts, S. 1996, A&AS, 117, 393
Bessel, M. S. 1990, A&AS, 83, 357
Bessell, M. S. 1991, AJ, 101, 662
Bessell, M. S., & Weis, E. W. 1987, PASP, 99, 642
Beuzit, J.-L., Ségransan, D., Forveille, T., et al. 2004, A&A, 425, 997
Bidelman, W. P. 1985, ApJS, 59, 197
Biller, B. A., & Close, L. M. 2007, ApJL, 669, L41
Biller, B. A., Kasper, M., Close, L. M., Brandner, W., & Kellner, S. 2006, ApJL, 641, L141
Binney, J., & Merrifield, M. 1998, Galactic Astronomy (Princeton, NJ: Princeton Univ. Press)
Blake, C. H., Charbonneau, D., White, R. J., et al. 2008, ApJL, 678, L125
Bonfils, X., Delfosse, X., Udry, S., et al. 2013, A&A, 549, A109
Bonnefoy, M., Chauvin, G., Dumas, C., et al. 2009, A&A, 506, 799
Bowler, B. P., Liu, M. C., Shkolnik, E. L., & Tamura, M. 2015, ApJS, 216, 7
Burningham, B., Pinfield, D. J., Leggett, S. K., et al. 2009, MNRAS, 395, 1237
Chanamé, J., & Gould, A. 2004, ApJ, 601, 289
Cortes-Contreras, M., Caballero, J. A., & Montes, D. 2014, Obs, 134, 348
Costa, E., Méndez, R. A., Jao, W.-C., et al. 2005, AJ, 130, 337
Costa, E., Méndez, R. A., Jao, W.-C., et al. 2006, AJ, 132, 1234
Cvetković, Z., Pavlović, R., & Boeva, S. 2015, AJ, 149, 150
Daemgen, S., Siegler, N., Reid, I. N., & Close, L. M. 2007, ApJ, 654, 558
Dahn, C. C., Harrington, R. S., Kallarakal, V. V., et al. 1988, AJ, 95, 237
Dahn, C. C., Harris, H. C., Vrba, F. J., et al. 2002, AJ, 124, 1170
Davison, C. L., White, R. J., Jao, W.-C., et al. 2014, AJ, 147, 26
Davison, C. L., White, R. J., Henry, T. J., et al. 2015, AJ, 149, 106
Dawson, P. C., & De Robertis, M. M. 2005, PASP, 117, 1
Deacon, N. R., & Hambly, N. C. 2001, A&A, 380, 148
Deacon, N. R., Hambly, N. C., & Cooke, J. A. 2005a, A&A, 435, 363
Deacon, N. R., Hambly, N. C., Henry, T. J., et al. 2005b, AJ, 129, 409
Delfosse, X., Forveille, T., Beuzit, J.-L., et al. 1999a, A&A, 344, 897
Delfosse, X., Forveille, T., Perrier, C., & Mayor, M. 1998, A&A, 331, 581
Delfosse, X., Forveille, T., Udry, S., et al. 1999b, A&A, 350, L39
Dhital, S., West, A. A., Stassun, K. G., & Bochanski, J. J. 2010, AJ, 139, 2566
Díaz, R. F., González, J. F., Cincunegui, C., & Mauas, P. J. D. 2007, A&A, 474, 345
Dieterich, S. B., Henry, T. J., Golimowski, D. A., Krist, J. E., & Tanner, A. M. 2012, AJ, 144, 64
Dieterich, S. B., Henry, T. J., Jao, W.-C., et al. 2014, AJ, 147, 94
Docobo, J. A., Tamazian, V. S., Balega, Y. Y., & Melikian, N. D. 2006, AJ, 132, 994
Docobo, J. A., Tamazian, V. S., Balega, Y. Y., & Melikian, N. D. 2010, AJ, 140, 1078
Doyle, J. G., & Butler, C. J. 1990, A&A, 235, 335
Duchêne, G., & Kraus, A. 2013, ARA&A, 51, 269
Dupuy, T. J., & Liu, M. C. 2012, ApJS, 201, 19
Duquennoy, A., & Mayor, M. 1988, A&A, 200, 135
Endl, M., Cochran, W. D., Kürster, M., et al. 2006, ApJ, 649, 436
Fabricius, C., & Makarov, V. V. 2000, A&AS, 144, 45
Faherty, J. K., Burgasser, A. J., Walter, F. M., et al. 2012, ApJ, 752, 56
Falin, J. L., & Mignard, F. 1999, A&AS, 135, 231
Femenía, B., Rebolo, R., Pérez-Prieto, J. A., et al. 2011, MNRAS, 413, 1524
Fischer, D. A., & Marcy, G. W. 1992, ApJ, 396, 178
Forveille, T., Beuzit, J.-L., Delorme, P., et al. 2005, A&A, 435, L5
Frankowski, A., Jancart, S., & Jorissen, A. 2007, A&A, 464, 377
Freed, M., Close, L. M., & Siegler, N. 2003, ApJ, 584, 453
Fu, H.-H., Hartkopf, W. I., Mason, B. D., et al. 1997, AJ, 114, 1623
Gaia Collaboration, Brown, A. G. A., Vallenari, A., et al. 2018, A&A, 616, A1
Gaia Collaboration, Prusti, T., de Bruijne, J. H. J., et al. 2016, A&A, 595, A1
Gatewood, G. 2008, AJ, 136, 452
Gatewood, G., & Coban, L. 2009, AJ, 137, 402
Gatewood, G., Coban, L., & Han, I. 2003, AJ, 125, 1530
Gatewood, G., de Jonge, K. J., & Stephenson, B. 1993, PASP, 105, 1101
Gershberg, R. E., Katsova, M. M., Lovkaya, M. N., Terebizh, A. V., & Shakhovskaya, N. I. 1999, A&AS, 139, 555
Gianninas, A., Bergeron, P., & Ruiz, M. T. 2011, ApJ, 743, 138
Gizis, J. E. 1997, AJ, 113, 806
Gizis, J. E. 1998, AJ, 115, 2053
Gizis, J. E., Reid, I. N., & Hawley, S. L. 2002, AJ, 123, 3356
Golimowski, D. A., Leggett, S. K., Marley, M. S., et al. 2004, AJ, 127, 3516
Gould, A., & Chanamé, J. 2004, ApJS, 150, 455
Graham, J. A. 1982, PASP, 94, 244
Gray, R. O., Corbally, C. J., Garrison, R. F., McFadden, M. T., & Robinson, P. E. 2003, AJ, 126, 2048
Harlow, J. J. B. 1996, AJ, 112, 2222
Harrington, R. S., & Dahn, C. C. 1980, AJ, 85, 454
Harrington, R. S., Kallarakal, V. V., Christy, J. W., et al. 1985, AJ, 90, 123
Harrington, R. S., Dahn, C. C., Kallarakal, V. V., et al. 1993, AJ, 105, 1571
Hartkopf, W. I., Tokovinin, A., & Mason, B. D. 2012, AJ, 143, 42
Hawley, S. L., Gizis, J. E., & Reid, I. N. 1996, AJ, 112, 2799
Heintz, W. D. 1976, MNRAS, 175, 533
Heintz, W. D. 1985, ApJS, 58, 439
Heintz, W. D. 1986, AJ, 92, 446
Heintz, W. D. 1987, ApJS, 65, 161
Heintz, W. D. 1990, ApJS, 74, 275
Heintz, W. D. 1991, AJ, 101, 1071
Heintz, W. D. 1992, ApJS, 83, 351
Heintz, W. D. 1993, AJ, 105, 1188
Heintz, W. D. 1994, AJ, 108, 2338
Hełminiak, K. G., Konacki, M., Kulkarni, S. R., & Eisner, J. 2009, MNRAS, 400, 406
Henry, T. J. 1991, PhD thesis, Arizona Univ., Tucson.
Henry, T. J., Franz, O. G., Wasserman, L. H., et al. 1999, ApJ, 512, 864
Henry, T. J., Ianna, P. A., Kirkpatrick, J. D., & Jahreiss, H. 1997, AJ, 114, 388
Henry, T. J., Jao, W.-C., Subasavage, J. P., et al. 2006, AJ, 132, 2360
Henry, T. J., & McCarthy, D. W., Jr. 1990, ApJ, 350, 334
Henry, T. J., Subasavage, J. P., Brown, M. A., et al. 2004, AJ, 128, 2460
Henry, T. J., Jao, W.-C., Winters, J. G., et al. 2018, AJ, 155, 265
Herbig, G. H., & Moorhead, J. M. 1965, ApJ, 141, 649
Hershey, J. L., & Taff, L. G. 1998, AJ, 116, 1440
Høg, E., Fabricius, C., Makarov, V. V., et al. 2000, A&A, 355, L27
Holman, M. J., & Wiegert, P. A. 1999, AJ, 117, 621
Horch, E. P., Bahi, L. A. P., Gaulin, J. R., et al. 2012, AJ, 143, 10
Horch, E. P., Casetti-Dinescu, D. I., Camarata, M. A., et al. 2017, AJ, 153, 212
Horch, E. P., Falta, D., Anderson, L. M., et al. 2010, AJ, 139, 205
Horch, E. P., Gomez, S. C., Sherry, W. H., et al. 2011a, AJ, 141, 45
Horch, E. P., Robinson, S. E., Meyer, R. D., et al. 2002, AJ, 123, 3442
Horch, E. P., van Altena, W. F., Demarque, P., et al. 2015a, AJ, 149, 151
Horch, E. P., van Altena, W. F., Howell, S. B., Sherry, W. H., & Ciardi, D. R. 2011b, AJ, 141, 180
Horch, E. P., van Belle, G. T., Davidson, J. W., Jr., et al. 2015b, AJ, 150, 151
Horch, E. P., Veillette, D. R., Baena Gallé, R., et al. 2009, AJ, 137, 5057
Hosey, A. D., Henry, T. J., Jao, W.-C., et al. 2015, AJ, 150, 6
Houdebine, E. R. 2010, MNRAS, 407, 1657

Howell, S. B. 2000, Handbook of CCD Astronomy (Cambridge: Cambridge Univ. Press)
Howell, S. B. 2012, PASP, 124, 263
Ianna, P. A., Patterson, R. J., & Swain, M. A. 1996, AJ, 111, 492
Ireland, M. J., Kraus, A., Martinache, F., Lloyd, J. P., & Tuthill, P. G. 2008, ApJ, 678, 463
Jahreiß, H., Meusinger, H., Scholz, R.-D., & Stecklum, B. 2008, A&A, 484, 575
Jancart, S., Jorissen, A., Babusiaux, C., & Pourbaix, D. 2005, A&A, 442, 365
Janson, M., Bergfors, C., Brandner, W., et al. 2014a, ApJ, 789, 102
Janson, M., Bergfors, C., Brandner, W., et al. 2014b, ApJS, 214, 17
Janson, M., Hormuth, F., Bergfors, C., et al. 2012, ApJ, 754, 44
Jao, W.-C., Henry, T. J., Beaulieu, T. D., & Subasavage, J. P. 2008, AJ, 136, 840
Jao, W.-C., Henry, T. J., Subasavage, J. P., et al. 2003, AJ, 125, 332
Jao, W.-C., Henry, T. J., Subasavage, J. P., et al. 2005, AJ, 129, 1954
Jao, W.-C., Henry, T. J., Subasavage, J. P., et al. 2014, AJ, 147, 21
Jao, W.-C., Henry, T. J., Subasavage, J. P., et al. 2011, AJ, 141, 117
Jao, W.-C., Henry, T. J., Winters, J. G., et al. 2017, AJ, 154, 191
Jao, W.-C., Mason, B. D., Hartkopf, W. I., Henry, T. J., & Ramos, S. N. 2009, AJ, 137, 3800
Jenkins, J. S., Ramsey, L. W., Jones, H. R. A., et al. 2009, ApJ, 704, 975
Jódar, E., Pérez-Garrido, A., Díaz-Sánchez, A., et al. 2013, MNRAS, 429, 859
Khovritchev, M. Y., Izmailov, I. S., & Khrutskaya, E. V. 2013, MNRAS, 435, 1083
Kirkpatrick, J. D., & McCarthy, D. W., Jr. 1994, AJ, 107, 333
Kleinman, S. J., Harris, H. C., Eisenstein, D. J., et al. 2004, ApJ, 607, 426
Koen, C., Kilkenny, D., van Wyk, F., Cooper, D., & Marang, F. 2002, MNRAS, 334, 20
Koen, C., Kilkenny, D., van Wyk, F., & Marang, F. 2010, MNRAS, 403, 1949
Köhler, R., Ratzka, T., & Leinert, C. 2012, A&A, 541, A29
Kraus, A. L., Ireland, M. J., Huber, D., Mann, A. W., & Dupuy, T. J. 2016, AJ, 152, 8
Kürster, M., Endl, M., & Reffert, S. 2008, A&A, 483, 869
Kürster, M., Zechmeister, M., Endl, M., & Meyer, E. 2009, Msngr, 136, 39
Lampens, P., Strigachev, A., & Duval, D. 2007, A&A, 464, 641
Landolt, A. U. 1992, AJ, 104, 372
Landolt, A. U. 2007, AJ, 133, 2502
Landolt, A. U. 2009, AJ, 137, 4186
Landolt, A. U. 2013, AJ, 146, 131
Law, N. M., Dhital, S., Kraus, A., Stassun, K. G., & West, A. A. 2010, ApJ, 720, 1727
Law, N. M., Hodgkin, S. T., & Mackay, C. D. 2006, MNRAS, 368, 1917
Law, N. M., Hodgkin, S. T., & Mackay, C. D. 2008, MNRAS, 384, 150
Leinert, C., Henry, T., Glindemann, A., & McCarthy, D. W., Jr. 1997, A&A, 325, 159
Leinert, C., Weitzel, N., Richichi, A., Eckart, A., & Tacconi-Garman, L. E. 1994, A&A, 291, L47
Lèpine, S., & Shara, M. M. 2005, AJ, 129, 1483
Lèpine, S., Thorstensen, J. R., Shara, M. M., & Rich, R. M. 2009, AJ, 137, 4109
Lindegren, L., Mignard, F., Söderhjelm, S., et al. 1997, A&A, 323, L53
Lurie, J. C., Henry, T. J., Jao, W.-C., et al. 2014, AJ, 148, 91
Luyten, W. J. 1979a, LHS Catalogue (2nd ed.; Minneapolis, MN: Univ. Minnesota)
Luyten, W. J. 1979b, NLTT Catalogue, Vol. I and Vol. II (Minneapolis, MN: Univ. Minnesota)
Luyten, W. J. 1980a, NLTT Catalogue, Vol. III (Minneapolis, MN: Univ. Minnesota)
Luyten, W. J. 1980b, NLTT Catalogue, Vol. IV (Minneapolis, MN: Univ. Minnesota)
Malo, L., Artigau, É., Doyon, R., et al. 2014, ApJ, 788, 81
Mamajek, E. E. 2016, in IAU Symp. 314, Young Stars & Planets Near the Sun, ed. J. H. Kastner, B. Stelzer, & S. A. Metchev, 21
Mamajek, E. E., Bartlett, J. L., Seifahrt, A., et al. 2013, AJ, 146, 154
Marcy, G. W., & Benitz, K. J. 1989, ApJ, 344, 441
Marcy, G. W., Lindsay, V., & Wilson, K. 1987, PASP, 99, 490
Martin, C., & Mignard, F. 1998, A&A, 330, 585
Martín, E. L., Koresko, C. D., Kulkarni, S. R., Lane, B. F., & Wizinowich, P. L. 2000, ApJL, 529, L37
Martinache, F., Lloyd, J. P., Ireland, M. J., Yamada, R. S., & Tuthill, P. G. 2007, ApJ, 661, 496
Martinache, F., Rojas-Ayala, B., Ireland, M. J., Lloyd, J. P., & Tuthill, P. G. 2009, ApJ, 695, 1183
Mason, B. D., Hartkopf, W. I., Gies, D. R., Henry, T. J., & Helsel, J. W. 2009, AJ, 137, 3358
Mason, B. D., Hartkopf, W. I., Miles, K. N., et al. 2018, AJ, 155, 215
McAlister, H. A., Hartkopf, W. I., Hutter, D. J., & Franz, O. G. 1987, AJ, 93, 688
McLean, I. S., McGovern, M. R., Burgasser, A. J., et al. 2003, ApJ, 596, 561
Meyer, R. D., Horch, E. P., Ninkov, Z., van Altena, W. F., & Rothkopf, C. A. 2006, PASP, 118, 162
Monet, D. G., Levine, S. E., Canzian, B., et al. 2003, AJ, 125, 984
Montagnier, G., Ségransan, D., Beuzit, J.-L., et al. 2006, A&A, 460, L19
Montet, B. T., Crepp, J. R., Johnson, J. A., Howard, A. W., & Marcy, G. W. 2014, ApJ, 781, 28
Morgan, D. H. 1995, in ASP Conf. Ser. 84, IAU Coll. 148: The Future Utilisation of Schmidt Telescopes, ed. J. Chapman et al. (San Francisco, CA: ASP), 137
Nidever, D. L., Marcy, G. W., Butler, R. P., Fischer, D. A., & Vogt, S. S. 2002, ApJS, 141, 503
Perryman, M. A. C., Lindegren, L., Kovalevsky, J., et al. 1997, A&A, 323, L49
Platais, I., Pourbaix, D., Jorissen, A., et al. 2003, A&A, 397, 997
Pokorny, R. S., Jones, H. R. A., Hambly, N. C., & Pinfield, D. J. 2004, A&A, 421, 763
Pourbaix, D., Platais, I., Detournay, S., et al. 2003, A&A, 399, 1167
Pourbaix, D., Tokovinin, A. A., Batten, A. H., et al. 2004, A&A, 424, 727
Poveda, A., Herrera, M. A., Allen, C., Cordero, G., & Lavalley, C. 1994, RMxAA, 28, 43
Pravdo, S. H., & Shaklan, S. B. 2009, ApJ, 700, 623
Pravdo, S. H., Shaklan, S. B., Henry, T., & Benedict, G. F. 2004, ApJ, 617, 1323
Pravdo, S. H., Shaklan, S. B., Wiktorowicz, S. J., et al. 2006, ApJ, 649, 389
Raghavan, D., McAlister, H. A., Henry, T. J., et al. 2010, ApJS, 190, 1
Reid, I. N., Cruz, K. L., Laurie, S. P., et al. 2003, AJ, 125, 354
Reid, I. N., Gizis, J. E., Kirkpatrick, J. D., & Koerner, D. W. 2001, AJ, 121, 489
Reid, I. N., Hawley, S. L., & Gizis, J. E. 1995, AJ, 110, 1838
Reid, I. N., Kilkenny, D., & Cruz, K. L. 2002, AJ, 123, 2822
Reiners, A., & Basri, G. 2010, ApJ, 710, 924
Reiners, A., Joshi, N., & Goldman, B. 2012, AJ, 143, 93
Riddle, R. K., Priser, J. B., & Strand, K. A. 1971, PUSNO, 20, 1
Riedel, A. R., Blunt, S. C., Lambrides, E. L., et al. 2017, AJ, 153, 95
Riedel, A. R., Finch, C. T., Henry, T. J., et al. 2014, AJ, 147, 85
Riedel, A. R., Murphy, S. J., Henry, T. J., et al. 2011, AJ, 142, 104
Riedel, A. R., Silverstein, M. L., Henry, T. J., et al. 2018, AJ, 156, 2
Riedel, A. R., Subasavage, J. P., Finch, C. T., et al. 2010, AJ, 140, 897
Salim, S., & Gould, A. 2003, ApJ, 582, 1011
Schilbach, E., Röser, S., & Scholz, R.-D. 2009, A&A, 493, L27
Schmidt, S. J., Cruz, K. L., Bongiorno, B. J., Liebert, J., & Reid, I. N. 2007, AJ, 133, 2258
Schneider, A., Melis, C., Song, I., & Zuckerman, B. 2011, ApJ, 743, 109
Scholz, R.-D. 2010, A&A, 515, A92
Ségransan, D., Delfosse, X., Forveille, T., et al. 2000, A&A, 364, 665
Shakht, N. A. 1997, A&AT, 13, 327
Shkolnik, E. L., Anglada-Escudé, G., Liu, M. C., et al. 2012, ApJ, 758, 56
Shkolnik, E. L., Hebb, L., Liu, M. C., Reid, I. N., & Collier Cameron, A. 2010, ApJ, 716, 1522
Siegler, N., Close, L. M., Cruz, K. L., Martín, E. L., & Reid, I. N. 2005, ApJ, 621, 1023
Simons, D. A., Henry, T. J., & Kirkpatrick, J. D. 1996, AJ, 112, 2238
Skrutskie, M. F., Forrest, W. J., & Shure, M. 1989, AJ, 98, 1409
Skrutskie, M. F., Cutri, R. M., Stiening, R., et al. 2006, AJ, 131, 1163
Smart, R. L., Ioannidis, G., Jones, H. R. A., Bucciarelli, B., & Lattanzi, M. G. 2010, A&A, 514, A84
Smart, R. L., Lattanzi, M. G., Jahreiß, H., Bucciarelli, B., & Massone, G. 2007, A&A, 464, 787
Snodgrass, C., & Carry, B. 2013, Msngr, 152, 14
Söderhjelm, S. 1999, A&A, 341, 121
Subasavage, J. P., Henry, T. J., Hambly, N. C., Brown, M. A., & Jao, W.-C. 2005a, AJ, 129, 413
Subasavage, J. P., Henry, T. J., Hambly, N. C., et al. 2005b, AJ, 130, 1658
Subasavage, J. P., Jao, W.-C., Henry, T. J., et al. 2009, AJ, 137, 4547
Subasavage, J. P., Jr. 2007, PhD thesis, Georgia State Univ.
Tamazian, V. S., Docobo, J. A., Melikian, N. D., & Karapetian, A. A. 2006, PASP, 118, 814
Tanner, A. M., Gelino, C. R., & Law, N. M. 2010, PASP, 122, 1195
Teegarden, B. J., Pravdo, S. H., Hicks, M., et al. 2003, ApJL, 589, L51
Teixeira, R., Ducourant, C., Chauvin, G., et al. 2009, A&A, 503, 281
Tinney, C. G. 1996, MNRAS, 281, 644
Tinney, C. G., Reid, I. N., Gizis, J., & Mould, J. R. 1995, AJ, 110, 3014
Tody, D. 1986, Proc. SPIE, 627, 733

Tody, D. 1993, in ASP Conf. Ser. 52, Astronomical Data Analysis Software and Systems II, ed. R. J. Hanisch, R. J. V. Brissenden, & J. Barnes (San Francisco, CA: ASP), 173
Tokovinin, A., & Lépine, S. 2012, AJ, 144, 102
Tokovinin, A. A. 1992, A&A, 256, 121
van Altena, W. F., Lee, J. T., & Hoffleit, D. 1995, yCat, 1174, 0
van Biesbroeck, G. 1974, ApJS, 28, 413
van de Kamp, P. 1975, ARA&A, 13, 295
van de Kamp, P., & Worth, M. D. 1972, AJ, 77, 762
van Dessel, E., & Sinachopoulos, D. 1993, A&AS, 100, 517
van Leeuwen, F. 2007, A&A, 474, 653
von Braun, K., Boyajian, T. S., Kane, S. R., et al. 2011, ApJL, 729, L26
Wahhaj, Z., Liu, M. C., Biller, B. A., et al. 2011, ApJ, 729, 139
Wang, J., Fischer, D. A., Xie, J.-W., & Ciardi, D. R. 2014, ApJ, 791, 111
Ward-Duong, K., Patience, J., De Rosa, R. J., et al. 2015, MNRAS, 449, 2618
Weis, E. W. 1984, ApJS, 55, 289
Weis, E. W. 1986, AJ, 91, 626
Weis, E. W. 1987, AJ, 93, 451
Weis, E. W. 1988, Ap&SS, 142, 223
Weis, E. W. 1991a, AJ, 102, 1795
Weis, E. W. 1991b, AJ, 101, 1882
Weis, E. W. 1993, AJ, 105, 1962
Weis, E. W. 1994, AJ, 107, 1135
Weis, E. W. 1996, AJ, 112, 2300
Weis, E. W. 1999, AJ, 117, 3021
Winn, J. N., & Fabrycky, D. C. 2015, ARA&A, 53, 409
Winters, J. G., Henry, T. J., Jao, W.-C., et al. 2011, AJ, 141, 21
Winters, J. G., Henry, T. J., Lurie, J. C., et al. 2015, AJ, 149, 5
Winters, J. G., Irwin, J., Newton, E. R., et al. 2018, AJ, 155, 125
Winters, J. G., Sevrinsky, R. A., Jao, W.-C., et al. 2017, AJ, 153, 14
Woitas, J., Tamazian, V. S., Docobo, J. A., & Leinert, C. 2003, A&A, 406, 293
Worley, C. E. 1961, PASP, 73, 167
Worley, C. E. 1962, AJ, 67, 396
Worley, C. E., & Mason, B. D. 1998, AJ, 116, 917
Young, A., Sadjadi, S., & Harlan, E. 1987, ApJ, 314, 272
Zechmeister, M., Kürster, M., & Endl, M. 2009, A&A, 505, 859